Decoding the microbial signature in the formation of *Hells Bells* underwater speleothems on the Yucatán Peninsula, Mexico

Zur Erlangung des akademischen Grades einer

DOKTORIN DER NATURWISSENSCHAFTEN

(Dr. rer. nat.)

von der KIT-Fakultät für Chemie und Biowissenschaften

des Karlsruher Instituts für Technologie (KIT)

genehmigte

DISSERTATION

von

Kerstin Meike Leberecht

ERKLÄRUNG AN EIDES STATT

Hiermit versichere ich, dass ich die folgende Arbeit selbständig verfasst und keine anderen als die angegebenen Hilfsmittel und Quellen verwendet habe. Alle wörtlich oder dem Sinn nach aus anderen Texten entnommenen Stellen sind von mir durch Angabe der Quelle gekennzeichnet. Diese Arbeit ist in gleicher oder ähnlicher Fassung noch nicht Bestandteil einer Prüfungsleistung. Weiterhin habe ich beim Anfertigen dieser Arbeit die Regeln zur Sicherung der guten wissenschaftlichen Praxis des KIT beachtet und alle Primärdaten gemäß Abs. A (6) am Institut für Angewandte Biowissenschaften archiviert. Des Weiteren versichere ich, dass die elektronische mit der schriftlichen Form dieser Arbeit übereinstimmt.

Die Untersuchungen zur vorliegenden Arbeit wurden von November 2018 bis Juli 2021 am Institut für Angewandte Biowissenschaften der Fakultät für Chemie und Biowissenschaften des Karlsruher Instituts für Technologie unter der Leitung von Professor Johannes Gescher durchgeführt.

_____   _____
Ort, Datum   Unterschrift

PUBLICATIONS, CONTRIBUTIONS TO CONFERENCES AND WORKSHOPS

Publications

Leberecht, K., Ritter, S. M., Lapp, C. J., Klose, L., Eschenröder, J., Scholz, C., Stinnesbeck, W., Kletzin, A., Isenbeck-Schröter, M., & Gescher, J. (in revision). Microbially promoted calcite precipitation in the pelagic redoxcline: Elucidating the formation of the turbid layer. *Geobiology*.

Grießmeier, V., Leberecht, K. and Gescher, J. (2019), NO_3^- removal efficiency in field denitrification beds: key controlling factors and main implications. *Environmental Microbiology Reports*, 11: 316-329.

Benkisser-Petersen M., Buchner M., Dörffel A., Dühren-von-Minden M., Claus R., Kläsener K., Leberecht K., Burger M., Dierks C., Jumaa H., Malavasi F., Reth M., Veelken H., Duyster J., Zirlik K. (2016), Spleen Tyrosine Kinase Is Involved in the CD38 Signal Transduction Pathway in Chronic Lymphocytic Leukemia. *PLoS One*; 11(12):e0169159

Contributions to conferences

03/2020   Talk at the Conference of the Association for General and Applied Microbiology, Leipzig, Germany

09/2019   Poster Presentation at the 24th European Nitrogen Cycle Meeting (ENCM), Lisbon, Portugal

03/2019   Poster Presentation at the Conference of the Association for General and Applied Microbiology, Mainz, Germany

Workshops

2020   Acceptance to the „International Geobiology training course 2020" of the California Institute of Technology (Caltech), California (postponed due to corona)

ABSTRACT

In association with rising temperatures, increased eutrophication and stratification can be expected in the future resulting in the spread of oxygen minimum zones. Oxygen minimum zones set the basis for the increased emergence of sulfidic water zones. Microbes can play an important role in the detoxification of hydrogen sulfide. Pelagic redoxclines as biogeochemical transformation zones represent ideal environments to study the complex role of microorganisms in this process and the corresponding key controlling factors. In this work, the microbial ecology of the redoxcline of cenote El Zapote on the Yucatán Peninsula was studied. In cenote El Zapote, the world's largest underwater speleothems named *Hells Bells* were discovered. Previous studies on the hydrogeochemistry of the cenote indicated that the development of these calcite formations is most likely based on microbial activity in the redoxcline. To elucidate if these enigmatic calcareous structures grow by microbially induced mineralization, the functional diversity of the different sub-biotopes (freshwater, halocline, redoxcline, biofilm on the speleothems) was determined via 16S rRNA amplicon sequencing and connected to a metagenomic and -transcriptomic profiling of the microbial community to identify the microbial key players and their diverse metabolic activity.

This study revealed that in this electron acceptor limited environment, chemolithoautotrophic Hydrogenophilales catalyze an incomplete nitrate-driven sulfide oxidation with elemental sulfur as the main product instead of sulfate. This proton-consuming process is responsible for a local pH shift towards the more alkaline, which in turn favors calcite precipitation and finally the formation of the turbid layer and growth of Hells Bells. Based on this conclusion, calcite precipitation by this metabolic activity was investigated and successfully confirmed on a laboratory scale using microfluidic chips system. Thus, the key findings of previous hydrogeochemical studies could be validated. A subproject based on the metatranscriptomic data even allowed to develop the basis for an antibody-based isolation method for the enrichment of Thaumarchaeota from the redoxcline of El Zapote.

To further understand the origin of Hells Bells, the microbial ecology of the redoxcline of cenote Angelita, which exhibits no speleothems, was studied next. Metatranscriptomic analyses revealed that photolithoautotrophic Chlorobiales and chemolithoautotrophic Campylobacterales play a central role. Anoxygenic photosynthesis and anaerobic sulfide oxidation with the main product of sulfate mediate a pH decrease in the less oxidant-deficient

redox regime, which in turn results in calcite undersaturation and inhibition of calcite precipitation. This study was able to unravel the microbial key players, their complex pathways and key genes involved in biogeochemical cycling in these redoxclines and thus elevates the understanding of Hells Bells growth to a molecular biological level.

ZUSAMMENFASSUNG

In Zusammenhang mit steigenden Temperaturen ist in Zukunft mit einer verstärkten Eutrophierung und Stratifizierung zu rechnen, was zur Ausbreitung von Sauerstoffminimumzonen führt. Sauerstoffminimumzonen bilden wiederum die Grundlage für das verstärkte Aufkommen von sulfidischen Wasserzonen. Mikroben können eine wichtige Rolle bei der Entgiftung von Schwefelwasserstoff spielen. Pelagische Redoxklinen als biogeochemische Transformationszonen stellen ideale Umgebungen dar, um die komplexe Rolle von Mikroorganismen in diesem Prozess und die entsprechenden wichtigen Kontrollfaktoren zu untersuchen. In dieser Arbeit wurde die mikrobielle Ökologie der Redoxkline der Cenote El Zapote auf der Yucatán Halbinsel untersucht. In der Cenote El Zapote wurden die größten Unterwasser-Speläotheme der Welt, die sogenannten *Hells Bells*, entdeckt. Frühere Studien zur Hydrogeochemie der Cenote deuteten darauf hin, dass die Entwicklung der Kalzitformationen höchstwahrscheinlich auf mikrobieller Aktivität in der Redoxkline beruht. Um zu klären, ob diese enigmatischen Kalkstrukturen durch mikrobiell induzierte Mineralisierung entstehen, wurde die funktionelle Vielfalt der verschiedenen Subbiotope (Süßwasser, Halokline, Redoxkline, Biofilm auf den Speläothemen) mittels 16S rRNA-Amplikonsequenzierung bestimmt und mit einem metagenomischen und -transkriptomischen *Profiling* der mikrobiellen Gemeinschaft verbunden, um die mikrobiellen Hauptakteure und ihre vielfältigen Stoffwechselaktivitäten zu identifizieren.

Diese Studie konnte aufdecken, dass chemolithoautotrophe Hydrogenophilales in dieser elektronenakzeptorlimitierten Umgebung eine unvollständige nitratgetriebene Sulfid-oxidation mit elementarem Schwefel als Hauptprodukt anstelle von Sulfat katalysieren. Dieser protonenverbrauchende Prozess ist für eine leichte lokale pH-Verschiebung ins Alkalische verantwortlich, welche wiederum Kalzitfällung und schließlich die Bildung der Trübeschicht und das Wachstum der Hells Bells fördert. Auf Grundlage dieser Schlussfolgerung wurde Kalzitfällung durch diese Stoffwechselaktivität mit Hilfe von mikrofluidischen Chip-Systemen im Labormaßstab untersucht und erfolgreich bestätigt. Folglich konnten die Kernaussagen vorrausgehender hydrogeochemischer Studien beleget werden. Ein Teilprojekt, das auf den metatranskriptomischen Daten basierte, ermöglichte es

sogar, die Grundlage für eine antikörperbasierte Isolierungsmethode zur Anreicherung von Thaumarchaeota aus der Redoxkline von El Zapote zu schaffen.

Um den Ursprung von Hells Bells besser zu verstehen, wurde als Nächstes die mikrobielle Ökologie der Redoxkline von Cenote Angelita untersucht, die keine Speläotheme aufweist. Metatranskriptomische Analysen zeigten, dass photolithoautotrophe Chlorobiales und chemolithoautotrophe Campylobacterales eine zentrale Rolle spielen. Die anoxygene Photosynthese und anaerobe Sulfidoxidation mit dem Hauptprodukt Sulfat bewirken in dem weniger elektronenakzeptorlimitierten Redoxregime eine pH-Absenkung, die wiederum zu einer Kalzituntersättigung und Hemmung der Kalzitfällung führt. Mit dieser Studie konnten die mikrobiellen Hauptakteure, ihre komplexen Stoffwechselwege und Schlüsselgene, die am biogeochemischen Kreislauf in diesen Redoxklinen beteiligt sind, aufgedeckt und damit das Verständnis des Wachstums von Hells Bells auf eine molekularbiologische Ebene gehoben werden.

TABLE OF CONTENTS

TABLE OF FIGURES

LIST OF TABLES

ABBREVIATIONS

Abbreviation	Description
3-HP	3-Hydroxypropionate
3-HP-4-HB	3-Hydroxypropionate/4-hydroxybutyrate
AA	Amino acid
ANAMMOX	Anaerobic ammonium oxidation
BLAST	Basic Local Alignment Search Tool
BP	Before present
bp	Base pairs
cDNA	Complementary DNA
CDS	Coding sequence
DCS	Double cone sampling
DNRA	Dissimilatory nitrate reduction to ammonium
DO	Dissolved oxygen
E	Equation
EC	Electric conductivity
EPS	Extracellular polymeric substances
FNU	Formazin nephelometric units
KEGG	Kyoto Encyclopedia for Genes and Genomes
kyr	Thousand years
MICCP	Microbially induced calcium carbonate precipitation
NCBI	National Center for Biotechnological Information
NGS	Next Generation Sequencing
OTU	Operational Taxonomic Unit
PCR	Polymerase chain reaction
PE	Paired-end
SE	Single-end
SI	Saturation index
S-layer	Surface layer
TCA	Tricarboxylic acid
TPM	Transcripts per million

1 INTRODUCTION

Microorganisms are important biocatalysts for geochemical transitions and have significantly shaped the planetary history and evolution. In turn, geochemical conditions define the local microbial community and predominant metabolic pathways (Druschel & Kappler, 2015; Schopf, 1983). Reviewing the history of the earth, it becomes clear that microbes can bring about changes at the lowest level, such as on a molecular basis, but microbial activity can also reach global dimensions (e.g. the Great Oxidation Event during the Paleoproterozoic period) (Druschel & Kappler, 2015). However, at geological sites it is not always obviously distinguishable whether microbiology is involved. This thesis revolves around such a question. On the Yucatán Peninsula in eastern Mexico extraordinary subaqueous calcite ($CaCO_3$) formations were found in 2009 by the cave diver Vincente Fito Dahne in the dark deeps of a sinkhole, locally termed *cenote*. These underwater speleothems of cenote El Zapote extend from the cave walls into the central water body and are characterized by their unusual structure and bell-shaped contour with a hollow interior (Fig. 1). After the discovery, the "new type" of formations gained more and more attention and the cenote El Zapote was further explored by other local divers. Finally, the first exploration divers called these structures *Hells Bells* (or in Spanish *campanas*) - based on their shape and the hell-like environmental conditions: they appear in darkness, above a white, cloudy turbid layer and a toxic, sulfidic halocline with a typical rotten smell.

The first scientific studies in the cenote were carried out by Stinnesbeck et al. (2017), however, were not dedicated to the Hells Bells, but to the skeleton of a new species (and genus) of giant ground sloth *Xibalbaonyx oviceps* that was found at the bottom of the cenote (Stinnesbeck et al., 2017). Shortly thereafter, a series of investigations on the speleothems followed. Firstly, Stinnesbeck et al. (2018) intensively studied the morphology of the speleothems and concluded that the Hells Bells must have grown underwater. Dr. Simon Ritter (from the research group of Prof. Isenbeck-Schröter, the department for Hydrogeochemistry and Hydrogeology at the University of Heidelberg) then build up on this fundamental study in form of his doctoral thesis and thereby greatly advanced the understanding of the hydrogeochemistry of the cenote and hydrogeobiochemical requirements for the appearance of Hells Bells (Ritter, 2020; Ritter et al., 2019). Already in the first study on the Hells Bells formations it was hypothesized that the microbial

communities in the water body and possibly also in the biofilm on the speleothems are involved in calcite precipitation and thus in speleothem growth (Stinnesbeck et al., 2018).
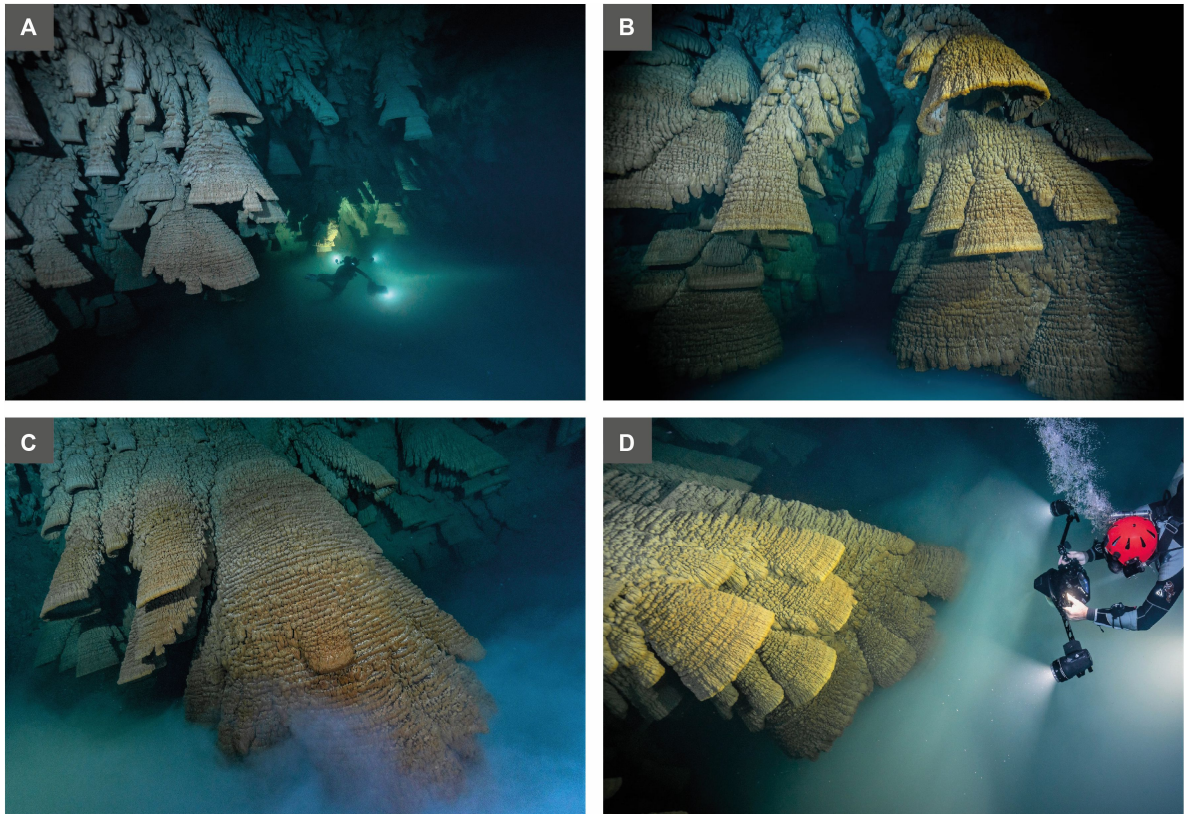
Figure 1: The Hells Bells speleothems of cenote El Zapote. A) In the dome-like submerged cave, Hells Bells cover the cave walls in a water depth from about 28 to 38 m. B) Hells Bells are characterized by their hollow bell-like shape and reach a size of up to 4 m. C) Some speleothems reach into the white turbid layer and redoxcline, the growth zone of Hells Bells. D) The calcite formations show horizontal layers with distinct swellings. Fotos provided by Valentina Cucchiara (Liquid Jungle Media, Playa del Carmen, Mexico; 2020).

However, to date, there have been no specific microbiological studies on this important aspect of Hells Bells growth that went beyond a phylogenetic diversity analysis (Stinnesbeck et al., 2018; see section 1.3). Accordingly, the specific role of defined microbial key players in the proposed process of microbially induced calcium carbonate precipitation (MICCP) is still unknown. Speleothem-forming calcite precipitation in caves usually occurs abiotically by the degassing of carbon dioxide and/or evaporation at the water-atmosphere interface. Results of these physiochemical processes are for example dripstone formations (Huggett, 2003) and calcite rafts (e.g. Kovacs et al., 2017) in cave environments. Hells Bells, however, grow subaqueous and in an otherwise carbonate dissolving karst aquifer environment. For some calcareous settings, it has been found that biological influences play an important role in the formation process (Bontognali et al., 2016; Enyedi et al., 2020; Holmes et al., 2001;

Melim et al., 2001; Queen & Melim, 2006; Reid et al., 2000). It should therefore be verified whether this is also the case for the development of Hells Bells of El Zapote. In form of this thesis, the aim was to provide precisely this important biological piece of the puzzle that was still missing from the overall picture of the biogeochemical formation processes of Hells Bells in El Zapote, and to complement the previous fundamental findings on hydrogeochemistry with microbial ecology.

1.1 How microbes impact carbonate balances

In nature, many examples from MICCP can be found in diverse environments, such as soils, freshwater and marine to hypersaline environments, in the form of aragonitic shells, stromatolites, encrusted surfaces or microbial mats (Dupraz et al., 2009).

MICCP is a well-known effect of microbes on geochemistry. The term refers to the process of calcium carbonate ($CaCO_3$) mineral formation from solution as the result of microbial metabolic activity and/or physical presence of microbial cells. However, microbes can only induce MICCP if their influence results in calcium carbonate supersaturation. This is the case when the product of Ca^{2+} and CO_3^{2-} exceeds the solubility product of $CaCO_3$ (Bosak, 2011). The solubility product K_{sp} can be described as:

$$K_{sp\ calcite} = [Ca^{2+}] \times [CO_3^{2-}]$$

whereas the $[Ca^{2+}]$ and $[CO_3^{2-}]$ describes the respective ion activities in the mineral saturated solution at a specific temperature, pressure and salinity. Likewise, the saturation index (SI) of a solution with regards to this mineral depends on these parameters and be defined as:

$$SI_{calcite} = \log \left[\frac{[Ca^{2+}] \times [CO_3^{2-}]}{K_{sp\ calcite}} \right]$$

Accordingly, an $SI_{calcite} > 0$ indicates mineral supersaturation, a value < 0 indicates undersaturation of calcite (de Moel et al., 2013).

The equilibrium equation (E) between calcite and carbonic acid can be described as:

$$Ca^{2+} + 2\,HCO_3^- \leftrightarrow CaCO_3 + CO_2 + H_2O \qquad\qquad (E1)$$

$$Ca^{2+} + CO_3^{2-} \leftrightarrow CaCO_3 \qquad\qquad (E2)$$
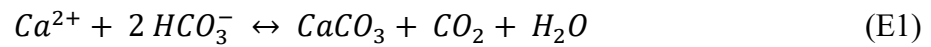
In principle, two different ways how microbial organisms shift the equilibrium towards calcite precipitation have been identified. Firstly, microbes cause the increase of the concentration of dissolved carbonate ions and the local pH of their environment, which finally induces calcite precipitation. With a higher pH, the concentration of carbonate also increases, hence, mineral precipitation in turn will also be reinforced. Secondly, the microbiome may also favor the nucleation of calcite and eliminate inhibitory factors on the kinetics of calcite precipitation (Bosak, 2011).

To date, many environmental studies have already identified several microbial metabolic pathways that have led to calcite precipitation in a wide variety of habitats. Among those, autotrophic processes such as anoxygenic and oxygenic photosynthesis and methanogenesis, as well as microbial activity in the nitrogen and sulfur cycle such as denitrification, the dissimilatory reduction of nitrate, ammonification, ureolysis and the dissimilatory reduction of sulfate were related to MICCP (Castanier et al., 1999; Seifan & Berenjian, 2019; Zhu & Dittrich, 2016). The metabolization of organic acids and conversion to calcium carbonate can also induce calcium carbonate precipitation (Seifan & Berenjian, 2019). A selection of these listed processes and their effect on the mineralization of $CaCO_3$ will now be exemplarily explained in more detail (Fig. 2).

1.1.1 Photosynthesis

In mineralization of CO_2 mediated by photosynthesis, cyanobacteria often play an important role (Altermann et al., 2006; Popall et al., 2020). Many environmental calcareous scenes have been recognized as the product of photosynthetic bacteria, such as stromatolites (Gautret & Trichet, 2005; Rodríguez-Martínez et al., 2012; Visscher et al., 1998) and annual limnic water withing events (Thompson et al., 1997). Microbes that conduct oxygenic photosynthesis favor calcite precipitation by their uptake of CO_2, which leads to a local positive pH shift just around the cells (Fig. 2 A).
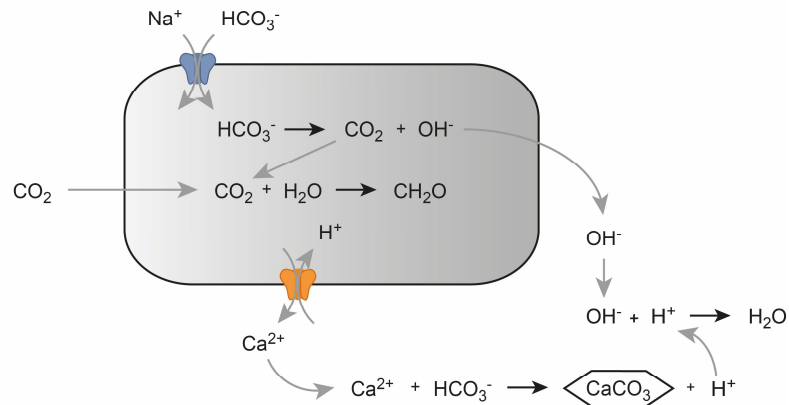
Figure 2: Microbially induced calcite precipitation. Schematic diagram on the mechanisms how microbes can promote calcite precipitation through metabolic activity such as A) photosynthesis, B) denitrification, and C) dissimilatory sulfate reduction. In these processes, the uptake of CO_2 and the consumption of protons and oxidized species (such as nitrate and sulfate) play a role in causing a local pH increase and thus calcite supersaturation. Scheme based on Zhu & Dittrich (2016).

Carbon dioxide either diffuses through the cell wall or is imported in form of HCO_3^- via a symporter (together with Na^+) into the cell (Zhu & Dittrich, 2016). In the cell interior, CO_2 is directly used to produce biomass by the enzyme Ribulose-1,5 bisphosphate carboxylase/oxygenase (RubisCo) of the Calvin cycle. This pathway is fueled by NADPH and ATP generated by photophosphorylation. Especially aquatic photosynthetic organisms were challenged to evolve an optimized CO_2 fixation process to compensate the limited CO_2 availability as the diffusion rate of CO_2 is 10^4 times slower in water than in air. The adaption can be found in many organisms (including many cyanobacteria) in form of a CO_2-concentrating intracellular system that is based on the activity of the enzyme carbonic anhydrase which converts imported HCO_3^- to CO_2 and H_2O (E3; Fig. 2 A):

$$H^+ + HCO_3^- \leftrightarrow CO_2 + H_2O \qquad\qquad (E3)$$
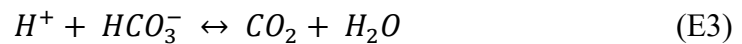
Finally, the H^+ consumption in this reaction contributes to the alkalinity on the cell surface that is mainly realized by the photosynthetic electron transport chain (Kamennaya et al., 2012). Furthermore, cells create an increased availability of Ca^{2+} ions at the outer cell membrane though the export of Ca^{2+} ions via Ca^{2+}/H^+ antiporters (Fig. 2). Increased pH levels on the cell surface and an excess of Ca^{2+} ions together favor $CaCO_3$ supersaturation (Kamennaya et al., 2012; Zhu & Dittrich, 2016).

Anoxygenic photosynthetic microorganisms, which use hydrogen sulfide, hydrogen and small organic carbon compounds as electron donors, may also contribute to calcification (Bosak et al., 2007; Bundeleva et al., 2012; Castanier et al., 1999). By their uptake of hydrogen sulfide and the formation of neutral extracellular or intracellular sulfur deposits, they promote a local pH increase (Castanier et al., 1999).

1.1.2 Denitrification

Nitrate is used as an alternative electron acceptor by many microorganisms, when oxygen is absent and high nitrate concentrations are available together with a carbon source (Chapin III et al., 2011). Most denitrifying organisms are facultative anaerobes and adapt their growth strategies to the environmental conditions. During a complete denitrification process nitrate (NO_3^-) is reduced via the intermediates nitrite (NO_2^-), nitric oxide (NO), nitrous oxide (N_2O) to the neutral product of dinitrogen (N_2) (Zumft, 1997) (Fig. 2 B). The alkalinity that results

from the proton consuming process of denitrification, together with the production of CO_2 can induce calcite precipitation (Erşan et al., 2015; Zhu & Dittrich, 2016) (E4):

$$5\ CH_3COO + 13\ H^+ + 8\ NO_3^- \rightarrow 10\ CO_2 + 4\ N_2 + 14\ H_2O \qquad \text{(E4)}$$
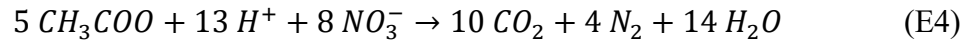
1.1.3 Dissimilatory reduction of sulfate

In anoxic environments enriched with organic matter and sulfate, sulfate reducing bacteria are also described to promote the precipitation of calcite (Baumgartner et al., 2006; Castanier et al., 1999) (Fig. 2 C) – especially, when their product, hydrogen sulfide, is used by sulfide oxidizing bacteria for an incomplete oxidation to zero-valent sulfur (Castanier et al., 1999). According to Baumgartner et al. (2006), the sum of metabolic processes of the dissimilatory reduction of sulfate can be summarized as:

$$SO_4^{2-} + 2\ [CH_2O] + OH^- + Ca^{2+} \rightarrow CaCO_3 + CO_2 + 2\ H_2O + HS^- \qquad \text{(E5)}$$
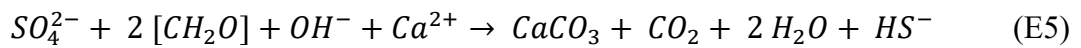
Based on this reaction (E5), one mole calcium carbonate can precipitate as calcite for every mole of sulfate and every two organic carbon molecules. As the product hydrogen sulfide is a much weaker acid compared to the substrate sulfate (sulfuric acid), the reduction of sulfate increases alkalinity and favors calcite supersaturation (Baumgartner et al., 2006).

1.1.4 Microbes as nucleation sites

Besides of the microbial metabolic activity, microorganisms may also contribute to calcite precipitation by the physical characteristics of their cellular surfaces (as cell walls) and surrounding extracellular polymeric substance (EPS) of biofilms. Both represent local sites for the adsorption of ions thus for the nucleation of minerals (Seifan & Berenjian, 2019; Zhu & Dittrich, 2016). Negatively charged functional groups on the cell walls of microbes (such as amine, carboxyl and phosphate groups) may show high affinity to aqueous metals and favor the adsorption of metal ions, such as Na^+, Ca^{2+}, Mn^{2+}, Mg^{2+}, Fe^{3+} (among others) as described for *Bacillus subtilis* (Beveridge & Murray, 1976; Fein et al., 1997). In presence of carbonate, mineralization is favored by the increased availability of metal cations in the micro-environment around the microbial cells to which carbonate anions are attracted (Zhu & Dittrich, 2016). In biofilms, the EPS functions as a physical barrier between the embedded cells and predators, other bacteria, and biocide compounds but also serves bacteria in many

other ways. These include adhesion, stressful environmental conditions (such as droughts), communication between cells in the biofilm and entrapment of nutrients (Costa et al., 2018; Tourney & Ngwenya, 2014). Within such a biofilm community, many different microbial metabolisms co-exist in close proximity.

The EPS is both described in association with calcite precipitation and inhibition of calcite supersaturation depending on the EPS properties. Large amounts of mono- or divalent cations can be included in EPS with negatively charged acidic groups, which promotes the maintenance of the EPS gel. Thereby, the removal of free Ca^{2+} ions from the aquatic environment inhibits the formation of calcium carbonate minerals. In the EPS, inhibitors such as acidic amino acids and carboxylated polysaccharides are often responsible for this calcite precipitation preventing effect. On the other hand, microbial metabolic activities that are associated with EPS degradation may actively promote calcite precipitation by releasing calcium ions bound to EPS polymers resulting in a local increase in the Ca^{2+} availability. Additionally, some EPS degrading metabolic pathways may also promote local alkalinity. These two effects combined result in microbially induced mineralization (Dupraz et al., 2009). A second mechanism is described for conditions where a continuous supply of calcium is provided, and the calcium binding capacity is reached. Wherever this is the case, the presence of free Ca^{2+} and a local alkalinity at the EPS matrix can cause calcite precipitation (Arp et al., 1999).

1.2 The Yucatán Peninsula and studied field sites

The two cenotes studied in this thesis are located in the Mexican state of Quintana Roo on the Yucatán Peninsula. The Yucatán Peninsula exhibits many different ecosystems, including tropical forests, coral reefs and wetlands. On the Caribbean coast of Quintana Roo there is the Sian Ka'an Biosphere Reserve (Sian Ka'an, Mayan for "where the sky is born"), a UNESCO World Heritage Site due to its importance of its groundwater-dependent wetlands (Bauer-Gottwein et al., 2011; Mazzotti et al., 2005). The weather on the Yucatán Peninsula is basically marked by three seasons: from November to February there is a winter storm season, followed by a dry and warm period from March to June, and finally from June to October a rainy season dominates with the highest precipitation in September. The average annual temperature is 26.1 °C (Schmitter-Soto et al., 2002).

The Yucatán Peninsula is a calcareous platform. As a result of permanent dissolution of limestone, the karst aquifer of the Yucatán Peninsula probably represents the largest contiguous underwater cave system worldwide. During infiltration, percolating rainwater is enriched with CO_2 and thus dissolves the carbonate rock (Bauer-Gottwein et al., 2011; Schmitter-Soto et al., 2002). This process has formed a network of conduits and caves. Sinkholes or cenotes, as they are called locally derived from the Mayan term *ts'onot*, are formed once the ceiling of a submerged cave collapsed (Schmitter-Soto et al., 2002). Cenotes are found in large numbers throughout the peninsula, but there are regions where cenotes are found in particularly high densities, such as the "ring of cenotes" in North-West Yucatán (Perry et al., 1995). Due to the porous limestone material, precipitation intrudes into the underlaying groundwater (Kovacs et al., 2017). The hydrogeological structure of the Yucatán karst aquifer system is rather complex (Fig. 3; Brankovits et al., 2017).
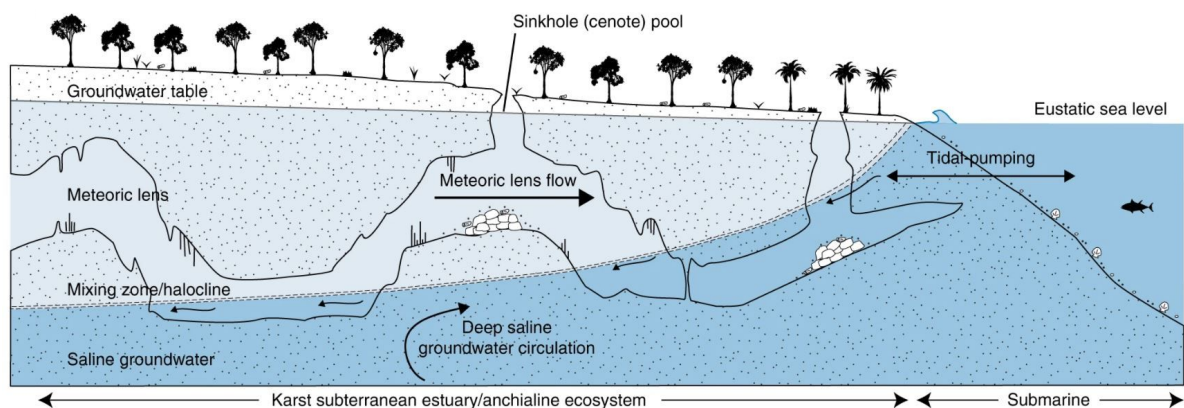
Figure 3: Schematic illustration of the Yucatán karst aquifer. The density-stratified aquifer consists of saline groundwater overlain by a freshwater mass. The transition zone between the two groundwater masses is termed halocline. Submerged sinkholes (cenotes) connect the complex underwater cave network with the surface. Scheme from Brankovits et al. (2017).

It comprises a saline groundwater, which is overlain by a meteoric freshwater groundwater lens. The transmission zone from salt- to freshwater is termed halocline. The depth of the halocline thereby depends on the distance to the coast, the freshwater mass (groundwater) and the global sea level (Bauer-Gottwein et al., 2011; Schmitter-Soto et al., 2002). The halocline itself also contributes to cave and conduit formation as this transmission zone is usually undersaturated with respect to calcium carbonate (Gulley et al., 2016).

In order to shed light on the role of microbes regarding the formation of Hells Bells, a comparative study between the microbial ecology in cenote El Zapote with Hells Bells and cenote Angelita was conducted as part of this study. Cenote Angelita was chosen as reference, as it shares the deep stratified water layering with cenote El Zapote (with Hells Bells) but does not exhibit calcite speleothems. This pair of cenotes thus provides an optimal setting to elucidate the role of microbiology in the origin of Hells Bells. Both cenotes are located in the North-East of the Yucatán Peninsula in the state of Quintana Roo (Fig. 4). The water bodies of these two cenotes exhibit all three water bodies of the Yucatan Karst Aquifer – freshwater, halocline and saltwater.

Figure 4: Location of the study sites cenote El Zapote and Angelita on the Yucatán Peninsula. Cenote El Zapote, in which the world's largest underwater speleothems were found, is located West of Puerto Morelos. Further south the coast, cenote Angelita, which does not display calcite speleothems, is located past of Tulum. Map extended from Stinnesbeck et al. (2018) and Ritter et al. (2019).

The main study site, the cenote El Zapote, is located in the North-Eastern part of Mexico on the Yucatán Peninsula, about 26 km west of Puerto Morelos (20°51'13.8" N 87°07'31.2" W). Cenote Angelita is sited South-West of Tulum (20°08'15.1" N 87°34'40.0" W) (Fig. 4). A narrow rain forest surrounds the environment of both cenotes. Figure 5 shows the water surface of these two cenotes and the extraordinary calcite speleothems that were found in the submerged cave of El Zapote.

Cenote El Zapote
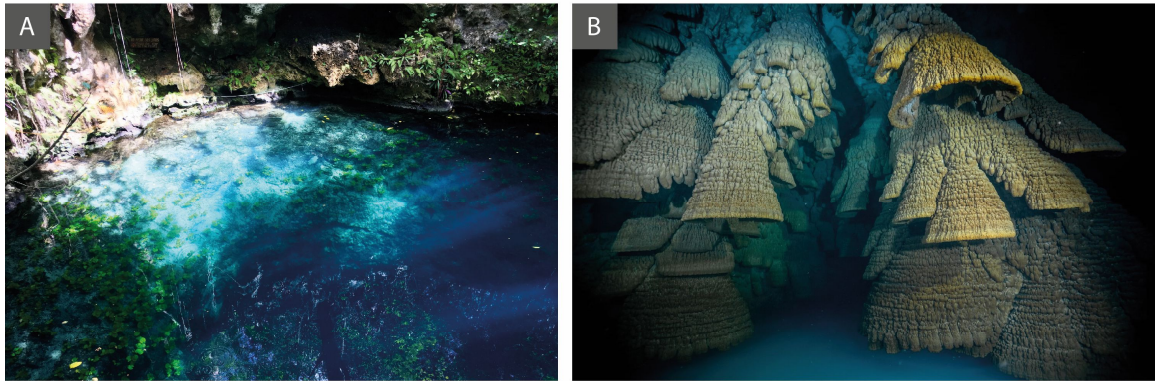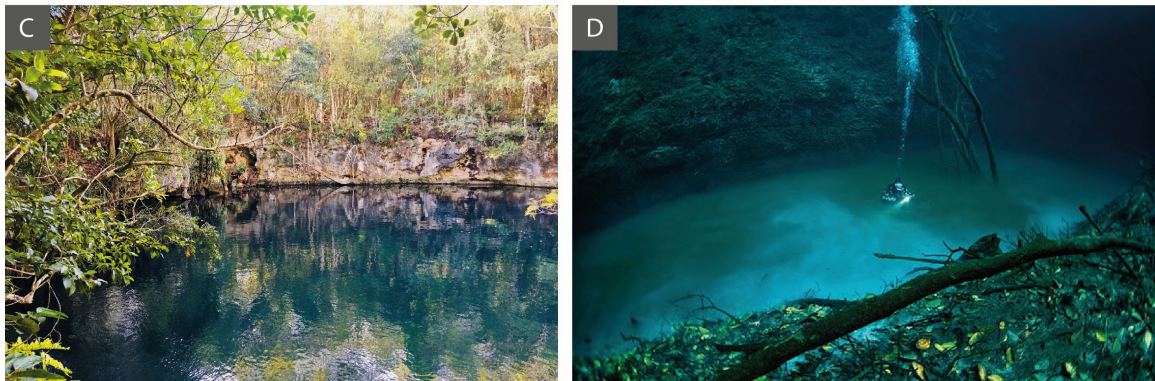
Cenote Angelita

Figure 5: The two study sites on the Yucatán Peninsula, Mexico. Cenote El Zapote (with Hells Bells) and Angelita (devoid of Hells Bells) are shown. A) and C) show the water surfaces of the cenotes. B) and D) show the water zone above the halocline and white, milky turbid layer of cenote El Zapote and Angelita. B) Cenote El Zapote exhibits extraordinary Hells Bells, whereas in D) cenote Angelita no calcite formations were found. Fotos A) and C) by Kerstin Leberecht (2020); B) by Valentina Cucchiara (Liquid Jungle Media, Playa del Carmen, Mexico; 2020); D) by Dirk Penzel (2020).

The underwater cave of El Zapote is characterized by a bottle-like shape with a 28 m long, narrow waterfilled shaft that connects the water surface to a dome-like subaqueous cave body with a diameter of 60 to 100 m (Fig. 6 A). So far, no conduits were found in the cenote that would connect El Zapote to other caves. In the central part, a debris mound has formed that reaches to a water depth of 36 m, whereas the lowest point of the cenote is reached at a total depth of ~54 m. Compared to El Zapote, cenote Angelita also has a bottle-like shape, but its shaft is much broader with a diameter of about 30 m. The water surface of the cenote is shown in Fig. 5 C, together with the underwater perspective on the turbid layer without a hint on calcite speleothems (Fig. 5 D). At the deepest point Angelita reaches a depth of 60 m (Ritter, 2020). In the center, a debris mound rises out of the turbid layer, as do some tree stems.

In the diving community, cenote Angelita is very well known for its very distinct turbid layer, the so-called "underwater river".
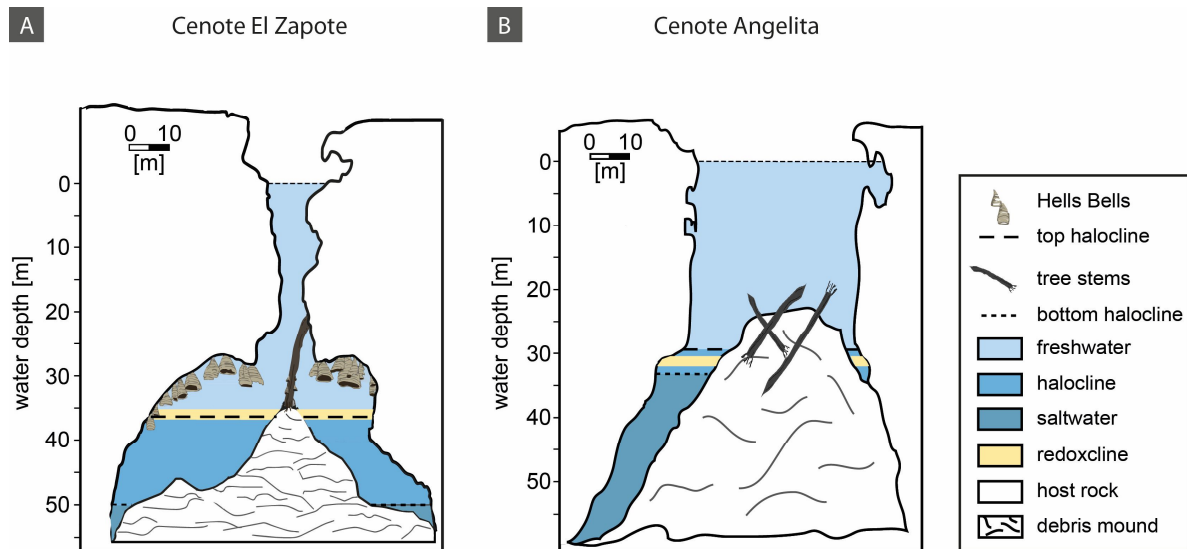
Figure 6: Schematic cave cross-sections of A) cenote El Zapote and B) Angelita. The water body of both cenotes comprises freshwater, a redoxcline, a halocline, and saltwater. However, only cenote El Zapote exhibits Hells Bells calcite speleothems. Hells Bells do not only cover the cave walls but also the surface of a fallen tree. Cave schemes modified from Ritter (2020).

The extraordinary, bell-shaped speleothems cover the cave walls of El Zapote in a water depth of 28 to 38 m, as well as the stem surface of fallen tree that stands right on top of the debris mound (see section 1.3). The complex water column of both cenotes comprises different water zones: freshwater, a white, milky turbid layer, a redoxcline, a halocline and finally saltwater (from top to bottom).

Pelagic redoxclines are characterized by strong vertical counter-gradients of upwards diffusing reduced products and downwards diffusing oxidized substrates such as electron acceptors. Furthermore, redoxclines represent the transmission zone from upper oxygenated water zones to anoxic, sulfidic waters below. Thus, a strong vertical redox gradient is established. The formation of redoxclines requires a high degree of water stagnancy (Ritter et al., 2019).

Research on the microbial ecology was based on the previous investigations that focused on the hydrogeochemistry of these two cenotes. The following section summarizes the most important findings on Hells Bells growth in cenote El Zapote and the absence of Hells Bells in cenote Angelita.

1.3 Hells Bells research – the status quo

The occurrence of Hells Bells is not exclusive to cenote El Zapote. So far, five other cenotes on the north-eastern Yucatán Peninsula have been reported to show similar underwater speleothems – cenote Tortugas, Maravilla, Siete Bocas, Kin-Ha and Holbox. In cenote El Zapote, Hells Bells developed at least since ~120 thousand years (kyr) before present (BP) and partially still grow (Ritter, 2020). Stinnesbeck et al. (2018) were the first to investigate the development of Hells Bells at cenote El Zapote. The most important conclusion was that these calcite speleothems must have grown underwater. This finding was strongly supported by the presence of small specimens of Hells Bells that developed on the surface of a tree, that has fallen into the cenote ~3.5 kyr BP, when the deeper part of the cenote had already been submerged for thousands of years. This also implicates that the calcifying, Hells Bells-forming conditions must have been (more or less) stable throughout this period. Furthermore, the freshwater zone above the halocline, the transition zone from freshwater to saltwater, was designated as the Hells Bells growth zone (Stinnesbeck et al., 2018).

Hells Bells are characterized by a bell-like morphology and an expanding hallow interior with a horse-shoe-like horizontal shape. The openings of the horseshoe-like shape always point towards the cave walls. The speleothems cover the cave ceiling in the dome-like cenote cave, but more dominantly the cave walls. Hells Bells do not necessarily grow individually by themselves. Larger Hells Bells often form the attachment surface for other small specimens or these grow out of them (Fig. 1). However, speleothems do not fuse with each other. They reach a size of up to four meters, thereby they represent the largest subaqueous speleothems worldwide (Stinnesbeck et al., 2018).

There seem to be different stages in the growth of Hells Bells (Stinnesbeck et al., 2018). It starts with a hemispherical base, which then develops a conical shape from a size of ~2 cm. From this stage, only the walls of the cone grow, continuously expanding downwards. From a size of ~3–4 cm the cones show ring patterns. At the same time, the lower edges of the speleothems always remain strictly horizontal, and the inner and outer walls of these ring walls always appear parallel to each other (Fig. 1 B). Irregular growth is indicated by the pattern of ring-like swellings and constrictions, but also the changes in color and thickness of individual layers in the vertical cross-section. Furthermore, layers of corroded dogtooth

spar crystals and microspars also indicate an inconstant growth and/or intermediate periods of dissolution (Stinnesbeck et al., 2018).

Together with the initial investigations of the hydrogeochemistry of El Zapote, microbial diversity was also investigated (Stinnesbeck et al., 2018). It was found that the microbial communities in the water column and in the biofilm on the Hells Bells differ significantly. In the planktonic phase, a dominance of Proteobacteria, more specifically the family Hydrogenophilaceae and the genus Sulfurovum was identified. Both taxa contain mainly chemolithotrophic sulfur or hydrogen oxidizers that use oxygen or oxidized nitrogen species as electron acceptors. Thaumarchaeota, ammonium-oxidizing representatives, was the only phylum of archaea identified. On the speleothems, organisms were detected that could be involved in the nitrogen cycle within the biofilm by denitrification, dissimilatory nitrate reduction to ammonium (DNRA) and nitrite oxidation. In addition, the family Anaerolineaceae, heterotrophic fermentative bacteria, was strongly represented. It was concluded that the processes of denitrification and autotrophy mediate calcite precipitation within the biofilm on the speleothem surface. In detail, DNRA conducting organisms could feed autotrophic nitrifying species. The produced nitrate may serve as oxidant for denitrifying representatives. Furthermore, it was hypothesized that the physical characteristics of the biofilm EPS could favor calcite precipitation (Stinnesbeck et al., 2018).

However, in the analysis described, the entire diversity of the water column and biofilm on the speleothems was analyzed as a whole. Considering the many different sub-epitopes of the cenote, it becomes clear that these niches and their microbial ecology must be analyzed separately in order to make a water zone-specific statement about the growth of calcite speleothems. This is especially true for the redoxcline, which Ritter et al. (2019) shortly after identified as the Hells Bells growth zone, and the biofilms on the speleothems that reach into this zone.

The 1–2 m thick redoxcline as Hells Bells growth zone is characterized by strong converging gradients of oxidized and reduced chemical species, which in turn leads to a vertical redox gradient. This implies that growth does not occur in the entire 10 m thick zone (28–38 m) where Hells Bells are found, but only within the narrow layer of the redoxcline. Since the hydrogeochemical water analyses showed that the concentration of oxygen already falls below the detection limit at the upper edge of the redoxcline, anaerobic processes should

dominate in this water layer. Based on the hydrogeochemical data, Ritter et al. (2019) and Ritter (2020) concluded that in addition to autotrophy, a proton-consuming process with nitrate as the electron acceptor and hydrogen sulfide as the electron donor could be the key process involved in Hells Bells growth. This assumption was supported by the fact that the concentrations of nitrate and hydrogen sulfide are consumed in the redoxcline at the same water depth. In addition, particulate sulfur was detected in water filtrates of the redoxcline, supporting the assumption that sulfur oxidation stops after the production of elemental sulfur instead of sulfate. The reason for the incomplete oxidation is the predominant electron-acceptor limitation in the central redoxcline. Such a process, summarized as chemolithoautotrophic nitrate-driven sulfide oxidation, would explain the local pH shift towards alkalinity and finally calcite supersaturation, which was only detected in the redoxcline (Ritter, 2020; Ritter et al., 2019).

Ritter et al. (2019) and Ritter (2020) explained why Hells Bells nevertheless exist in a range of 10 m by the fact that the water column of the cenote El Zapote is exposed to periodic hydraulic changes that result in a rise or fall of the halocline and thus of the redoxcline. In short, droughts lead to a reduction of the freshwater body and thus to an elevation of the underlying halocline. In contrary, recharge events and enormous rain fall mediate the lowering of the halocline and thus of the zone of calcite precipitation. Therefore, the position of the halocline is subject to a certain dynamic driven by annual tidal fluctuations and periods of droughts, and recharge events. The halocline responds to these changes in different time frames (Ritter, 2020; Ritter et al., 2019).

At cenote Angelita devoid of Hells Bells, the water column has been found to be less stagnant and to show a higher degree of advection (Ritter, 2020). According to the hydrogeochemical analyses, the redoxcline therefore does not seem to be as oxidant-deficient as in El Zapote. Instead of an incomplete anaerobic sulfide oxidation as in El Zapote (with Hells Bells), the aerobic complete oxidation of hydrogen sulfide to sulfate was identified as the major microbial metabolic activity. This process results in a negative pH shift and thus inhibition of calcite precipitation and speleothem development (Ritter, 2020).

After Stinnesbeck et al. (2018) hypothesized that the biofilm plays a central role in Hells Bells growth, the assumption by Ritter et al. (2019) followed that calcite precipitation and thus speleothem development is controlled by the planktonic phase of the redoxcline. Lately,

another hypothesis evolved. López-Martínez et al. (2020) stated the growth of Hells Bells is an abiotic mechanism based on the fact that no mineralized microbes or a stromatolitic structure were found as an indication of the involvement of microbes in calcite precipitation. Hells Bells were interpreted as folia (speleothems resembling, among others, the shape of inverted cups), which grow by calcite precipitation that occurs around carbon dioxide bubbles that are trapped at overhangs of the cave walls (López-Martínez et al., 2020). These controversial opinions underline that the formation mechanism of the speleothems is very complex. The influence of microbiology has been discussed intensively, even though no targeted, water zone-specific analysis of the microbial ecology has yet been conducted (beyond the diversity analysis of Stinnesbeck et al. (2018)). It is precisely this gap that this work aimed to fill.

1.4   Aim of this thesis

In order to understand the origin of the Hells Bells speleothems, a holistic study of the microbial ecology of cenote El Zapote was supposed to be conducted. A major focus was on the identification of the microbial key players and their metabolic activity in the hydrogeochemical gradients of the redoxcline (and overlapping turbid layer), the water zone that was identified as the zone in which Hells Bells grow (Ritter et al., 2019). Hence, the first leading question of this work was whether and, if so, to what extent the microbial diversity of the redoxcline differs from the adjacent water layers. Therefore, a comparative 16S rRNA-based analysis of the microbial diversity in the freshwater, redoxcline, halocline and biofilms on Hells Bells in the freshwater and redoxcline was conducted.

In the next step, the dominant microbial metabolic pathways should be determined in a metagenomic and -transcriptomic analysis to figure out whether the microbial community is indeed involved in Hells Bells development and which process is the crucial one to facilitate microbially induced calcite precipitation. Besides the planktonic phase, the role of the biofilm on the speleothems in the redoxcline was supposed to be addressed.

Having deciphered the microbial key players and the mechanism that is associated with calcite precipitation in the redoxcline and turbid layer of cenote El Zapote, the question arises as to what distinguishes cenote El Zapote with Hells Bells from other cenotes that also exhibit a turbid layer but no Hells Bells. In this context, cenote Angelita, which meets exactly these

criteria, was chosen for a comparative metagenomic and metatranscriptomic study to the redoxcline of El Zapote. This analysis aimed for a deeper understanding of the biogeochemical interplay in redoxclines and defining key controlling factors that regulate the growth of Hells Bells speleothems.

Based on the bioinformatic results, the involvement of the identified key microbial metabolic pathway in calcite precipitation in cenote El Zapote should be verified on a laboratory scale. Using microfluid chip systems, the conditions in the redoxcline were simulated in a very simplified manner. With this experiment, based on a biological duplicate and an abiotic control, it should be demonstrated that calcite precipitation occurs only through the identified microbially catalyzed key process. These results could provide significant support for previous hypotheses on the microbial contribution to calcite precipitation in the redoxcline of El Zapote.

Based on the findings on the microbial ecology in the redoxcline of El Zapote, a subproject evolved that focused on the cultivation of previously uncultivable microorganisms. Although at first glance this topic is not related to calcite precipitation in redoxclines, a closer look reveals that a redoxcline represents exactly the environment where highly niche-adapted organisms live. It is assumed that 99 % of all microbial species cannot yet be isolated, as they are part of consortia and do not grow axenically. Another factor is that it is very challenging to mimic complex environmental conditions during enrichments. In this work, attempts were made to isolate the identified microbial key player in the redoxcline of El Zapote using standard enrichment methods, but without success. In this context, the aim was therefore to establish a bioinformatically derived, antibody-based isolation workflow for the targeted isolation of organism from complex environmental niches. For this purpose, the redoxcline of El Zapote represents a complex environmental matrix and Thaumarchaeota as the target organisms were found to be optimal candidates based on the metatranscriptome.

2 MATERIALS AND METHODS

2.1 Field studies

2.1.1 Sampling campaigns

As part of this study, the microbial communities in cenote El Zapote were sampled for the first time in the period from May 31st to June 6th, 2018. The second sampling on site was carried out from 13th to 25th of February 2020, together with the cenote Angelita devoid of speleothems.

2.1.2 Water sampling and on-site measurements

The complex water biogeochemistry of the cenotes El Zapote was studied by the research group of Prof. Isenbeck-Schröter (department of Hydrogeochemistry and Hydrogeology) from the University of Heidelberg at the same time of microbiome sampling. To generate a biogeochemical profile throughout the waterbody, the 'EXO 1 Multiparameter Sonde' (Xylem Analytics, Norway. Fig. 7 B) was used that measures multiple *in-situ* parameters simultaneously: the pH (±0.1; relative accuracy ±0.01), dissolved oxygen (DO; ±0.1 mg l^{-1}, detection limit 0.1 mg l^{-1}), electrical conductivity (±0.05 % of value), redox potential (±20 mV), temperature (±0.01 °C), turbidity (±2 % of value), and water depths. Subsequently, the respective water depth values were corrected according to the air pressure and to the increasing salt concentration towards the halocline (below 36 m). To the peak of the debris mound (0-36 m), all measurements and sample collections were conducted from the surface via a winch-operated system (Fig. 7 A). The EXO 1 sonde was coupled with the FreeFlow bottle (HydroBios Kiel), which was used for sample collection, to simultaneously detect the corresponding hydrogeochemical *in-situ* parameters and the exact water depth (Fig. 7 B). The sampling depth was set according to the depth counter of the winch. Thus, the sample depths mentioned in this work represent the center of the FreeFlow bottle.
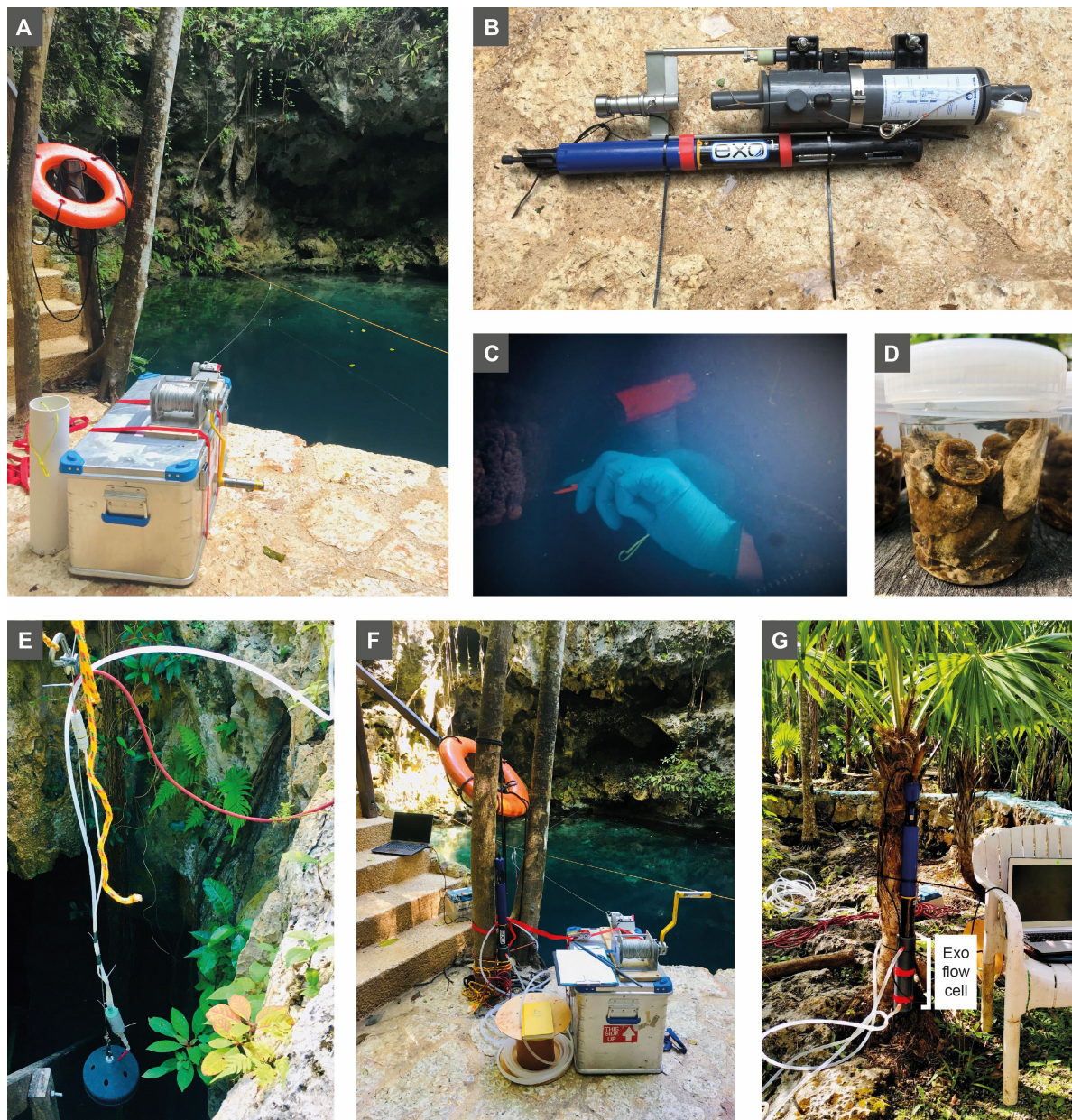
Figure 7: Sampling techniques and *in-situ* parameter measurements at the cenotes. A) In 2018, water samples were taken via an installed winch to regulate the FreeFlow bottle to the appropriate water depth for sample collection. B) The FreeFlow bottle was additionally coupled with the EXO-1 sonde to detect the *in-situ* parameters and the exact water depth for every single sample. C) Hells Bells samples for a metagenomic and metatranscriptomic analysis of the biofilm on the speleothem surface were collected by technical divers using hammer and chisel. D) The speleothem pieces were collected in sterile cups that were previously filled with water surrounding the speleothems. E) In 2020, the double cone sampling (DCS) system was used that allows water samples to be pumped from the desired water depths to the water surface without mixing with adjacent water layers. F) The sample depth for the system was set via the winch and recorded via a CTD logger. The pumped water then passed through the flow cell, where the EXO-1 probe measured the *in-situ* parameters above ground instead of underwater. Foto C) by Dirk Penzel (2020), all others by Kerstin Leberecht (2020).

From 36 to 52 m, the EXO 1 probe was directed through the deeper water zones by technical divers to create a water profile (for more information see Ritter, 2020). The halocline and saltwater were sampled by the technical divers using sterile polyethylene syringes (140 ml) connected to a three-way port. During sample collection, the technical divers carried the EXO 1 sonde attached to the mounted gas bottle to allow the detection of the water depth and *in-situ* parameters.

In 2020, the sampling of the water column of cenote Angelita and El Zapote was conducted with an optimized system. Whereas in 2018, water samples were collected via the FreeFlow bottle, a double cone sampling (DCS) system was used, which pumps water only from the side and thus allows sampling of very define stratified water layers or along gradients without interference with other surrounding water layers (Fig. 7 E and F). The pumped water (flow rate 500 ml min^{-1}) was then transferred through a connected pipe system to the water surface and further through the flow cell of the EXO 1 (Fig. 7 G) that was used for above ground *in-situ* parameter measurements of the water pumped from the respective water depth. The water depth was determined by a CTD-Logger that was combined with the DCS system. For more information on the DCS system, see Eschenröder (2020; unpub.).

For a detailed description of sample handling and hydrogeochemical analyses after sampling see Ritter (2020) for samples from El Zapote and Eschenröder (2020; unpub.) for samples from cenote Angelita.

2.1.3 Microbiome sampling

In 2018, the complex water body of the cenote El Zapote was sampled along the biogeochemical gradients to characterize the different sub-biotopes and its diverse microbial communities. Water samples were taken from the freshwater (sampled at 32 m), the central redoxcline (sampled at 35.8 m) and the halocline (sampled at 38 m). Except for the halocline, all other samples were collected using a winch-operated 1 L polyethylene FreeFlow bottle (HYDRO-BIOS, Kiel, Germany). Water samples from the halocline had to be collected by technical divers as the peak of the debris mound limits the accessibility of the deeper waters (below 36 m water depth). For the investigation of the biofilm on the Hells Bells surface and its potential role in speleothem formation, Bell material was also collected from the central redoxcline (35.8 m) and freshwater (32 m) by technical divers. Samples of the speleothems

(5 pieces) were collected and transferred to the surface in sterile 50 ml cups filled with water of the respective water layer.

For the planktonic microbiome samples, 200 ml of collected water from the respective water zone were immediately filtered through a MCE membrane filter (0.22 µm; Merck KGaA, Darmstadt, Germany) on site. Subsequently, filters as wells as the collected Bell material were then preserved in Allprotect Tissue Reagent (for later DNA analyses) or RNAprotect Bacteria Reagent (for metatranscriptomic samples) (Qiagen, Hilden, Germany). Cooling at 4 °C was ensured from the time of sampling through the sample transport to the laboratory to stabilize DNA/RNA until long time storage at -80 °C and further analysis. For 16S rRNA-based diversity analyses, biological duplicates were taken. The metagenomic and -transcriptomic data from the planktonic microbiome of the redoxcline of El Zapote are based on one sample set that was sequenced with high depth due to limited possibilities to retrieve the samples with technical divers.

For cenote El Zapote, the main goal in 2020 was to successfully collect sufficient RNA material from the Hells Bells biofilm for metatranscriptome sequencing, which was not possible with the limited sample material from 2018. Therefore, technical divers took much more speleothem material (filling two 250 ml cups) from several Bells in the center of the redoxcline (which was at 34.95 m in 2020) using hammer and chisel and collected them in sterile cups filled with ambient redoxcline water (Fig. 7 C and D). This time, the Hells Bells surface was fastly and extensively scraped with a sterile scalpel on site (B. Braun Melsungen AG, Melsungen, Germany) and the extracted material was immediately conserved in Allprotect Tissue Reagent/RNAprotect Bacteria Reagent and stored at 4 °C.

Beside the cenote El Zapote, cenote Angelita (without Hells Bells) was also studied during the sampling campaign in 2020. At site, the planktonic microbiome samples were collected from the central redoxcline using the DCS system. At cenote Angelita, the respective sampling depth was 29.9 m. Otherwise, the samples were treated as described above for samples from El Zapote.

2.2 Laboratory experiments

2.2.1 Chemicals, materials and kits

If not mentioned otherwise, chemicals and biochemicals used in this work were purchased from Qiagen (Hilden, Germany), Sigma-Aldrich (Steinheim, Germany), Bioline (Luckenwalde, Germany), New England Biolabs (Frankfurt am Main, Germany), Carl Roth GmbH & Co. KG (Karlsruhe, Germany), AppliChem (Darmstadt, Germany), and Thermo Scientific (Karlsruhe, Germany).

2.2.2 Microorganisms

In the following table (Table 1) all microorganisms relevant for this work are listed, including the official strain number of the German Collection of Microorganisms and Cell Cultures (DSM).

Table 1: Strains used in this work in pure culture.

Species (strain number)	DSM No.	Strain	Reference
Thiobacillus denitrificans	12475, Type strain	AB7	(Kelly & Wood, 2000)

2.2.3 Primers

In the following table (Table 2) a list of all primers used in this study is provided. The primer synthesis was conducted by Sigma-Aldrich (Steinheim, Germany).

Table 2: List of all primers used in this study.

Primer name	Primer sequence (5'→3')	Purpose
A519F	CAGCMGCCGCGGTAA	Degenerated forward primer for the detection of 16S rRNA genes of archaea for Illumina amplicon sequencing
A906R	CAATTCMTTTAAGTTTC	Degenerated reverse primer for the detection of 16S rRNA genes of archaea for Illumina amplicon sequencing
Bact_341F	CCTACGGGNGGCWGCAG	Degenerated forward primer for the detection of 16S rRNA genes of bacteria for Illumina amplicon sequencing
Bact_805R	GACTACHVGGGTATCTAATCC	Degenerated reverse primer for the detection of 16S rRNA genes of bacteria for Illumina amplicon sequencing
Pro341F	CCTACGGGNBGCASCAG	Degenerated forward primer for the detection of 16S rRNA genes of both bacteria and archaea (for Nanopore sequencing)
Universal_1492rev	GGTTACCTTGTTACGACTT	Degenerated reverse primer for the detection of 16S rRNA genes of both bacteria and archaea (for Nanopore sequencing)
Arch-amoAF	STAATGGTCTGGCTTAGACG	Forward primer for the detection of *amoA* genes of archaea
Arch-amoAR	GCGGCCATCCATCTGTATGT	Reverse primer for the detection of *amoA* genes of archaea

2.2.4 Media

All buffers, solutions and media were prepared with deionized water from an ultrapure water system (TKA Micropure, TKA, Niederelbert, Germany) and, if necessary, autoclaved (Systec VE-150, Systec, Wettenberg, Germany) or sterilized by filtration (Filtropur S 0.2 μm, Sarstedt, Nümbrecht, Germany).

Design of Thaumarchaeota medium

To culture Thaumarchaeota from water samples of the upper redoxcline (taken during the sampling campaign 2020), a minimal medium (hereafter referred to as Thaumarchaeota medium; Table 3) was derived from the *in-situ* parameters (see Fig. 9). The anion/cation concentrations 1.5–2 m above and below the upper redoxcline, respectively, were considered. In line with other studies on Thaumarchaeota enrichments (such as Jung et al., 2011; Könneke et al., 2005; Sauder et al., 2017), the non-chelated trace element solution, the selenite-tungstate solution and vitamin mix were taken from Widdel (1992).

Table 3: Components of the self-compiled Thaumarchaeota medium.

Thaumarchaeota medium	
Component	**Amount/Volume**
KH_2PO_4	54 mg
KCl	74 mg
$MgSO_4$ x 7 H_2O	49 mg
NaCl	548 mg
$CaCO_3$ (will stay as precipitate)	2.5 g
Cresol red stock solution (as pH indicator; 47 mg in 100 ml ddH_2O)	2 ml
ddH_2O	Ad 1000 ml

After the medium was autoclaved, the excess calcium carbonate was removed, and the medium was complemented according to Table 4.

Table 4: Supplements for 1 L Thaumarchaeota medium.

Nonchelated trace element mixture (Table 5)	1 ml
Vitamin mixture (Table 6)	1 ml
Selenite-tungstate solution (Table 7)	1 ml
NH_4Cl solution (1 M)	20 µl

Subsequently, the pH of the medium was adjusted to pH 6.9 by addition of sterile 10 % HCl.

Table 5: Components of the non-chelated trace element mixture from Widdel (1992) used for the Thaumarchaeota medium.

Non-chelated trace element mixture	
Component	**Amount/Volume**
HCl (25 %, 7.7 M)	12.5 ml
$FeSO_4$ x 7 H_2O	2100 mg
H_3BO_3	30 mg
$MnCl_2$ x 4 H_2O	100 mg
$CoCl_2$ x 6 H_2O	190 mg
$NiCl_2$ x 6 H_2O	24 mg
$CuCl_2$ x 2 H_2O	2 mg
$ZnSO_4$ x 7 H_2O	144 mg
Na_2MoO_4 x 2 H_2O	36 mg
ddH_2O	987 ml

Table 6: Components of the vitamin mixture from Widdel (1992) used for the Thaumarchaeota medium.

Vitamin mixture	
Component	**Amount/Volume**
Sodium phosphate buffer (10 mM; pH 7.1)	100 ml
4-Aminobenzoic acid	4 mg
D(+)-Biotin	1 mg
Nicotinic acid	10 mg
Calcium D(+)-pantothenate	5 mg
Pyridoxine dihydrochloride	15 mg

Table 7: Components of the selenite-tungstate solution from Widdel (1992) required for the Thaumarchaeota medium.

Selenite-tungstate solution	
Component	**Amount/Volume**
NaOH	0.4 g
Na_2SeO_3 x 5 H_2O	6 mg
Na_2WO_4 x 2 H_2O	8 mg
ddH_2O	ad 1000 ml

The trace element and selenite-tungstate solutions were autoclaved once, the vitamin mixture was filter-sterilized.

Design of redoxcline medium

To proof microbially induced calcite precipitation under *in-vitro* conditions (see section 2.2.6 for the description of the experiment), a minimal mineral medium (called redoxcline medium (Table 8)) saturated with calcium carbonate, sulfide as electron donor and nitrate as electron acceptor was designed to mimic the water chemistry of the redoxcline. The ratio of electron donor (sulfide) to acceptor (nitrate) was taken into account (10:1), and the applied concentrations corresponded to the respective measured availability one meter above or below the center of the redoxclines (Fig. 9; 0.2 mM sulfide, 0.02 mM nitrate). The pH was adjusted to ~6.9 according to the pH in the central redoxcline.

Table 8: Composition of the self-compiled redoxcline medium derived from El Zapote.

Redoxcline medium	
Component	**Amount/Volume**
KH_2PO_4	1 mg
NaCl	0.58 g
NH_4Cl	0.2 g
KNO_3	20 mg
$CaCO_3$ (will stay as precipitate)	3.5 g
Distilled water	ad 1000 ml

After sterilization by autoclaving, the medium was transferred in a sterile flask without the undissolved calcium carbonate. Subsequently, the medium was complemented with 2 ml of Trace element solution SL-4 (Table 10) and a final sulfide concentration of 0.2 mM (from a sterile-filtered 10x stock of Na_2S x 9 H_2O) was set. Subsequently, the pH was adjusted to 6.9.

Thiobaciullus denitrificans medium

The *Thiobacillus denitrificans* medium was used for precultures of *T. denitrificans*. The composition is shown in Table 9.

Table 9: Composition of the *Thiobacillus denitrificans* medium.

Thiobacillus denitrificans medium (DSMZ medium 113)	
Component	**Amount/Volume**
Solution A (pH 7.0, adjusted with NaOH)	
KH_2PO_4	2 g
KNO_3	2 g
NH_4Cl	1 g
$MgSO_4$ x 7 H_2O	0.8 g
Trace element solution SL-4 (Table 10)	3.5 g
Distilled water	ad 960 ml
Solution B	
$Na_2S_2O_3$ x 5 H_2O	5 g
ddH_2O	20 ml
Solution C	
$NaHCO_3$	1 g
ddH_2O	20 ml
Solution D	
$FeSO_4$ x 7 H_2O	2 mg
0.1 N H_2SO_4	1 ml

Except for solution C, which was sterilized by filtration and gassed with N_2/CO_2 (80 %:20 %) (v/v), all solutions were gassed with N_2 and sterilized by autoclaving.

Table 10: Composition of the trace element solution SL-4 required for the *T. denitrificans* medium.

Trace element solution SL-4 (DSMZ medium 14)	
Component	**Amount/Volume**
Na_2-EDTA (dissolved first, pH 7.0)	0.5 g
$FeSO_4$ x 7 H_2O	0.2 g
$ZnSO_4$ x 7 H_2O	0.1 g
$MnCl_2$ x 4 H_2O	0.03 g
H_3BO_3	0.3 g
$CoCl_2$ x 6 H_2O	0.2 g
$CuCl_2$ x 2 H_2O	0.01 g
$NiCl_2$ x 6 H_2O	0.02 g
Na_2MoO_4 x 2 H_2O	0.03 g
ddH_2O	ad 1000 ml

2.2.5 Antibody-based isolation approach for Thaumarchaeota

In the context of this work, the development of an isolation method for so far uncultivable microbes was aimed. The procedure is based on magnetic beads coupled with a secondary antibody and a primary antibody that binds the antigen on the cell surface of the target cells to be isolated (see Fig. 30). In the first step, the magnetic beads with bound secondary antibodies are incubated with the primary antibody. The cell sample (from which the cells are to be isolated) is then added to the antibody-bead complex. After an incubation period, the cells of interest were supposed to be separated via magnetic separation over the antibody-bead-cell complex.

Thaumarchaeota from the redoxcline of El Zapote were used as an exemplary enrichment target. First, the highly expressed S-layer proteins of Thaumarchaeota were studied in detail and a suitable epitope was selected as a starting point for an antibody-based isolation method (see section 2.6.3). Subsequently, a medium was designed that mimics the conditions in the upper redoxcline and meets previously known cultivation requirements of Thaumarchaeota (section 2.2.4). In this medium the cells should be transferred after isolation.

For the isolation of Thaumarchaeota goat-anti rabbit IgG magnetic beads (New England Biolabs, Frankfurt am Main, Germany) and the costume primary antibody against the selected Thaumarchaeota S-layer protein (hereafter referred to as rabbit anti-T-SL) was used. The isolation procedure was conducted according to the protocol shown in Table 11, which includes several adjustments (see description in section 3.5). Most steps were performed at 24 °C, which corresponds to the temperature in the upper redoxcline.

Table 11: Protocol of the antibody-based pulldown method for the isolation of Thaumarchaeota.

Antibody-based pulldown method		
Step	**Details**	**Repeats, Temperature**
Concentrating the cell community	12 ml Redoxcline sample, 12,000 g, 10 min	4 °C
Resuspension	in 6 ml Thaumarchaeota medium	24 °C
Washing magnetic beads	100 µl goat-anti rabbit IgG magnetic beads in 2 ml 1x PBS	3x; 24 °C
Magnetic separation	-	24 °C
Binding primary antibody	Resuspension in 2 ml 1x PBS; Addition of primary rabbit anti-T-SL (ratio of 2:1 of primary:secondary antibody); Incubation for 2 h on Hula-Mixer	24 °C
Magnetic separation	-	24 °C
Washing magnetic beads for removal of unbound primary antibody	With 2 ml 1x PBS	4x; 24 °C
Magnetic separation	-	24 °C
Incubation with cells of interest	Resuspension of magnetic bead pellet with the 6 ml of cell suspension; Incubation for 4 h on Hula-Mixer	24 °C
Magnetic separation	Cells of interest are bound to the antibody-bead complex	24 °C

2.2.6   Proof of microbially induced calcite precipitation on the laboratory scale

In order to demonstrate calcite precipitation by the identified key process in the El Zapote redoxcline, nitrate-driven sulfide oxidation, on a laboratory scale, the conditions in the redoxcline were mimicked in a very simplified manner using microfluidic chips systems.

The characteristics of the microfluidic meandric chip systems is given in Hansen et al. (2019). The base area of the meandric chips was 76 x 26 mm, which corresponds to the standard size of microscopy slides. The cultivation channel had a volume of ~150 µl. For the fabrication of polydimethylsiloxane (PDMS) chips, the basic component (Sylgard 184 Silicone Elastomer Kit (Dow Corning, Michigan, USA)) was prepared according to the manufacturer's instructions. The PDMS mixture was transferred into brass replication molds and placeholder cannulas (Sterican, B. Braun Melsungen AG, Germany) were inserted into the molds to provide space for later connecting cannula channels. Subsequently, the chips were solidified for 3 h at 60 °C. In the next step, using oxygen plasma treatment (Plasma Flecto 10; Plasma Technology, Herrenberg, Germany) the PDMS chips were bonded to a glass cover slide, thereby closing the meandric cultivation channel. The plasma treatment protocol included the following steps: lowering of the system pressure to 0.2 mbar; stabilization for 15 s; plasma treatment for 30 s; ventilation for 15 s. Subsequently, the covalent bonds were strengthened by incubation at 100 °C for 20 min.

The setup of the chip-based cultivation environment was adapted to provide anoxic conditions. Two meandric chips were connected in line (Fig. 8). An upstream gassing chip was connected in order to allow anaerobic conditions in the downstream cultivation chip. Both chips were gassed with N_2 (Tyczka Industrie-Gase GmbH, Mannheim, Germany) via viton tubing (Carl Roth, Karlsruhe, Germany) to create anaerobic conditions. While the first chip only had access points for medium inflow and outflow, the cultivation chip also had an inlet point for inoculation at the first meander. For sterilization, all components of the setups, except for the three-way ports, were autoclaved. The redoxcline medium was filled into sterile 50 ml syringes (B. Braun Melsungen AG, Germany). Medium supply was achieved by syringe pumps (Nexus3000, Chemyx, Stafford, USA) that continuously delivered medium to the chips via silicone tubing (Carl Roth, Karlsruhe, Germany), three-way ports (BD

Connecta; Medi-KS Berlin Gmbh, Germany) and cannulas (B. Braun Melsungen AG, Germany) (Fig. 8 A). The gassing and cultivation chips were connected via a cannula.
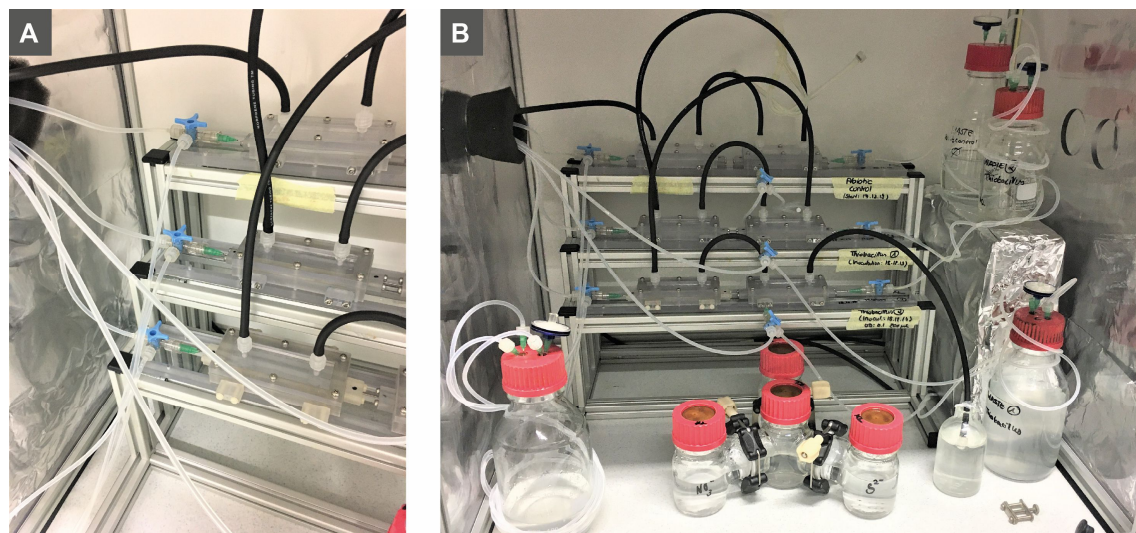
Figure 8: Setup of three microfluidic meandric chip systems for the evaluation of microbially induced calcite precipitation by nitrate-driven sulfide oxidation. A) Redoxcline medium was introduced into the front gassing chip via a syringe pump. B) Both the gassing and cultivation chips were gassed with N_2 via viton tubings (black). A duplicate of chips inoculated with *Thiobacillus denitrificans*, as well as an abiotic control were incubated for four weeks at 25 °C.

In total, 3 chip setups were installed, a biotic duplicate of chips inoculated with *T. denitrificans* together with an abiotic control. For inoculation, a pre-culture (48 h at 30 °C, 180 rpm) of *T. denitificans* in the respective medium (Table 9) was centrifuged (16,000 g, 5 min, 4 °C) and the cell pellet was washed two times with redoxcline medium (Table 8). The cell suspension was adjusted to an optical density of 0.1. Using syringe pumps, inoculation occurred at a flow rate of 0.1 ml min^{-1} and with a simultanous medium flow rate of 0.4 ml min^{-1} for 4 h. Subsequently, the medium flow rate was set to 0.5 ml min^{-1}. The whole experimental setup was incubated at 25 °C and operated for four weeks.

Microscopic images were taken after four weeks of cultivation using a Leica microscope type DM5500B (Leica Microsystems GmbH, Wetzlar, Germany) through a 10× bright field objective.

2.3 Molecular biological methods

2.3.1 DNA/RNA extraction

After sampling, during which the microbial cells were concentrated by filtering the cenote water, the filters were first washed with 1x PBS to carefully remove the viscous Allprotect Tissue Reagent (Qiagen, Hilden, Germany). The subsequent DNA isolation from cells on the filters was performed with the DNeasy PowerWater Kit. The DNA was finally eluted in 50 μl of nuclease-free water at room temperature and stored at -20 °C.

Similar procedures were applied to the biofilm samples. Hells Bells samples collected during the sampling in 2018 were stored in Allprotect Tissue Reagent. To this end, the first step was to wash the speleothem pieces in 1x PBS to remove the reagent. Subsequently, the surface of the speleothem pieces was extensively scraped with a sterile scalpel and the material was then processed with the DNeasy PowerBiofilm Kit (Qiagen, Hilden, Germany) according to the manufacturer's instructions. The mechanical cell disruption step included in this protocol was performed with the cell mill Mixer Mill 400 (Retsch, Haan) for 7 minutes at 30 Hz. DNA was then eluted with 50 μl of nuclease-free water. After the second sampling campaign in 2020, when much more Hells Bells material was collected, the scraping step was already performed directly on site. The subsequent purification was also conducted with the RNeasy/DNeasy PowerBiofilm Kit.

For the samples from cenote El Zapote (from 2018), the isolation of RNA was conducted by the sequencing company IMGM Laboratories GmbH (Martinsried, Germany) using the RNeasy PowerWater Kit (Qiagen, Hilden, Germany). This was not the case for the samples of cenote Angelita and the Hells Bells Biofilm from cenote El Zapote from the second sampling campaign. Instead, isolation of RNA from cenote water and biofilm samples was performed in the laboratory in an analogous way to DNA isolation using the same kits and protocols. Isolated RNA was eluted in nuclease-free water at room temperature and stored at -20 °C. Due to the very limited yield of total RNA, no rRNA depletion was conducted for any samples.

2.3.2   Quantification of nucleic acid concentrations and purity

For both DNA and RNA, sample concentrations and their purity were determined using a NanoDrop ND-1000 spectrophotometer (Thermo Scientific, Waltham, Massachusetts). For this application, 1 μl of the DNA/RNA sample was loaded and measured photometrically at 260 nm. Prior to sequencing of metagenomes or metatranscriptomes, a more accurate quantification of the double-stranded DNA was conducted using a Qubit dsDNA HS Assay Kit protocol (ThermoFisher Scientific, Waltham, Massachusetts). From the same manufacturer, the Qubit RNA BR Assay Kit was used for the determination of RNA concentrations. Using the Infinite M200 PRO Multimode Microplate Reader (TECAN Infinite m200 Pro, Tecan Trading AG, Schweiz), fluorescence intensity was measured at 480/530 nm for DNA and at 630/660 nm for RNA. Furthermore, the fragment length distribution was measured using a 2100 Bioanalyzer (Agilent, Santa Clara, USA) according to the High Sensitivity DNA Assay protocol. The samples were stored at -80 °C until further processing.

2.3.3   Polymerase chain reaction (PCR)

In this work, regions of the 16S rRNA and the archaeal *amoA* gene (encoding the ammonia monooxygenase subunit A) were amplified by Polymerase Chain Reaction (PCR). The primers used are listed in section 2.2.3, together with the respective primer sequences. Purified genomic DNA or (in the case of Thaumarchaeota) cell pellets were used as templates. Thaumarchaeota cells in planktonic culture or cenote water were centrifuged (16,000 g, 5 min, 4 °C) before PCR, and the resulting pellet was treated in an ultrasonic bath for 25 s and incubated at 95 °C for 5 min.

For an analytical PCR, MangoMix (Bioline, Luckenwalde, Germany) was used as a PCR approach containing all components (Mango*Taq* DNA Polymerase, red and orange reference dyes and 3 mM MgCl, dNTPs) except of the template DNA and primers (Table 12). The respective polymerase has an error rate of about 10^{-4} per bp and was therefore only used if no amplicon sequencing followed. For a preparative approach, a polymerase with proofreading function was used (Table 13), which significantly reduces the error rate during amplification ($\sim 2.2 \times 10^{-8}$ per bp). In this work, the PCRBIO HiFi DNA Polymerase (PCR Biosystems, London, UK) was applied according to the manufacturer's instructions.

Table 12: Standard reaction (50 µl) for analytical PCRs using MangoMix.
(*For the amplification of the *amoA* gene, a higher amount of template was added).

MangoMix standard reaction	
Component	**Volume**
2x MangoMix	25 µl
Forward Primer (10 µM)	1.25 µl
Reverse Primer (10 µM)	1.25 µl
Template	1 µl/5 µl*
ddH$_2$O	Up to 50 µl

Table 13: Standard reaction (50 µl) for preparative PCRs using the PCRBIO HiFi Polymerase.

PCRBIO HiFi Polymerase standard reaction	
Component	**Volume**
5x PCRBIO Reaction Buffer (incl. dNTPs)	25 µl
Forward Primer (10 µM)	2 µl
Reverse Primer (10 µM)	2 µl
Hifi Polymerase	0.5 µl
DMSO	1 µl
Template	1 µl
ddH$_2$O	Up to 50 µl

For amplification, the PCR reactions were incubated in a thermocycler (S1000, BioRad, Munich, Germany), according to the following programs (Tables 14 and 15):

Table 14: Thermocycler program for the amplification of *amoA* according to Francis et al. (2005).

Temperature [°C]	Time [min]		PCR step
95	5:00		Initial denaturation
94	0:45		Denaturation
53	1:00	35–45 x	Annealing of primers
72	1:00		Elongation
72	15:00		Final elongation
12	∞		Cooling

Table 15: Thermocycler program for the amplification of the 16S rRNA gene (for amplicon sequencing) using the PCRBIO HiFi Polymerase.

Temperature [°C]	Time [min]		PCR step
95	5:00		Initial denaturation
95	0:15		Denaturation
Primer-specific annealing temp. (56 Bacteria and universal primers; 50 Archaea primer)	30 s per kb	30 x	Annealing of primers
72	0:20		Elongation
72	10:00		Final elongation
12	∞		Cooling

2.3.4 Whole genome amplification

To determine an enrichment factor after the antibody-based isolation of Thaumarchaeota, the abundance of Thaumarchaeota before and after the isolation method procedure were supposed to be compared. Due to the very limited number of cells, a total DNA amplification was conducted. To this end, the EquiPhi29 DNA Polymerase (Thermo Fisher Scientific, Waltham, USA) was used according to the manufacturer's instructions.

Before the amplification, DNA was denatured in a 5 µl mix of nuclease-free water, 100 µM of exo-resistant random primers (Thermo Fisher Scientific, Waltham, USA) and EquiPhi29 Reaction buffer. The DNA sample was heated at 95 °C for 3 min and subsequently cooled for 5 min. The DNA was then added to the amplification reaction mixture (Table 16).

Table 16: Standard reaction (20 µl) for DNA amplification using the EquiPhi29 DNA Polymerase.

EquiPhi29 DNA Polymerase standard reaction	
Component	**Volume**
10x Reaction Buffer	1.5 µl
dNTP Mix 10 mM each (New England Biolabs)	2 µl
DTT (100 mM)	0.2 µl
Denatured DNA	5 µl
EquiPhi29 Polymerase (10 U/µl)	1µl
Nuclease-free water	Ad 20 µl

For the isothermal amplification, the reaction was incubated at 45 °C for 3 h and subsequently inactivated at 65 °C for 10 min.

2.3.5   Agarose gel electrophoresis and PCR product purification

For separation by size, visualization and purification, DNA fragments from PCR preparations were subjected to gel electrophoresis. To prepare a 1 % (w/v) agarose gel, the TAE buffer-agarose mixture was boiled and subsequently 0.6 µg/ml FastGene Midori Green Direct (Nippon Genetic, Dueren, Germany) were added and the entire mixture was transferred into gel chamber in which placeholders for pockets were inserted. After polymerization, the gel was inserted into the gel electrophoresis chamber filled with TAE buffer (Table 17). The PCR samples were mixed with 6x DNA Loading dye (Thermo Fisher Scientific, Waltham, USA) and transferred into the preformed pockets. If the PCR reactions were based on the MangoMix, which already contains the loading buffer, this step was not required. As a DNA size standard marker, the GeneRuler 1 kb DNA ladder (Thermo Fisher Scientific, Waltham, USA) was used for each run to allow the determination of a relative DNA fragment size. Fragment separation occurred by applying a voltage of 120 V using a Powerpac HC (BioRad, Munich, Germany).

The evaluation of the gels was conducted using a ChemiDoc XRS+ (Bio-Rad Laboratories GmbH, Munich, Germany) and the associated Image Lab 5.1 software.

To purify individual fragment bands from a preparative PCR, fragments in the gel were detected on a FastGene Blue/Green transilluminator (Nippon Genetics, Dueren, Germany) and isolated with a scalpel. These gel pieces were subsequently processed using the Wizard SV Gel and PCR Clean-Up System (Promega, Mannheim, Germany) according to the manufacturer's instructions. The purified DNA was finally eluted in 30 µl of nuclease-free water at room temperature and stored at -20 °C.

Table 17: Composition of 1x TAE buffer. (The pH of Tris-HCl was adjusted with acetic acid).

1x TAE buffer		
Component	**Amount [g/l]**	**Concentration**
Tris-HCl, pH 8	4.85	40 mM
EDTA	0.37	1 mM

2.4 Protein biochemical techniques

2.4.1 Sodium dodecyl sulfate polyacrylamide gel electrophoresis (SDS-PAGE)

In order to obtain an analytical separation of proteins according to their molecular weight, discontinuous SDS-PAGE (Laemmli, 1970) was conducted for Thaumarchaeota-containing cell lysates.

For the preparation of cell lysates, 50 ml of Thaumarchaeota-containing freshwater and samples from the upper redoxcline of cenote El Zapote were centrifuged at 12,000 g for 15 min at 4 °C. For protein denaturation, the cell pellet was resuspended in 25 µl protein buffer, supplemented with 5 µl 6x SDS Loading buffer and subsequently, the samples were incubated at 95 °C for 5 min. Heat, SDS and the β-mercaptoethanol included in the loading buffer promote the disruption of the tertiary and secondary protein structure. Furthermore, SDS in turn allows the separation of the proteins along the electrical field by providing proteins with a negative net charge.

The separation of the denatured proteins occurred via the application of a voltage of 120 V (Powerpac HC, Biorad). The polymerized gel matrix consisted of a separating gel and a stacking gel. The gels were covered with Running buffer and loaded with the corresponding

samples and a reference protein marker (BlueStar Prestained Protein Marker, Nippon Genetics). All buffers relevant for this method are listed in Tables 18–21.

Table 18: Components of a Separating gel (12 % acrylamide (w/v)).

Separating gel (12 %)		
Component	**Composition**	**Volume**
ddH$_2$O	-	3.1 ml
Separating gel buffer	2 M Tris/HCl, pH 8.8	2.25 ml
Acrylamide solution	30 % (w/v) Acrylamid, 0.8 % (w/v) Bisacrylamide	3.6 ml
Sodium dodecyl sulfate (SDS)	20 % (w/v) in ddH$_2$O	45 µl
Tetramethylethylenediamine (TEMED)	-	9 µl
Ammonium persulfate (APS)	10 % (w/v) in ddH$_2$O	45 µl

Table 19: Components of a Stacking gel (4 % acrylamide (w/v)).

Stacking gel (4 %)		
Component	**Composition**	**Volume**
ddH$_2$O	-	4.38 ml
Stacking gel buffer	1 M Tris/HCl, pH 6.8	375 µl
Acrylamide solution	30 % (w/v) Acrylamide, 0.8 % (w/v) Bisacrylamide	3.6 ml
SDS	20 % (w/v) in ddH$_2$O	45 µl
Tetramethylethylenediamine (TEMED)	-	9 µl
Ammonium persulfate (APS)	10 % (w/v) in ddH$_2$O	45 µl

Table 20: Components of the 10x Running buffer (pH 8.8).

10x Running buffer	
Component	**Amount [g/l]**
Tris-base	30
SDS	10
Glycine	144

Table 21: Components of the 6x Loading buffer.

6x Loading buffer	
Component	**Volume**
1 M Tris/HCl, pH 6.8	1.5 ml
20 % (w/v) SDS	3.0 ml
Glycerin	5.0 ml
β-Mercaptoethanol	3.0 ml
0.5 % (w/v) Bromphenol blue	3.0 ml

2.4.2 Western Blot

After the separation of proteins according to their molecular weight, a semi-dry Western Blot was conducted to transfer the proteins from the SDS gel onto a nitrocellulose membrane. For this purpose, a layering of the following components (from the anode to the cathode) was prepared in the Trans-Blot Turbo blotting chamber (Bio-Rad Laboratories GmbH, Munich, Germany): two filter papers (Whatman GB003, GE Healthcare, Munich, Germany) fully saturated with Blotting buffer (Table 22), a nitrocellulose membrane (Carl Roth, Karlsruhe, Germany), the SDS gel containing the proteins, and finally another two filter papers fully saturated with Blotting buffer. The transfer was accomplished by applying a voltage of 13 A and 25 V for 12 min.

Table 22: Components of the Blotting buffer.

Blotting buffer	
Component	**Amount/Volume**
Tris	40 g
Glycine	20 g
Methanol	50 ml
Ethanol	150 ml
ddH$_2$O	Ad 1000 ml

2.4.3 Immunodetection

For the subsequent detection of proteins of interest, immunodetection was performed. This method involves the use of primary and secondary antibodies (see Table 23 for details), as well as a series of incubation and washing steps. For the detection of the Thaumarchaeota S-layer protein, the bioinformatically derived rabbit anti-Thaumarchaeota S-layer (anti-T-SL) antibody was used for primary detection (produced by Genscript, Leiden, Netherlands), diluted 1:1,000 in 15 ml TBS 3 % BSA. The mouse anti-rabbit antibody coupled with alkaline phosphatases (AP) (1:10,000 in 15 ml TBS, 3 % milk powder) was used as secondary antibody. Subsequent staining was performed using the AP Conjugate Substrate Kit (Bio-Rad Laboratories GmbH, Munich, Germany) according to the standard protocol. The membrane was incubated in the staining solution for 10 min to 4 h, depending on the signal strength. The signals on the nitrocellulose membrane were then detected and visualized using the ChemiDoc XRS+ system (Bio-Rad Laboratories GmbH, Munich, Germany).

Table 23: Immunodetection procedure.

Immunodetection procedure		
Step	**Buffer/solution**	**Incubation time and repeats**
Washing	1x TBS	2x 10 min
Blocking	1x TBS 3 % (w/v) milk powder	1 h-o/n
Primary Ab	1x TBS 3 % (w/v) BSA + 1:1,000 primary Ab	≥1 h
Washing	1x TBSTT	2x 10 min
Washing	1x TBS	1x 10 min
Secondary Ab	1x TBS 3 % (w/v) milk powder + 1:10,000 secondary Ab	1 h
Washing	TBS-T	4x 5 min
Washing	ddH_2O	5x 2 min
Staining	ddH_2O 11.75 ml AP detection buffer (500 µl) Color Reagent A (125 µl) Color Reagent B (125 µl)	> 10 min
Washing	ddH_2O	2 min

Table 24: Components of different washing buffers (pH 7.5) used for immunodetection.

Component	TBSTT buffer	TBST buffer	TBS buffer
Tris	20 mM	20 mM	10 mM
NaCl	500 mM	500 mM	150 mM
Triton-X100	0.2 %	-	-
Tween-20	0.05 %	0.05 %	-

2.5 Sequencing methods

2.5.1 Sanger sequencing

Sequencing of PCR products was performed using the Mix2Seq kit (MWG eurofins Genomics GmbH, Ebersberg, Germany). The respective PCR primers served as sequencing primers for sequencing according to method of Frederick Sanger (Sanger et al., 1977).

2.5.2 Illumina sequencing

In this study, Illumina sequencing was used for microbial diversity analysis via 16S rRNA gene amplicon sequencing (El Zapote) and for metagenome and metatranscriptome analysis of the redoxcline community of cenote Angelita and El Zapote.

The sequencing material were the DNA and RNA samples isolated as described in chapter 2.3.1. All samples from cenote El Zapote (from 2018), which included 16S rRNA amplicon samples, metagenomes and metatranscriptomes, were sequenced by IMGM Laboratories GmbH (Martinsried, Germany). The microbial diversity of the freshwater, redoxcline, halocline and Hells Bells biofilm in the freshwater and redoxcline were analyzed by 16S rRNA amplicon sequencing. The amplicons were generated (by the sequencing company) with the primer set Bact_341F/Bact_805R for Bacteria and A519F/A906R for Archaea (for primers, see section 2.2.3). Sequencing of these amplicons was conducted on an Illumina MiSeq platform (Illumina, San Diego, USA) with paired-end 250 nucleotide (nt) reads (PE250).

For the microbial community in the redoxcline and on the Hells Bells speleothems in the same water zone, metagenome libraries were generated with the NEBNext Ultra II FS DNA Library Preparation Kit (New England Biolabs, Frankfurt am Main, Germany).

Subsequently, the metagenome libraries were processed on the Illumina NextSeq 500 platform (Illumina, San Diego, USA) with paired-end 150 nt reads (PE150) and a sequencing depth of minimum 100 million reads.

The libraries on RNA extracted from the Hells Bells biofilm and the planktonic phase of the redoxcline community, were prepared with the TruSeq total RNA Sample Prep Kit (Illumina, San Diego, USA) and sequencing was conducted on the Illumina NextSeq 500 platform with single-read 150 nt reads (SR150) and a sequencing depth of min. 100 million reads.

The metagenomes and -transcriptomes of the redoxcline community of cenote Angelita and Hells Bells biofilm material from cenote El Zapote (from 2020) was not sequenced by IMGM, but in the research group of Prof. Dr. Kaster (Karlsruhe Institute of Technology, Institute for Biological Interfaces 5 (IBG 5), Eggenstein-Leopoldshafen). Analogous to the metagenome of El Zapote, the NEBNext Ultra II FS DNA Library Preparation Kit (New England Biolabs, Frankfurt am Main, Germany) was used. The PE sequencing was conducted on a NextSeq550 System (Illumina, San Diego, USA) with 150 cycles and a sequencing depth of minimum 100 million reads. The respective metatranscriptome libraries were prepared with the NEBNext Ultra II Directional RNA Library Kit (New England Biolabs, Frankfurt am Main, Germany). The sequencing parameters were the same as for the metagenome. However, the PE sequenced metatranscriptone was analyzed as SE data. For simultaneous sequencing of multiple samples, the NEBNext Multiplex Oligos Index Primer Set 2 was used. The Supplementary Tables S1-3 summarize the quantitative sequencing results for each sample.

2.5.3   Nanopore sequencing

The sequencing method from Oxford Nanopore Technologies (Oxford, UK) was used for 16S rRNA gene amplicon sequencing of samples related to the Thaumarchaeota isolation approach. These included the cells on the magnetic beads and in the bead supernatant after the isolation procedure, as well as the original redoxcline community from which Thaumarchaeota were to be isolated.

Samples were prepared using the Ligation Sequencing Kit protocol (SQK-LSK109; Oxford Nanopore Technologies, Oxford, UK), and markers were applied using the Native Barcoding Expansion Kit (EXP-NBD104; Oxford Nanopore Technologies, Oxford, UK) to generate a

barcoded sequencing library. Sequencing of the 16S rRNA gene amplicons (based on the amplification with Pro341/Universal_1492rev primers) was performed on a flongle flow cell (FLO-FLG001; Oxford Nanopore Technologies, Oxford, UK).

2.6 Bioinformatic analyses

Demultiplexing and trimming of adapter sequences after Illumina sequencing was conducted using the Illumina software MiSeq Reporter (MSR) v2.5.1.3 and the Illumina Sequence Analysis Viewer (SAV) v1.9.1. Base calling of Nanopore reads was accomplished with the Guppy software v4.0.4 (Oxford Nanopore Technology, Oxford, UK) with the high accuracy model followed by demultiplexing with the Epi2me software (Oxford Nanopore Technologies, Oxford, UK).

All tools and software programs that were used for the bioinformatic analyses are listed in Table 25. Unless explicitly described otherwise, the tools were used with standard parameters.

Table 25: Software and bioinformatic tools used in this work.

Tool/Software	Version	Reference
Bowtie2	2.3.4.3	Langmead & Salzberg (2012)
CLC Genomics Workbench	20	Qiagen, Aarhus, Denmark
DIAMOND	0.9.24	Buchfink et al. (2015)
eggNOG mapper	2.0.0	Huerta-Cepas et al. (2017, 2019)
I-TASSER	-	Roy et al. (2010); Yang et al. (2015); Yang & Zhang (2015)
Kallisto	v0.45.0	Bray et al. (2016)
Megahit	1.1.4-2	Li et al. (2015, 2016)
phyloFLASH	3.3b1	Gruber-Vodicka et al. (2019)
Prodigal	2.6.1	Hyatt et al. (2010)
PyMol	2.4.1	Schrödinger LLC (New York, USA)
SignalP	5.0	Almagro Armenteros et al. (2019)
TMHMM	2.0	Krogh et al. (2001)
Trimmomatic	0.38	Bolger et al. (2014)

2.6.1   16S rRNA gene amplicons

After sequencing, the first step in the 16S rRNA amplicon data analysis was the quality (with the threshold of 0.05) and primer trimming. Subsequently, the paired reads of the individual samples were merged. The clustering of operational taxonomic units (OTUs) was conducted against the SILVA 16S database release v132 97 % to obtain a taxonomic profile. All amplicon data from cenote El Zapote are based on duplicates. Since the duplicates of every sample were very similar with regards to the microbial diversity, these were merged, and the relative abundance was averaged for every OTU. Very low abundant OTUs with a minimum combined abundance of less than 50 were excluded from the analysis. All steps of the 16S rRNA amplicon analysis were conducted with the CLC Genomic Workbench Software including the 'Microbial genomic module 4.0' plugin.

2.6.2   Metagenomic and metatranscriptomic analyses

Using Trimmomatic, the first step in the metatranscriptomic and -genomic data analysis was the quality and adapter trimming of the Illumina raw reads. For trimming, the following parameters were set: 'LEADING:3 TRAILING:3 SLIDINGWINDOW:4:15 MINLEN:105'. Based on the high quality paired metagenomic reads, the metagenomes were assembled with the assembly tool Megahit. For the metagenome of the redoxcline community of El Zapote, the settings of k-mer x 21-141 and steps of 20 were chosen. For the two metagenomes of the Hells Bells biofilm and the redoxcline community of cenote Angelita, the best assembly result was achieved with the sensitive assembly preset. Subsequently, the coding sequences (CDS) within the metagenome was determined using prodigal in -p meta mode (Hyatt et al., 2010). At the same time, the tool enables the translation of CDS into protein sequences. Using DIAMOND blastp in sensitive metagenome mode, the protein sequences were annotated by blasting against the Uniprot database (entry version 36, state: 28.05.2019). In parallel, orthology prediction and functional annotation was acquired using eggNOG mapper. Transcript abundances were determined by the alignment against the metagenomic CDS reference index using Kallisto. To allow comparison between metatranscriptomic samples, gene expression levels were calculated in transcripts per million (TPM).

In contrast to amplicon sequencing, the microbial diversity on the basis of metagenomes and metatranscriptomes can be determined independent of primer biases. For this purpose, the

metagenomic and metatranscriptomic (filtered) raw reads were blasted against the assembled metagenome using bowtie2 in default mode. For following steps, a custom python script was written (together with Christian Jonas Lapp; provided in the digital appendix; filename 'lappleb'). Taxonomic assignments of the annotated metagenome were merged with calculated abundance information. Additionally, for quantitative information, the number of mapped reads was aggregated on the taxonomic level of family and order. The resulting microbial diversity was verified by a second, alternative analysis using phyloFLASH.

2.6.3 *In silico* **analysis and modelling of a Thaumarchaeota S-layer protein**

Thaumarchaeota were noted for their dominance in the metatranscriptome. S-layer proteins were found to be highly expressed. A number of genes annotated as uncharacterized proteins shared the assignment to the 'S-layer protein' (ID: A0A388QJN8_9ARCH) as the next best annotated hit in the Uniprot database. Since the original gene sequences and thus the translated protein sequences were not fully represented in the genome, the complete protein sequence of the common hit 'S-layer protein' was taken and further studied as described in the following.

In the first step, the S-layer protein sequence was screened for signal peptides as well as putative transmembrane domains using SignalP and TMHMM (see Table 24). Subsequently, protein structure prediction was obtained using the I-TASSER server. The embedded algorithms serve to identify the best matching protein structure template, thereby forcing the fragments of the amino acid sequence and the complete protein into already known conformation templates from structural databases. Finally, a putative model structure is then assembled. Using PyMol, the S-layer protein of Thaumarchaeota was then plotted according to the determined protein folding and structure model. The company Genscript (Leiden, Netherlands), which produced the antibody against the selected antigen, provided a list of peptides of the S-layer protein that had the best properties for binding to antibodies (based on factors such as hydrophobicity, peptide charge, antigenicity). Finally, the peptide from amino acid 503 to 516 ("ANRNSRADEDLDVN") in the extracellular domain of the protein (Fig. 31) was chosen as the optimal epitope because it provided the best accessibility and peptide characteristics for antibody binding.

2.6.4 Data availability

The complete hydrogeochemical data set is available online under https://doi.org/10.11588/data/TMYLWS (cenote El Zapote (2018)) and https://doi.org/10.11588/data/GYLDH5 (cenote Angelita and El Zapote (2020)). All 16S rRNA amplicon and metagenomic/-transcriptomic raw reads included in this study are publicly available through the NCBI BioProjects PRJNA635010 and PRJNA784917.

3 RESULTS

Previous hydrogeochemical investigations by Ritter et al. (2019) and Ritter (2020) indicated that the development of Hells Bells might be catalyzed by microorganisms in the redoxcline and turbid layer of cenote El Zapote. To achieve a thorough understanding of the Hells Bells formation process, a microbiological investigation in form of this thesis was attempted to complement the previous hydrogeochemical findings to a holistic study. The compiled data resulted from two sampling periods in Mexico. The first sampling campaign was carried out from 31st of May to 6th of June 2018 and focused on the detailed sampling of cenote El Zapote. Data on cenote Angelita are based on samples collected during the second sampling from 13th to 25th of February 2020. In this chapter, the results are structured in four subprojects associated with the microbiology of redoxclines and Hells Bells growth, followed by another one focusing on the establishment of a bioinformatically derived isolation method for Thaumarchaeota from the redoxcline of El Zapote:

The first part of this study revolved around the question if and (if so) how the microbial diversity distinguishes the redoxcline as the growth zone for Hells Bells from other zones of the water column of cenote El Zapote.

Subsequently, the aim was to answer whether microbiology is indeed involved in the development of Hells Bells speleothems. Metagenomic and metatranscriptomic analyses were conducted to identify the dominant microbial metabolic processes and the potential microbial key players in the planktonic phase of the redoxcline of cenote El Zapote. Furthermore, the role of the biofilm on the speleothems in the Hells Bells growth zone was evaluated.

In the following, unique features of the redoxcline of El Zapote with Hells Bells were examined in a comparative analysis to a similar cenote (in terms of the structure of the water column) in the vicinity, which, however, does not exhibit subaqueous calcite speleothems. In this context, the microbial ecology of the redoxcline of cenote Angelita without Hells Bells was studied in the same way as for El Zapote.

In addition, the elaborated theory on Hells Bells growth was tested in a highly simplified manner on a laboratory scale to substantiate the bioinformatic results.

Finally, based on the metatranscriptomic results of the El Zapote redoxcline, a side project arose that revolved around the isolation of so far uncultivable microorganisms. Thaumarchaeota stood out in the metagenomic and -transcriptomic study of the redoxcline of El Zapote. These archaea are known to be very challenging to cultivate. These archaeal ammonium oxidizers were used as an exemplary enrichment target to develop an antibody-based workflow for the specific enrichment of microorganisms based on metagenomic and -transcriptomic information.

3.1 Unique characteristics of the redoxcline as Hells Bells growth zone of El Zapote

3.1.1 Hydrogeochemistry of the redoxcline

At the time of microbiome sampling, the water chemistry of the redoxcline was simultaneously investigated by the research group of Prof. Isenbeck-Schröter (for Hydrogeochemistry and Hydrogeology, University of Heidelberg) to allow an accurate linkage of environmental parameters in the redoxcline (Ritter, 2020) to the microbial ecology studied in this work (Fig. 9). The redoxcline represents a water zone of steep counter-gradients of oxidized and reduced chemical species. In cenote El Zapote, the redoxcline overlapped with a turbid layer that is clearly distinguishable from the adjacent water layers by the white, cloud-like turbidity (Fig. 1). In June 2018, the turbid layer reached from about ~35–36.6 m and is indicated in Figure 9 by the increase in turbidity with a peak value of ~7 formazin nephelometric units (FNU). The redoxcline is localized to top of the halocline that is indicated by the increase in electric conductivity (EC) below a water depth of 36.6 m. The redoxcline itself was identified by the abrupt shift in the redox potential from ~400 to -150 mV. The center of the redoxcline was located at a water depth of 35.7 m, exactly where a positive peak of the pH could be measured. The pH was detected to be circumneutral in the freshwater above the turbid layer and redoxcline and slightly dropped just above the redoxcline to a value of 6.86. The availability of dissolved oxygen changed from above the turbid layer, where low concentrations were detectable, towards the top of the redoxcline, where these fell below the detection limit.
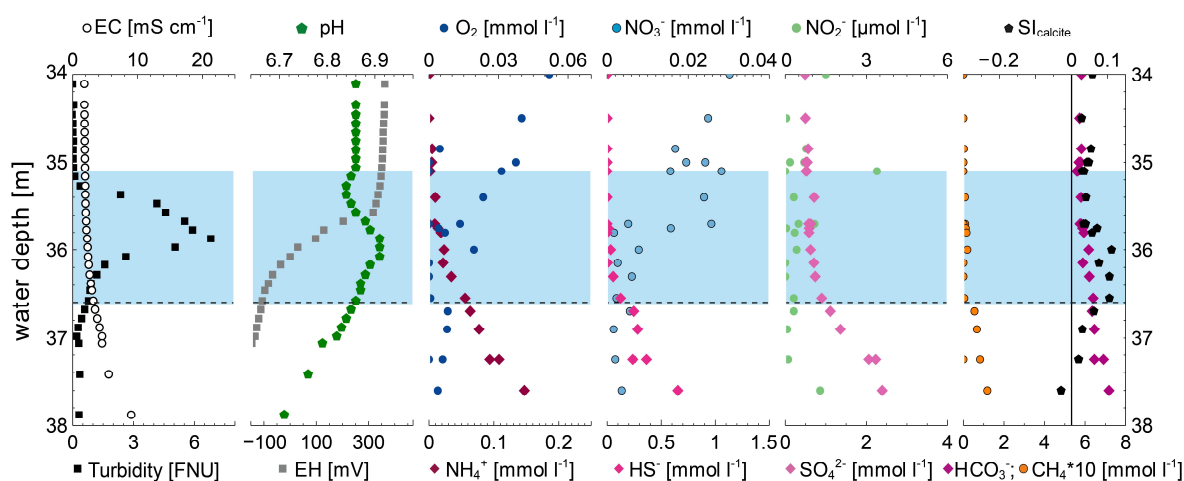
Figure 9: Hydrogeochemical profile of the pelagic redoxcline of cenote El Zapote. The redoxcline, which is located between the freshwater zone (above) and the halocline (below), is highlighted in light blue. The dashed line indicates the upper edge of the halocline. From the left to right side, the electric conductivity (EC; in mS cm^{-1}), turbidity in formazin nephelometric units (FNU), pH and redox potential (EH; in mV) are plotted. Furthermore, the measured concentrations of O_2, NH_4^+, NO_3^-, HS^-, NO_2^-, SO_4^{2-}, HCO_3^- and CH_4 are shown. The presented data were collected by the research group of Prof. Isenbeck-Schröter during the first sampling campaign in June 2018 (Ritter (2020)) at the same time of microbiome sampling. Modified from Leberecht et al. (in revision).

Similar profiles were detected for nitrate and nitrite. Concentrations of about ~30 μmol l^{-1} (NO_3^-) and ~1.5 μmol l^{-1} (NO_2^-) were measured in the freshwater at 34 m water depth, but both profiles showed decreasing trends towards the central redoxcline. Similarly, the concentrations of hydrogen sulfide (~1.1 mmol l^{-1} at 38 m), ammonium (~0.22 mmol l^{-1} at 38 m), methane (~0.1 mmol l^{-1} at 38 m) and bicarbonate (~7.25 mmol l^{-1} at 38 m) decreased from the source, the debris mound, towards the center of the redoxcline. Another important parameter in the context of the hypothesis of microbially induced calcite precipitation and growth of Hells Bells is the saturation index for calcite ($SI_{calcite}$). In the center of the redoxcline, parallel to the observed positive pH shift, a peak value in the $SI_{calcite}$ of ~0.12 at 36 m was measured, indicating a local calcite ($CaCO_3$) supersaturation. In the freshwater, however, SI values of 0.02–0.04 above the turbid layer implied a local calcite saturation but no supersaturation.

3.1.2   The microbial diversity

After examining the redoxcline of El Zapote regarding the local *in-situ* parameters, the first question addressed from a microbiological point of view was whether and if so, to what extent the microbial diversity in the Hells Bells growth zone differs from the adjacent water zones (freshwater above, halocline below) (Fig. 10).
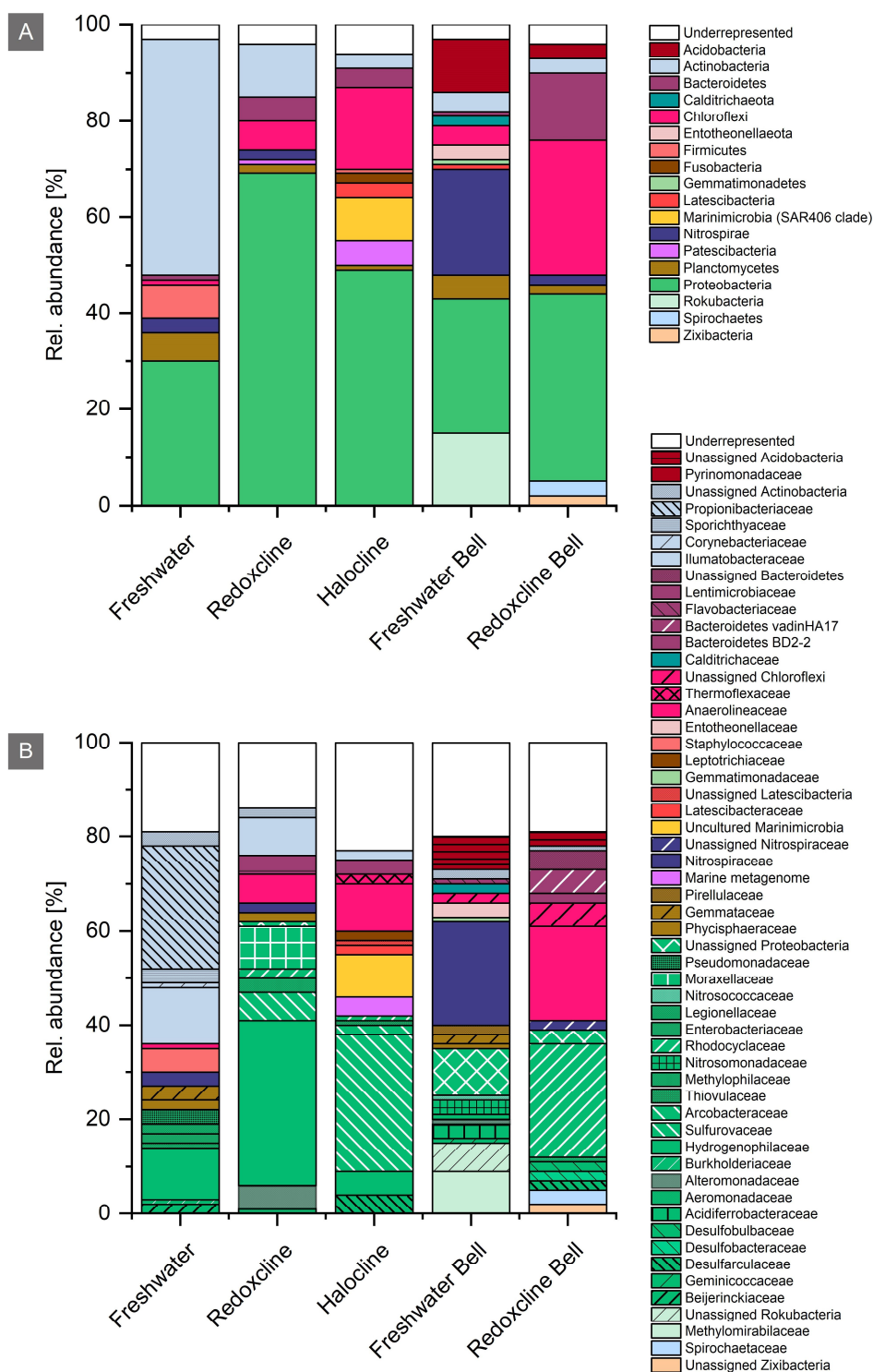
Figure 10: Relative abundance of OTUs of Bacteria throughout the water body of the cenote El Zapote. A) Taxonomy at phylum level. B) Taxonomy at family level. Based on 16S rRNA gene amplicon sequencing, the microbial diversity was determined for the planktonic communities in the freshwater, redoxcline and halocline and for the biofilm on Hells Bells speleothems in the freshwater zone (Freshwater Bell) and redoxcline (Redoxcline Bell). Phyla and families below a relative abundance of 1 % were grouped as underrepresented.

The 16S rRNA-based diversity analysis shows that the bacterial redoxcline community is clearly dominated by Proteobacteria, more than in the adjacent freshwater and halocline (Fig. 10 A). Already at the phylum level, it is evident that the redoxcline represents a transition zone between the freshwater above and the halocline below. The redoxcline shared phyla with the freshwater that were not found in the halocline, such as the Firmicutes, Planctomycetes and Nitrospirae. Conversely, certain phyla of the halocline were found in lower abundance in the redoxcline, but not or only to a very limited extent in the freshwater zone. This concerned the phyla Chloroflexi, Patescibacteria and Bacteroidetes. The phlya Latescibacteria, Marinimicrobia, and Fusobacteria could be assigned exclusively to the community in the halocline. When comparing the redoxcline biofilm with the planktonic redoxcline community, it turned out that the abundance of Proteobacteria on the Hells Bells was reduced and that the abundance of the phyla Chloroflexi and Bacteroidetes was much higher.

On the family level (Fig. 10 B), the freshwater community was mainly composed of Hydrogenophilaceae (11 %), Illumatobacteraceae (12 %) and Propionibacteriaceae (26 %). The redoxcline was clearly dominated by the family Hydrogenophilaceae (35 %). Besides Moraxellaceae and Sulfurovaceae, a few other Proteobacteria families were identified. In the halocline, the Sulfurovaceae were dominant among the Proteobacteria (29 %) instead of the Hydrogenophilaceae, which were less abundant than in the freshwater and redoxcline. Four unique operational taxonomic units (OTU) could be found in the halocline, which were not identified in neither of the other samples. The two biofilm samples of Hells Bells from different water zones seem to be markedly different in terms of the microbial diversity. The freshwater Bell biofilm is mainly composed of Nitrospiraceae (22 %), followed by unassigned Proteobacteria, Methylomiabilaceae and other unassigned Rokubacteria and unassigned Acidobacteria. In contrast to the freshwater biofilm, the Hells Bells biofilm in the redoxcline was not dominated by Nitrospiraceae but rather by the families Rhodocyclaceae (24 %) and Anaerolineaceae (20 %).

If the diversity of archaea is also considered, it becomes clear that the biofilm compositions differed further (Fig. 11). Both the planktonic and the biofilm phase in freshwater were dominated exclusively by Thaumarchaeota. However, only one family (Nitrosopumilaceae) was found in the planktonic phase, while various Thaumarchaeota families were identified on the Bell surface.
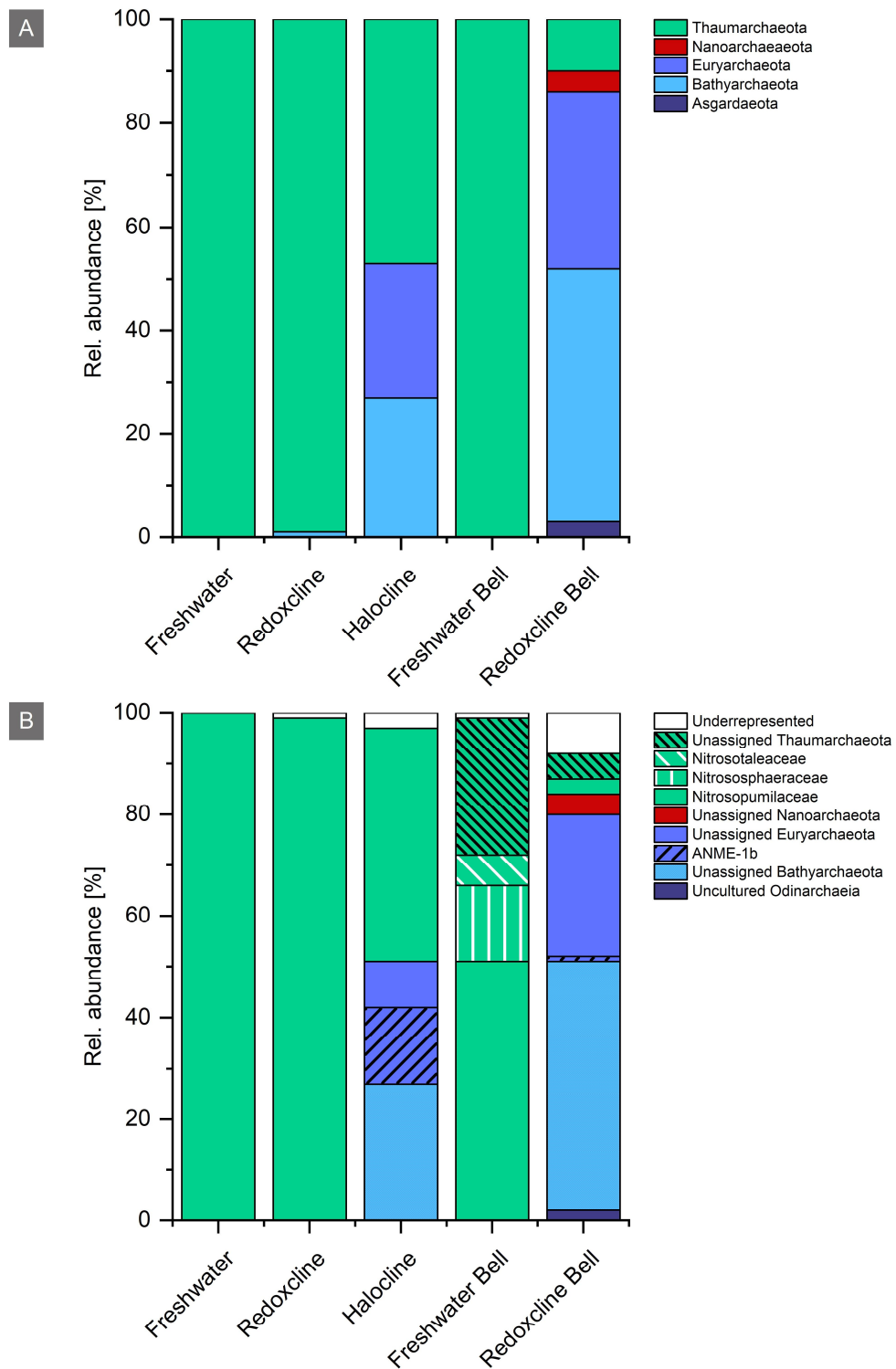
Figure 11: Relative abundance of OTUs of Archaea in the different water zones of the cenote El Zapote. A) Taxonomy at phylum level. B) Taxonomy at family level. The 16S rRNA amplicon analysis revealed the microbial diversity in the planktonic phase in the freshwater, redoxcline and halocline and for the solid phase (biofilm) on freshwater (Freshwater Bell) and redoxcline Hells Bells (Redoxcline Bell). The group of underrepresented microorganisms comprises phyla and families with a relative abundance < 1 %.

In the redoxcline, Thaumarchaeota of the family Nitrosopumilaceae were also found almost exclusively in the aqueous phase (Fig. 11 B). On the speleothems in the redoxcline, however, the highest archaeal diversity was determined among all samples. On the redoxcline Hells Bells, unassigned Odinarchaeia, Bathyarchaeota, Euryarchaeota, Nanoarchaeota, the family Nitrosopumilaceae and other unassigned Thaumarchaeota were detectable. Comparing the planktonic phases of the three water zones with each other, the highest archaeal diversity was found in the halocline. There was also a high proportion of Nitrosopumilaceae, but also unassigned Bathyarchaeota and Euryarchaeota. A part of the Euryarchaeota could be assigned to the OTU ANME-1b (*an*aerobic *me*thane oxidizers (ANMEs)).

In addition to the 16S rRNA amplicon data, the phylogenetic diversity of the community in the pelagic redoxcline of cenote El Zapote was also determined based on the taxonomic origin of metagenomic and metatranscriptomic raw reads (Fig. 12).
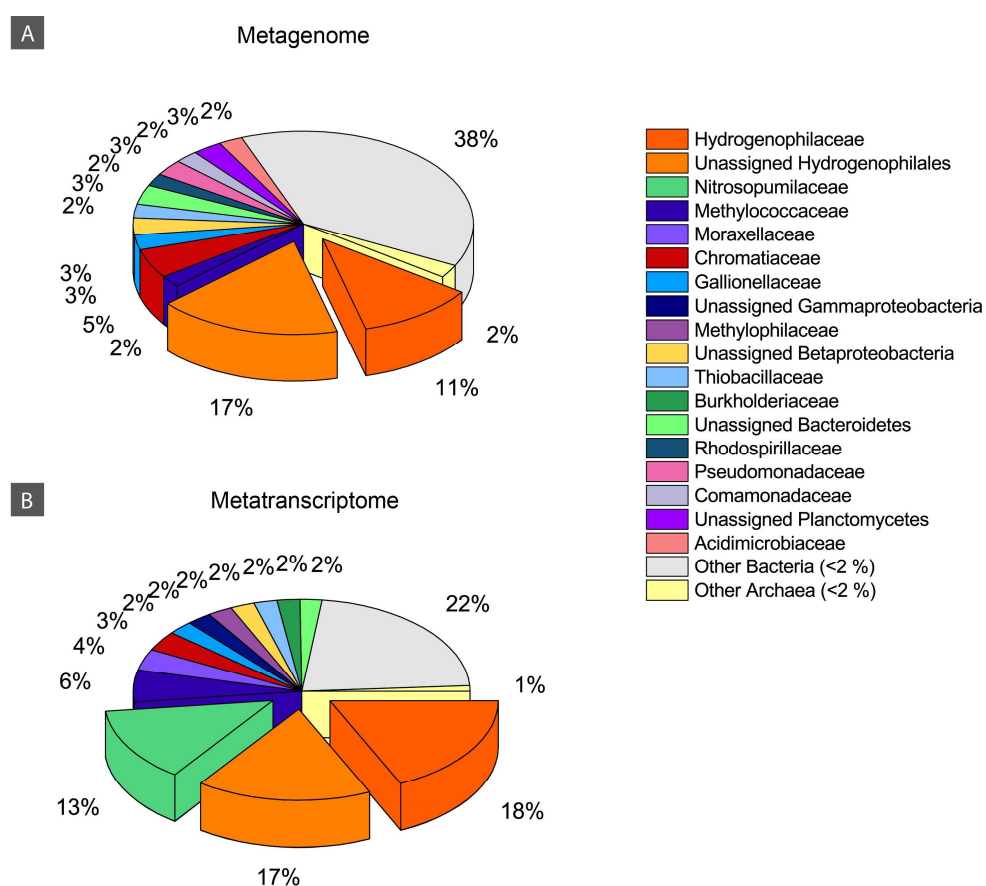
Figure 12: Microbial diversity of the planktonic phase of the redoxcline of El Zapote. A) The relative abundance of microbial families is based on the taxonomic assignment of metatranscriptomic raw reads, B) the same is shown based on the metagenomic raw reads. Families below a relative abundance of 2 % were grouped as underrepresented. Modified from Leberecht et al. (in revision).

As predicted by the amplicon data, the family of Hydrogenophilaceae (metatranscriptome: 18 %, metagenome: 11 %) and other not further classifiable Hydrogenophilales (17 % each) were also the most abundant organisms on the metatranscriptomic and -genomic level (together 35 %). One family stood out on the metatranscriptome-based diversity, but at the same time fell among the underrepresented families (< 2 %) in the metagenome. This concerned the Thaumarchaeota family Nitrosopumilaceae, which was represented at 17 % in the metatranscriptome and below 2 % in the metagenome. Thaumarchaeota transcripts were the second most abundant.

The remaining families varied only marginally between the two meta data sets. Among those, the Methylococcaceae, Moraxellaceae, Chromatiaceae, Gallionaceae, unassigned *β*-Proteobacteria and Bacteroidetes were identified in the redoxcline, and they made up 2 to 6 % of the community. There were fewer underrepresented families detected in the metatranscriptomic (Bacteria 22 %, Archaea 1 %) than in the metagenomic data (Bacteria 38 %, Archaea 2 %). For the dominant group of Hydrogenophilaceae/Hydrogenophilales, it may be of special interest to determine their metabolic contribution to the hydrogeochemistry of the redoxclines and thus potentially to calcite precipitation. The analysis of the 16S rRNA from Hydrogenophilales indicated that these bacteria may form a new genus within the order Hydrogenophilales. According to the SILVA database, the 16S rRNA sequence had a 93.7 % similarity to "uncultured Hydrogenophilales", based on the NCBI 16S ribosomal RNA database the sequence shared 92.8 % indentity with *Annwoodia aquaesulis* (of the order Nitrosomonadales).

3.2 Microbial ecology of the redoxcline - dominant metabolic pathways and microbial key players

3.2.1 The planktonic community

As the redoxcline was previously identified as the zone, in which Hells Bells develop and grow (Ritter, 2020; Ritter et al., 2019), the question arises whether the local calcite precipitation occurs abiotically or whether microbes in the redoxcline significantly contribute to that process by metabolically mediated changes of their microenvironment. Therefore, a metagenomic and -transcriptomic study of the microbiome in the redoxcline was conducted.

The resulting gene expression levels of genes involved in autotrophic and photosynthetic pathways, as well as the methane, sulfur and nitrogen cycle were determined in transcripts per million (TPM) and are plotted in Figure 13.
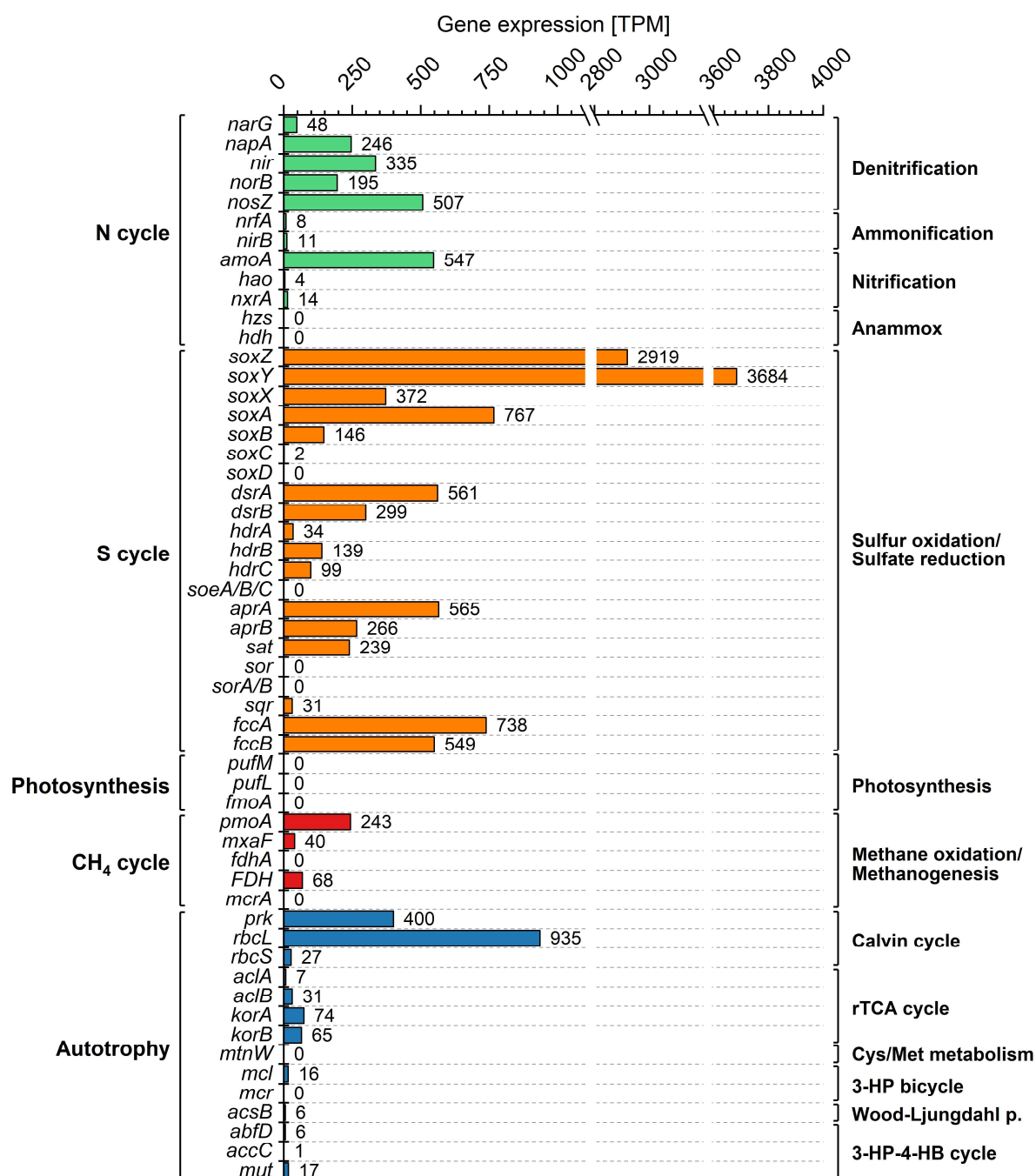
Figure 13: The metatranscriptomic analysis revealed dominant microbial metabolic pathways in the redoxcline. The gene expression levels of genes involved in the nitrogen, methane and sulfur cycle, photosynthesis and autotrophy were calculated in transcripts per million (TPM). Modified from Leberecht et al. (in revision).

Since the latter two cycles turned out to be of particular importance in the redoxcline, the transcript abundances were also linked to the respective metabolic reactions and visualized in Figure 14 (scheme based on Alvarez et al. (2014) and Rodionov et al. (2005)) and Figure 15 (scheme based on Grabarczyk and Berks (2017)).

The nitrogen cycle (Fig. 14) comprises the processes of ammonification/the dissimilatory nitrate reduction to ammonia (DNRA), denitrification, nitrification and the anaerobic ammonium oxidation (ANAMMOX). The complete denitrification pathway is based on the following enzymes that allow the reduction of nitrate to dinitrogen: the nitrate reductases (*narG*; 48 TPM and *napA* 246 TPM), the nitrite reductases (*nirK/S*; 335 TPM), the nitric oxide reductase (*norB*; 195 TPM) and nitrous oxide reductase (*nosZ*; 507 TPM). All genes encoding these listed enzymes were highly expressed and among these, transcripts of *nosZ* for the reduction of nitrous oxide (N_2O) to N_2 had the highest abundance.
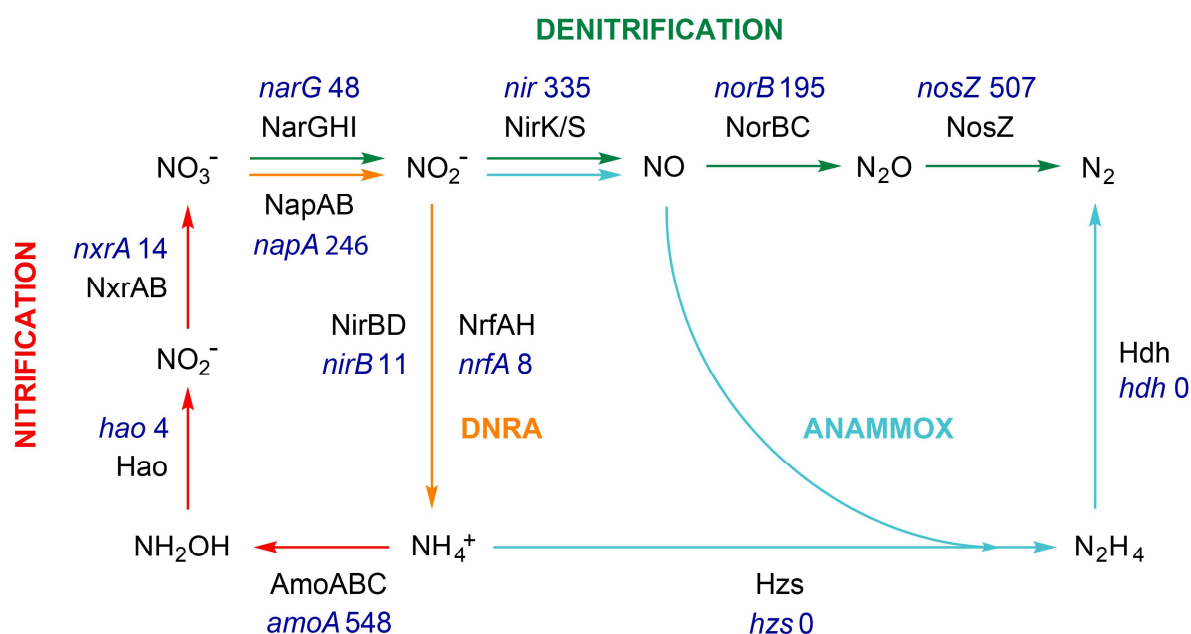
Figure 14: The gene expression levels of genes encoding enzymes that are involved in the nitrogen cycle are shown in context of the respective catalzyed reaction (according to Leberecht et al. (in revision)). The expression levels were calculated in transcripts per million [TPM] and are shown in dark blue. Scheme based on Alvarez et al. (2014) and Rodionov et al. (2005).

In contrast, the two different genes of the catalytic subunits of the nitrite reductases, *nrfA* (8 TPM) and *nirB* (11 TPM), which are relevant for the dissimilatory reduction of nitrate to ammonium (DNRA), were only weakly expressed. Likewise, the ANAMMOX pathway seemed to play a minor role in the redoxcline as the hydrazine synthase (*hzs*) and the hydrazine dehydrogenase (*hdh*) genes were hardly transcribed. Besides the process of denitrification, the oxidation of ammonia was identified as a dominant metabolic pathway in the redoxcline. The ammonia monooxygenase that catalyzes the first step in the oxidation reaction showed the highest expression level among all marker genes of the nitrogen metabolism (subunit A; *amoA;* 508 TPM). Only a very limited number of transcripts was assigned to the hydroxylamine oxidoreductase that oxidizes hydroxylamine in the next step of the ammonium oxidation process to nitrite (*hao*; 4 TPM). The same applies to the nitrite oxidoreductase (*nrxA;* 14 TPM) that allows the last step in nitrification from nitrite to nitrate. Thus, in the nitrogen cycle two processes seemed to dominate – the complete denitrification and the oxidation of ammonia. The denitrification is a proton consuming process (see chapter 1.1.2) and may thereby favor calcite precipitation in the redoxcline.

For specific genes of the sulfur cycle (Fig. 13 and 15), much higher transcript abundances were found compared to all previously described marker genes of the nitrogen cycle. Among those, the two genes, *soxZ* an *soxY,* that encode the two subunits of the periplasmic protein SoxYZ were found, which is the central heterodimeric carrier protein of the sulfur oxidation (Sox) system. The respective gene expression levels reached 3684 TPM for *soxY* and 2919 TPM for *soxZ*. The carrier protein binds reduced sulfur molecules at the C-terminal cysteine persulfide group of the SoxY peptide swinging arm, where the protein-bound oxidation of sulfur occurs (SoxZY-S-S$^-$) (Quentmeier & Friedrich, 2001; Sauvé et al., 2007). Other components of the Sox system, such as SoxXA, SoxCD and SoxB, catalyze a number of sulfur oxidation steps at this active site (Fig. 15). In the first step, SoxXA is responsible for the addition of reduced chemical species (such as sulfide, thiosulfate, elemental sulfur and other inorganic sulfur compounds) to the persulfide chain of the SoxY-cysteine (SoxZY-S-S-S-SO$_3^-$). After SoxXA, SoxB takes over the hydrolysis of the resulting sulfonate group and releases sulfate. The resulting sulfane sulfur (SoxZY-S-S-S$^-$) is then converted back into a sulfonate group by SoxCD (SoxZY-S-S-S-SO$_3^-$). As in the previous step, this residue can be hydrolyzed again by SoxB. SoxYZ is then back in its initial state (SoxZY-S-S$^-$) and another sulfate molecule has been produced (Grabarczyk & Berks, 2017; Rother et al., 2001).
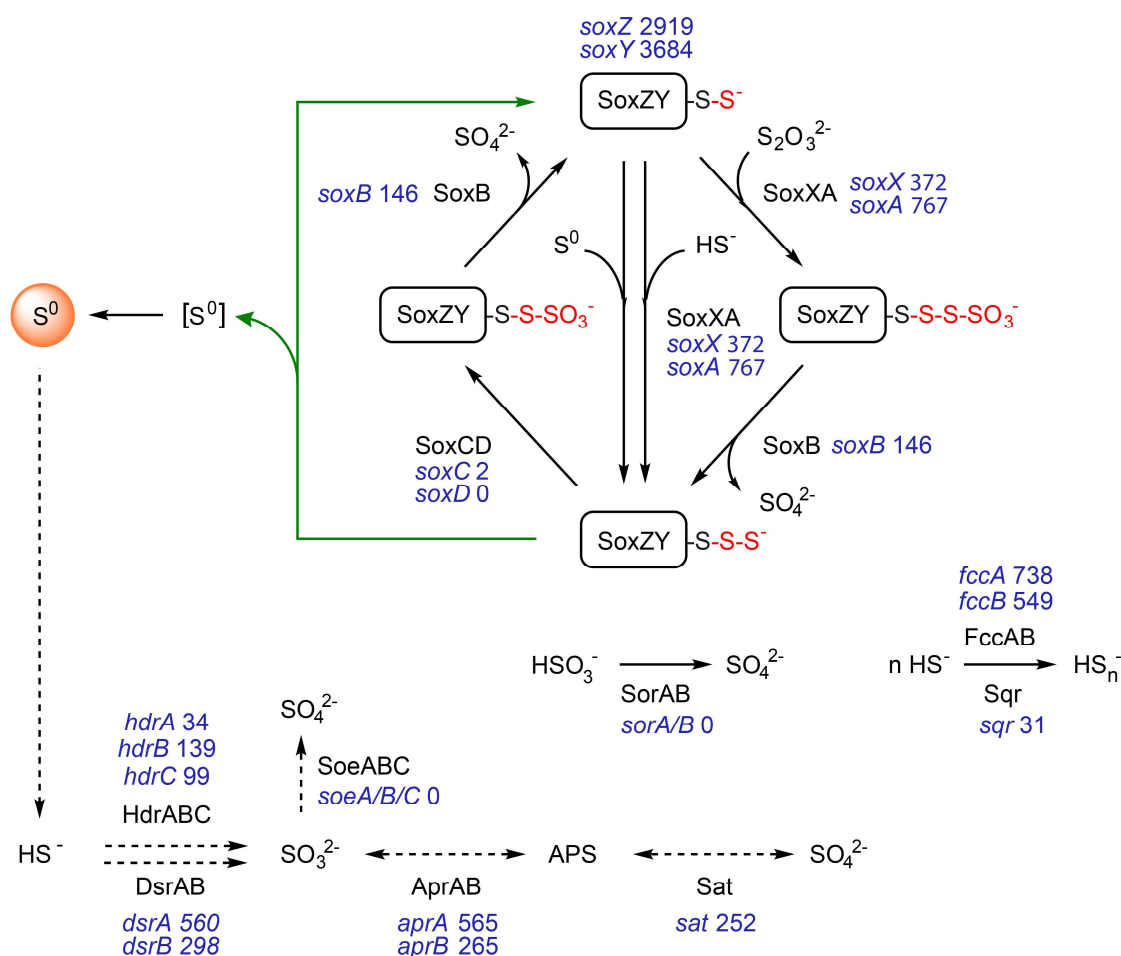
Figure 15: Microbial gene expression of genes involved in the sulfur cycle of the central redoxcline of El Zapote. Transcript abundances (shown in dark blue) were calculated in transcripts per million [TPM]. Normal arrows mark reactions that occur in the periplasm of microbial cells, dashed arrows indicate that the respective reaction takes place in the cytoplasm. The scheme of the Sox cycle is based on the revised model by Grabarczyk & Berks (2017). According to Leberecht et al. (in revision).

For these three Sox enzymes very different transcription levels were determined. While *soxB* was moderately expressed (146 TPM) and *soxXA* was highly expressed (372 TPM for *soxX*, and 767 TPM for *soxA*), the community in the redoxcline hardly expressed *soxCD* at all (*soxC*, 2 TPM; *soxD* 0 TPM). Organisms that lack *soxCD* genes or do not transcribe those often use an alternative step to regenerate SoxYZ again. They transfer the sulfane sulfur from SoxZY-S-S-S$^-$ to elemental sulfur particles (S^0) (Frigaard & Dahl, 2008; Sauvé et al., 2007) (Fig. 15).

Depending on the phylogeny, prokaryotes deposit this elemental sulfur either inside (e.g. Chromatiaceae, ɣ-Proteobacteria such as *Beggiatoa*) or outside the cell (e.g. Chlorobiaceae, Ectothiorhodospiraceae, Heliobacteriaceae). Hence, sulfur particles may accumulate as final

or intermediate products (Dahl & Prange, 2006). To link these results to the hydrogeochemistry in the redoxcline (Fig. 9), it is important to note that, consistent with the high expression of *soxXA* and the lack of *soxCD* transcripts, no sulfate production could be measured (Fig. 9). But interestingly, zero-valent sulfur was already detected in the redoxcline (Ritter et al., 2019).

For further oxidation of zero-valent sulfur, sulfur atoms form persulfides or polysulfides and are transported into the cytoplasm by carrier proteins such as the *Wolinella succinogenes* Sud or as low-molecular-mass thiols (Lin et al., 2004; Stockdreher et al., 2012). A cascade of additional carrier proteins transfers sulfur to DsrC (Cort et al., 2008; Stockdreher et al., 2014). The DsrC trisulfide is substrate for the dissimilatory sulfite reductase (rDsrAB) that produces sulfite with electron acceptors such as NAD^+ (Löffler et al., 2020). Sulfite is subsequently further oxidized by the adenylyl-sulfate reductase (AprAB) to adenosine-phosphosulfate (APS) (Frigaard & Dahl, 2008; Stockdreher et al., 2014; Tanabe et al., 2019). The last oxidation step is catalyzed by the sulfate adenylyltransferase (Sat) that oxidizes APS to sulfate, a process that allows ATP synthesis by substrate-level phosphorylation (Frigaard & Dahl, 2008). Looking at the expression levels of these three cytoplasmic sulfur-oxidizing enzymes, it is obvious that the transcripts are similarly abundant to those from periplasmic *soxXA*. However, DsrAB, AprAB and Sat are not only involved in the oxidative direction of this pathway but also in the reductive direction (sulfate reduction). Therefore, a bioinformatic analysis was conducted to determine whether an oxidative or reductive form of the enzyme DsrAB dominated. In detail, the gene sequences of the dominant *dsrAB*-expressing organisms (the orders Hydrogenophilales, Nitrosomonadales and Thiotrichales (Fig. 17)) were aligned against the *dsrAB* database of Müller et al. (2015), which was created to distinguish reductive from oxidative forms of DsrAB. The resulting classification indicated that all three orders expressed the reverse form of DsrAB that catalyzes the sulfide oxidation instead of sulfate reduction (Supplementary Tables S4-6). Apparently, a complete oxidation of sulfur to sulfate seems to occur at least to some extent, even if a sulfate production was not detectable in the redoxcline (Fig. 9) in contrast to zero-valent sulfur (the product of an incomplete oxidation) (Ritter et al., 2019). This also means that sulfate reduction played a rather negligible role in the turbid layer and redoxcline. Besides DsrAB, the microbial community also moderately expressed the heterodisulfide reductase Hdr (*hdrA/B/C*

34/139/99 TPM) that basically catalyzes the same oxidative reaction of sulfide to sulfite (Boughanemi et al., 2016; Koch & Dahl, 2018).

Apart from the sox system, there were other sulfide sinks in the periplasm identified. These included the periplasmic flavocytochrome c FccAB and the membrane-bound sulfide:quinone oxidoreductase (SQR) that both oxidize sulfides to polysulfides and/or elemental sulfur (Chen et al., 1994; Griesbeck et al., 2002; Marcia et al., 2009; Reinartz et al., 1998). However, SQR couples sulfite oxidation to the quinone pool, whereas FccAB feeds electrons to the electron transport chain. The expression of *fccAB* was much higher (738/549 TPM) than that of *sqr* (31 TPM).

A lack of transcripts encoding the three molybdoenzymes SoxCD (see above) and the sulfite oxidoreductases SorAB (periplasmic (Kappler et al., 2000; Kappler & Bailey, 2005); *sorA/B* 0/0 TPM) and SoeABC (membrane-bound (Dahl et al., 2013); *soeA/B/C* 0/0/0 TPM) was observed and indicates that the community in the redoxcline does not utilize alternative sulfite oxidation pathways but oxidizes sulfide via SoxYZXAB/FccAB, Dsr/Hdr, Apr and Sat with minor contributions of Sqr. Interestingly, the only oxygen-dependent enzyme among all of the sulfur cycle analyzed here, the sulfur oxygenase reductase, could not be identified on the transcriptome level (*sor* 0 TPM). Taken together, the oxidation of sulfide seems to be a key process in the central redoxcline, whereas the reverse pathway (sulfate reduction) plays a minor role.

Photosynthesis could be another process that induces local calcite supersaturation in the redoxcline and turbid layer (see chapter 1.1.1). Therefore, the expression levels of several marker genes of oxygenic and anoxygenic photosynthesis were also investigated (Fig. 13). However, the process of photosynthesis is not described here in as much detail as previously for the N and S cycle, as the genes relevant for photosynthesis were hardly represented at the metatranscriptome level. These included *psaA* (the photosystem I P700 chlorophyll a apoprotein A1) (Fromme, 1996), *petA* (apocytochrome f of the cytochrome *b6f* complex), *psbA* (the photosystem II P680 reaction center D1 protein) (Mulo et al., 2009) and the *bchP* (the bacteriochlorophyll synthesizing enzyme geranylgeranyl diphosphate/geranylgeranyl bacteriochlorophyllide reductase). These genes and all analyzed genes for anoxygenic photosynthesis (*fmoA*, *pufLM*) were hardly transcribed (TPM values < 1). Apparently, light-dependent reactions cannot be catalyzed at a water depth of 35.7 m.

Since methane was detected in the halocline and diffuses towards the redoxcline (Fig. 9), it was also verified whether important processes take place in the methane cycle (Fig. 13 and 16).

METHANE OXIDATION
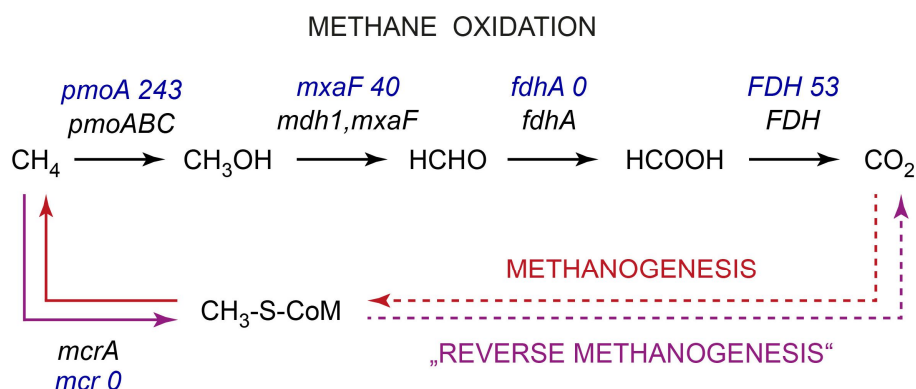
Figure 16: The transcript abundances of genes encoding enzymes that are involved in the methane cycle. The expression levels were calculated in transcripts per million [TPM] and are shown in dark blue.

Indeed, transcripts of the (particulate) methane monooxygenase were found, which is relevant for the first step of the aerobic methane oxidation from methane to methanol (243 TPM). The soluble form of the methane monooxygenase (*mmo*) was not found on the metatranscriptomic level. The next enzyme in this pathway is the formaldehyde-forming methanol dehydrogenase. Genes encoding this enzyme were much less expressed (*mxaF* 40 TPM). No transcripts at all were found for the formaldehyde dehydrogenase (*fdhA* 0 TPM), which catalyzes the oxidation of formaldehyde to formate. In contrast, 53 TPM could be assigned to genes encoding the formate dehydrogenase (*FDH* 53 TPM). This enzyme catalyzes the final oxidation step to CO_2. The key gene for the anaerobic respiration process of methanogenesis was not expressed at all (*mcr* 0 TPM). This gene encodes the methyl-coenzyme M reductase, which catalyzes the last of this process leading to the formation of methane. At the same time, this gene is also described in association with the "reverse methanogenesis"/anaerobic methane oxidation (Scheller et al., 2010). Accordingly, both reactions do not seem to play a role in the redoxcline.

In addition, the different carbon dioxide fixation pathways of the community in the redoxcline were analyzed in more detail at the metatranscriptomic level, such as the Calvin cycle, the reverse tricarboxylic acid (rTCA) cycle, the cysteine/methionine metabolism, 3-hydroxypropionate (3-HP) bicycle, the Wood-Ljungdahl pathway and 3-hydroxypropionate/

4-hydroxybutyrate (3-HP-4-HB) cycle (Fig. 13). Among those, the Calvin cycle was identified as the major sink for carbon dioxide in the redoxcline. The phosphoribulokinase (*prk*) reached 400 TPM and the large subunit of the ribulose-bisphosphate carboxylase (rubisCO; *rbcL*) even 935 TPM. Moderate and low expression levels were determined for the 2-oxoglutarate ferredoxin oxidoreductase (*korA* 74 TPM, *korB* 65 TPM) and ATP citrate lyase (*aclA* 7 TPM; *aclB* 31 TPM), two marker genes of the rTCA cycle. Marker genes that encode the malonyl-CoA reductase/3-hydroxypropionate dehydrogenase (*mcr* 0 TPM) and malyl-CoA lyase (*mcl* 16 TPM) of the 3-HP cycle were only marginally expressed. Likewise, the 2,3-diketo-5-methylthiopentyl-1-phosphate enolase (*mtnW* 0 TPM) of the cysteine and methionine metabolism and acetyl-CoA synthase (*acsB* 6 TPM) of the reductive acetyl-CoA pathway (Wood-Ljungdahl pathway). Marker genes of the 3-HP-4-HB cycle, the 4-hydroxybutyryl-CoA dehydratase (*abfD* 6 TPM), acetyl-CoA/propionyl-CoA carboxylase (*accC* 1 TPM) and methylmalonyl-CoA mutase (*mut* 17 TPM), were also transcribed on a very low level although Thaumarchaeota were highly abundant on the metatranscriptomic level (Fig. 12).

From the metabolic profiling (based on metatranscriptomic data), it can now be concluded that the key processes are denitrification and ammonium oxidation, as well as sulfide oxidation, and that the microbial community mainly uses the Calvin cycle for carbon fixation. Under the light-limited conditions in the turbid layer in the water depth of 35.7 m, no or only weak photosynthesis seems to be feasible. Based on this, it would of course be important to determine in the next step which organisms are now operating the major metabolic pathways that have been identified, as these might be the microbial key players that are possibly contributing to calcite precipitation and thus to the growth of Hells Bells. Therefore, the taxonomic classification of transcripts was analyzed to show, which phylogenetic groups expressed the respective key genes. In Figure 17, the gene expression levels were plotted for selected key genes together with the taxonomic assignment of the respective transcripts. One order immediately stands out, the order of Hydrogenophilales (highlighted in orange). The Hydrogenophilales dominantly expressed *soxY* (with 2472 TPM), *soxA* and *soxB* of the Sox system and *fccA*, which encodes an alternative periplasmic sulfide-oxidizing enzyme. The main portion of *dsrA* reads also originated from the Hydrogenophilales. They additionally seem to use nitrate as electron acceptor and are able to reduce nitrate completely to dinitrogen as they expressed all genes for the denitrification pathway (*napA*, *nir*, *nor*, *nosZ*).

Furthermore, the Hydrogenophilales highly expressed the large subunit of the RubisCo (*rbcL*) for carbon dioxide fixation via the Calvin cycle. Besides the Hydrogenophilales, unassigned Betaproteobacteria also highly expressed *soxY* and *fccA*.
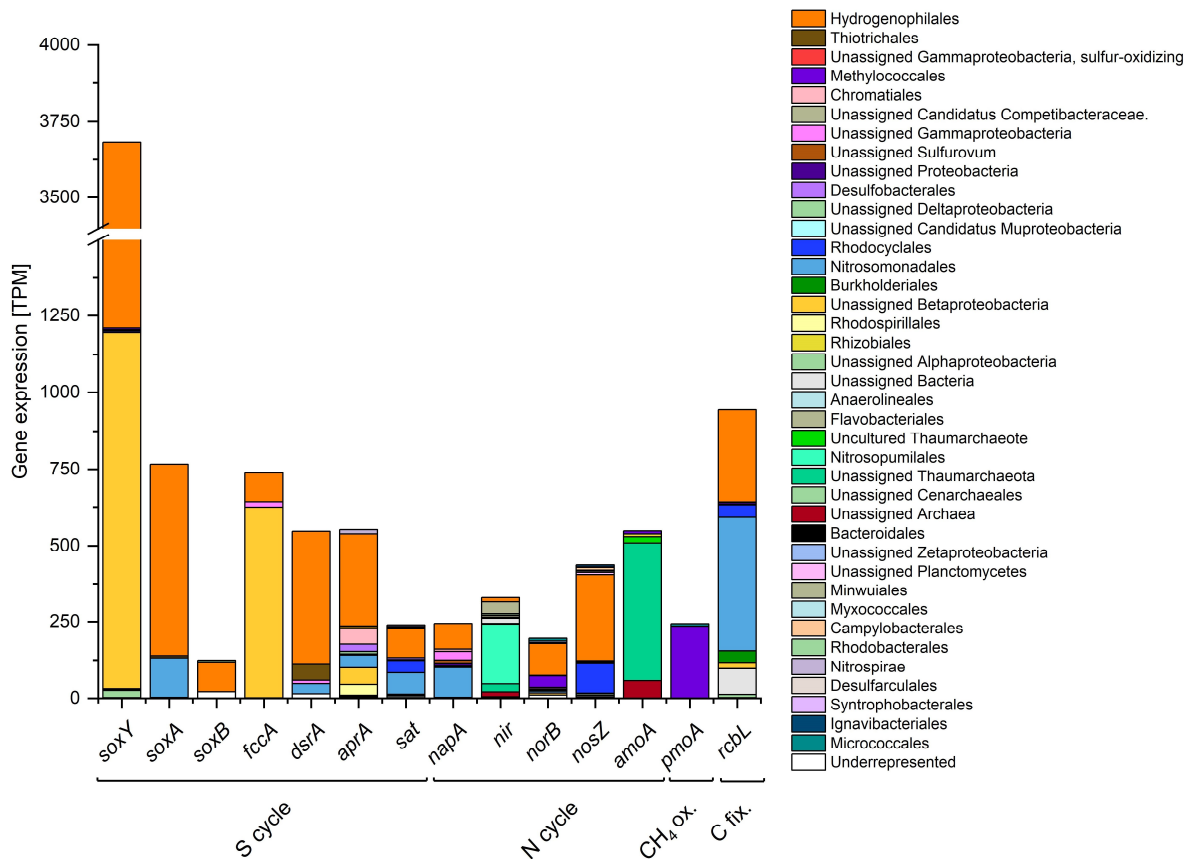
Figure 17: Taxonomic origin of transcripts of identified key marker genes. In addition to the respective gene expression levels (in transcripts per million [TPM]), the taxonomy (at the order level) of the gene-expressing organisms in the planktonic phase of the redoxclines is shown. Modified from Leberecht et al. (in revision).

The order Nitrosomonadales that belongs to the *β*-Proteobacteria also contributes to the expression level of *soxA*, *dsrA*, *aps* and *sat*, but especially to *rbcL*. In contrast to the Hydrogenophilales, the Nitrosomonadales only seem to reduce nitrate to nitrite but not further to dinitrogen. As mentioned before, the *dsrA* gene sequences of the dominant three *dsrA*-expressing orders Hydrogenophilales, Thiotrichales and Nitrosomonadales were classified as the reverse, sulfide-oxidizing form of DsrA (Supplementary Tables S4-6). To a minor part, the *rbcL* gene transcripts could also be assigned to Rhodocyclales and Burkholderiales. The transcripts of the nitrite reductases mostly originated from Thaumarchaeota of the order Nitrosopumilales, just as most of the reads of the ammonia monooxygenase subunit A gene *amoA* were from unassigned Thaumarchaeota.

In conclusion, denitrifying and sulfide-oxidizing Hydrogenophilales and the nitrate-reducing sulfide-oxidizers Nitrosomonadales (and unassigned β-Proteobacteria) were identified as microbial key players. Additionally, the ammonium oxidizing Thaumarchaeota order Nitrosopumilales stood out in the metatranscriptome by the high expression of the ammonia monooxygenase gene (*amoA*) and their high proportion of transcripts of the whole metatranscriptome (see Fig. 12).

3.2.2 The Hells Bells biofilm

To address the question of whether a biofilm on the Hells Bells surface is involved in the growth of the speleothems, a comparative study to the planktonic phase of the redoxcline was conducted. Therefore, the surface of the Hells Bells was scraped off and a metatranscriptomic and metagenomic analysis was planned using the same approach as for the planktonic phase. Since no reasonable metatranscriptome of the biofilm could be successfully generated even after several optimization attempts at sampling, the question could only be discussed based on the metagenome (Fig. 18) for the microbial community on the Hells Bells (based on a merged duplicate from the sampling campaigns in 2018 and 2020).

Figure 18: Microbial diversity of the biofilm community on Hells Bells in the redoxcline of El Zapote. The relative abundance of microbial orders is based on the taxonomic assignment of the metagenomic raw reads. Orders below a relative abundance of 1 % were grouped as underrepresented.

As already shown in the 16S rRNA amplicon-based diversity analysis (Fig. 10), the microbial communities in the redoxcline differed substantially between the planktonic and biofilm phases. This can be confirmed by the metagenome-based phylogenetic analysis (Fig. 18). As in the amplicon result, Chloroflexi dominated in the Hells Bells biofilm community. Thereby 5 % could be assigned to the order Anaerolineales, 3 % could not be classified further than to the class Anaerolineae and 13 % only broadly to the phylum Chloroflexi. In addition, 6 % unclassified δ-Proteobacteria were detected, as well as 5 % of the sulfate-reducing order Desulfobacterales, which also belong to the δ-Proteobacteria. Interestingly, in the microbial community, 3 % belonged to the Euryarchaea class of Methanomicrobia, known methanogens. According to the amplicon data, these could belong to the ANME-1b cluster. The Rhodocyclales were much lower abundant in the metagenome-based phylogenetic assemblage (3 %) than in the amplicon-based one (24 %). Together, the unclassified Planctomycetes and Planctomycetales also made up approximately 5 % of the community. All orders that made up less than 1 % of the total community were grouped as underrepresented. This made a total of 35 %.

Without a metatranscriptome that could shed light on this, it is difficult to determine which microbial metabolic pathways might actually be dominant or negligible under the *in-situ* parameters in the redoxcline. However, the phylogeny alone can already reveal some differences to the previously studied metabolic activity of the planktonic phase. The Anaerolineae are strictly anaerobic chemoorganotrophs that are often described in context of hydrocarbon degradation, fermentation and oxidation of alkanes (Liang et al., 2015; Rosenberg et al., 2014a; Yamada et al., 2006). The order Desulfobacterales (δ-Proteobacteria) is described as a taxonomic unit of sulfate reducers that also comprises known hydrogenotrophs (Burow et al., 2014). In contrast, sulfate reduction most likely plays a rather minor role in the water column of the redoxcline (see section 3.2.1). In addition, Methanomicrobia also could add methanogenesis as another metabolism that was not represented in the planktonic phase.

3.3 What distinguishes El Zapote from cenotes without Hells Bells - a comparative analysis (from a microbiological point of view)

After the metabolic and diversity profiling of the redoxcline of El Zapote with Hells Bells, the next step was to compare the hydro- and biogeochemistry of El Zapote with another cenote that also has a turbid layer and a similar water stratification but exhibits no calcite speleothems. In this context, the cenote called Angelita was chosen as it met these criteria and shares similar climatic conditions with El Zapote due to its location on the eastern Yucatán Peninsula.

At this point, it should be briefly mentioned that all sampling at cenote Angelita was done two years after the field study of cenote El Zapote with a different sampling system. Whereas cenote El Zapote was sampled with a FreeFlow bottle, which collected water over ~40 cm of water column as one sample, cenote Angelita was sampled with the double cone sampling (DCS) system (research group of Isenbeck-Schröter), which achieves a higher resolution in the 1–5 cm scale (see chapter 2.1.2). Thus, in the course of the Hells Bells research, the resolution could be significantly improved, which is very relevant considering the strong vertical gradients in the redoxcline.

3.3.1 Hydrogeochemistry of the redoxcline of cenote Angelita (devoid of Hells Bells)

Firstly, the water geochemistry of the redoxcline of cenote Angelita was analyzed during the second sampling campaign in February 2020 (simultaneously to the microbiome sampling). As mentioned above, the presented hydrogeochemical data were collected and analyzed by the cooperation partners (research group of Isenbeck-Schröter for Hydrogeochemistry and Hydrogeology, University of Heidelberg) to enable associations of microbial activity with the respective environmental conditions.

Just as for El Zapote, the focus of the water column analysis of cenote Angelita was again on the *in-situ* parameters in and around the redoxcline (Fig. 19 A). The halocline of cenote Angelita, which is indicated by the increase in electric conductivity, overlapped with the redoxcline, in which the redox potential changed significantly from about 400 mV (oxic conditions) to -200 mV (reducing conditions). The center of the redoxcline was detected at about 29.9 m of water depth. In El Zapote, the redoxcline was located just on top of the halocline (Fig. 19 B).
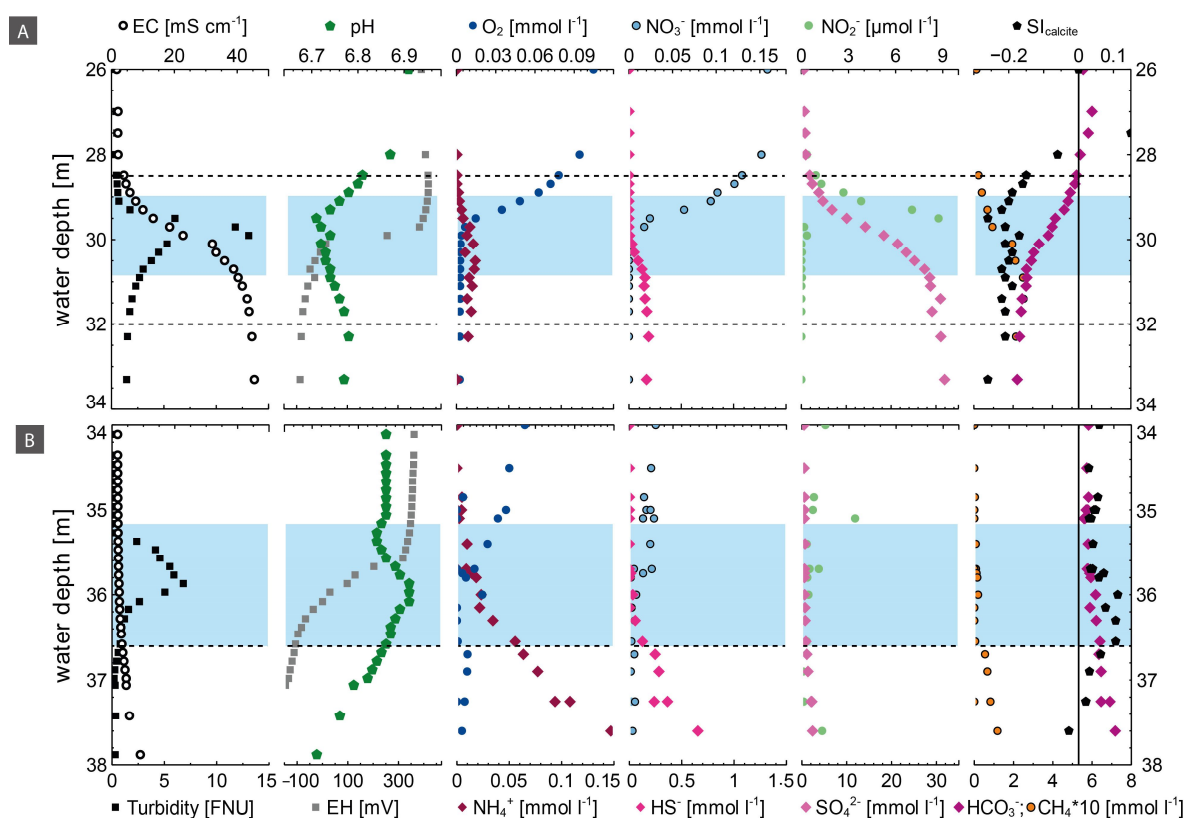
Figure 19: Comparative analysis of the hydrogeochemical profiles of the pelagic redoxcline of A) cenote Angelita (without Hells Bells) and B) cenote El Zapote (with Hells Bells). From the left to the right side, the electric conductivity (EC; in mS cm^{-1}), turbidity (in FNU), pH and redox potential (EH; in mV) are plotted. The measured concentrations of O_2, NH_4^+, NO_3^-, HS^-, NO_2^-, SO_4^{2-}; CH_4 and HCO_3^- are shown. The redoxcline is highlighted in light blue; the upper edge of the halocline is indicated by the dashed line. Data provided by the cooperation partners (research group of Isenbeck-Schröter for Hydrogeochemistry and Hydrogeology, University of Heidelberg).

In the central redoxcline, the peak value of ~15 FNU in turbidity was measured, which marked the center of the turbid layer. The maximum in turbidity could be detected at the exact same depth where sulfide appeared, and the concentration of dissolved oxygen fell below the detection limit. From above the redoxcline, the pH dropped to a minimum pH value of ~6.7 at the top of the redoxcline. Towards the bottom of the halocline and saltwater below, the pH slightly increased to 6.8. In cenote El Zapote, the opposite trend was observed with a positive pH shift in the center of the redoxcline. Compared to the redoxcline of El Zapote (with Hells Bells), the concentrations of ammonia were lower in cenote Angelita with values < 0.03 mmol l^{-1}. Roughly 2 m above the central redoxcline ~0.15 mmol l^{-1} of nitrate were measured.

The nitrate concentration decreased towards the redoxcline and showed a local minimum just above the water depth where sulfide was detectable. At the very top of the redoxcline and

halocline, the nitrite profile displayed a distinct peak in the nitrite concentration with a peak value of ~9 µmol l^{-1}. However, just a few centimeters below the concentrations fell below the detection limit. Below the redoxcline (at ~32 m water depth), the concentrations of sulfide reached about 0.2 mmol l^{-1} and decreased towards the redoxcline, where they fell below the detection limit at ~29.9 m. Much higher concentrations of sulfate were detected in cenote Angelita compared to cenote El Zapote. In El Zapote, sulfate concentrations of 0.2 mmol l^{-1} reached the bottom of the redoxcline, whereas nearly 30 mmol l^{-1} were measured in cenote Angelita. The sulfate concentrations decreased but stayed high throughout the redoxcline. Only in the freshwater zone above the redoxcline the concentrations strongly decreased. Similarly, the concentration of methane fell below the detection limit above the redoxcline. The profile of HCO$_3^-$ showed no distinct peaks but the trend of lower concentrations towards the bottom of the redoxcline and increasing availability in the freshwater above the redoxcline. The SI values for calcite predicted the opposite scenario in the redoxcline of cenote Angelita compared to El Zapote. Whereas in El Zapote the data indicated calcite supersaturation resulting from the positive pH shift in the redoxcline, in cenote Angelita decreasing and negative SI$_{calcite}$ values (that went in line with the negative pH shift) implied calcite undersaturation and dissolution.

3.3.2 Microbial diversity

Just as before for the redoxcline of cenote El Zapote with Hells Bells, a comparative diversity analysis and metabolic profiling was aimed for the microbial community in the redoxcline of cenote Angelita devoid of Hells Bells. The comparative diversity analysis based on the taxonomic annotation of the metagenomic and -transcriptomic raw reads is presented in Figure 20.

At first glance, it can be seen that the microbial composition of the communities in the two different redoxclines is very different and also that the complexity of the samples from cenote Angelita seems to be lower than from El Zapote. In both the metagenome and metatranscriptome of cenote Angelita, the photosynthetic green sulfur bacteria family Chlorobiaceae dominated significantly. This family could not be identified in cenote El Zapote. Based on the metagenome, they made up to 52 % of the community in the redoxcline, and about 57 % according to the metatranscriptome. Based on the metagenome, unassigned δ- (4 %) and γ-Proteobacteria (3 %), Helicobacteriaceae (2 %), Ectothiorhodospiraceae (3 %)

and unassigned Bacteroidetes (2 %) were still among the higher abundant microorganisms. However, these no longer appeared in the metatranscriptome-based diversity, except for the Helicobacteraceae. In the metatranscriptome, 15 % of all reads could be assigned to the family Helicobacteraceae. Apart from these, other δ-Proteobacteria were also identified as the dominant group in the metatranscriptome of cenote Angelita, such as unassigned *Sulfurovum* (4 %) and the family Campylobacteraceae (9 %).
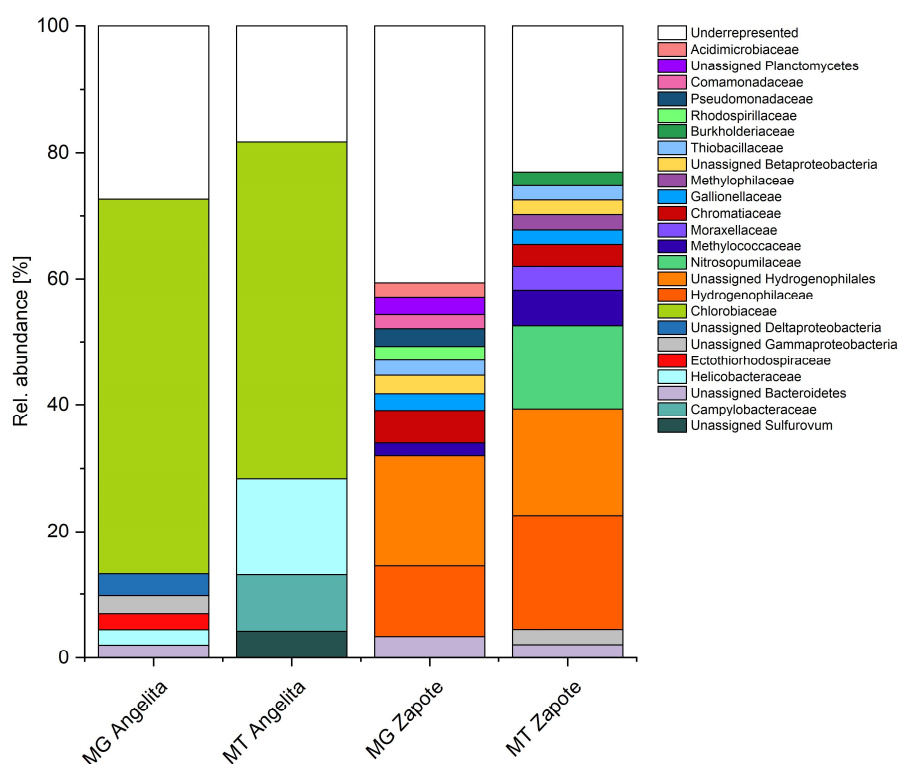
Figure 20: Microbial diversity of the planktonic phase of the redoxclines of cenote Angelita (without Hells Bells) and El Zapote (with Hells Bells). For both cenotes, the relative abundance of microbial families based on the taxonomic assignment of metatranscriptomic (MT) and metagenomic (MG) raw reads are shown.

Underrepresented families (< 2 %) accounted for approximately 27 % in metagenome and 18 % in metatranscriptome. Those families identified as dominant or even key players in cenote El Zapote with Hells Bells were not found among the higher abundant groups in cenote Angelita without Hells Bells and vice versa. Excluding the underrepresented families, it could be said that the microbial redoxcline communities have no commonalities with regard to the phylogenetic composition (except for unassigned Bacteroidetes).

3.3.3 Cenote Angelita - dominant metabolic pathways and microbial key players

Now that the processes of denitrification, ammonium oxidation, autotrophy and sulfide oxidation have been identified as key processes in the redoxcline of El Zapote with Hells Bells, the question arises as to what distinguishes the redoxcline of Angelita without Hells Bells in terms of the microbial ecology. Using the same approach as previously applied to El Zapote, a metabolic profile was established for the microbial community in the redoxcline of cenote Angelita. As before, the transcript abundances of genes involved in the nitrogen, sulfur and methane cycle were additionally plotted in context of the metabolic reaction network (Fig. 22, 24 and 26).

In the nitrogen cycle (Fig. 21 and 22), the microbial community of cenote Angelita's redoxcline highly expressed *napA*, the gene encoding the catalytic subunit of the nitrate reductase, with 773 TPM.
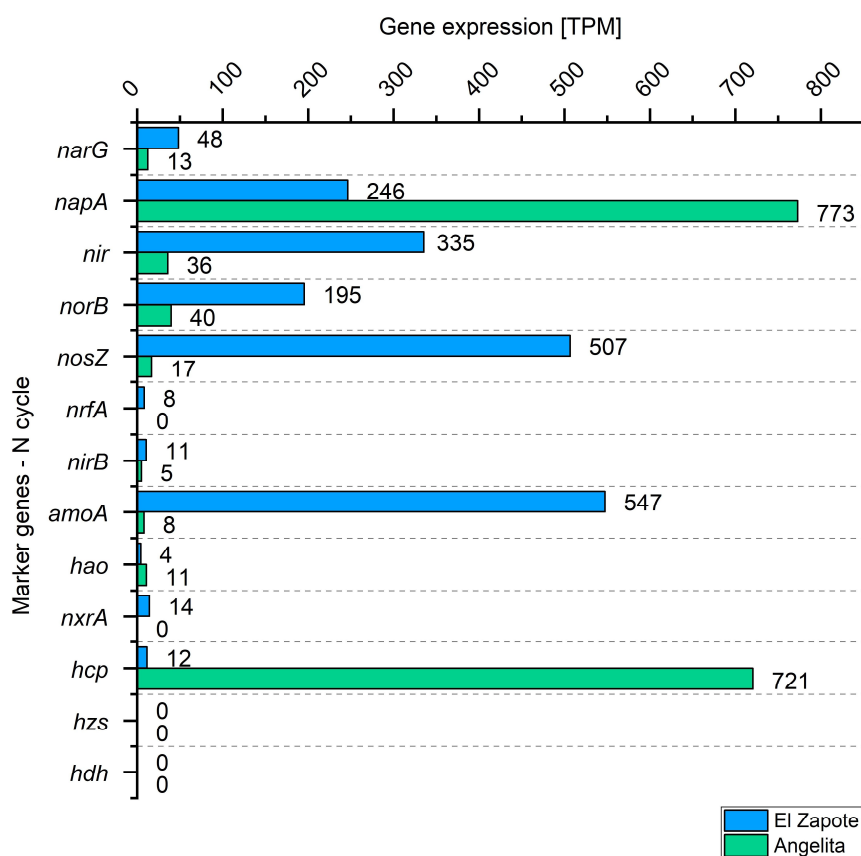
Figure 21: The metatranscriptomic analysis revealed dominant microbial metabolic pathways of the nitrogen cycle. The gene expression levels were calculated in transcripts per million (TPM). For a comparative analysis, the respective transcript abundances in the metatranscriptome of the redoxcline of cenote El Zapote with Hells Bells (shown in blue) and Angelita without Hells Bells (shown in green) are included.

NarG and all other genes relevant for the complete denitrification process from nitrate to dinitrogen were much less expressed (*narG* 48 TPM, *nir* 36 TPM; *norB* 40 TPM; *nosZ* 17 TPM). This was particularly evident for *nosZ*. The abundance of transcripts of *nrfA* and *nirB*, which are relevant for the process of ammonification were similarly low for both redoxcline communities (El Zapote and Angelita $\leq$ 11 TPM). Since the genes *amoA, hao* and *nrx*, which catalyze the process of nitrification from ammonium to nitrate, were only marginally expressed (Fig. 22), this process seems to play a minor role in the central redoxcline of cenote Angelita. In contrast, in El Zapote the *amoA* gene was highly expressed.
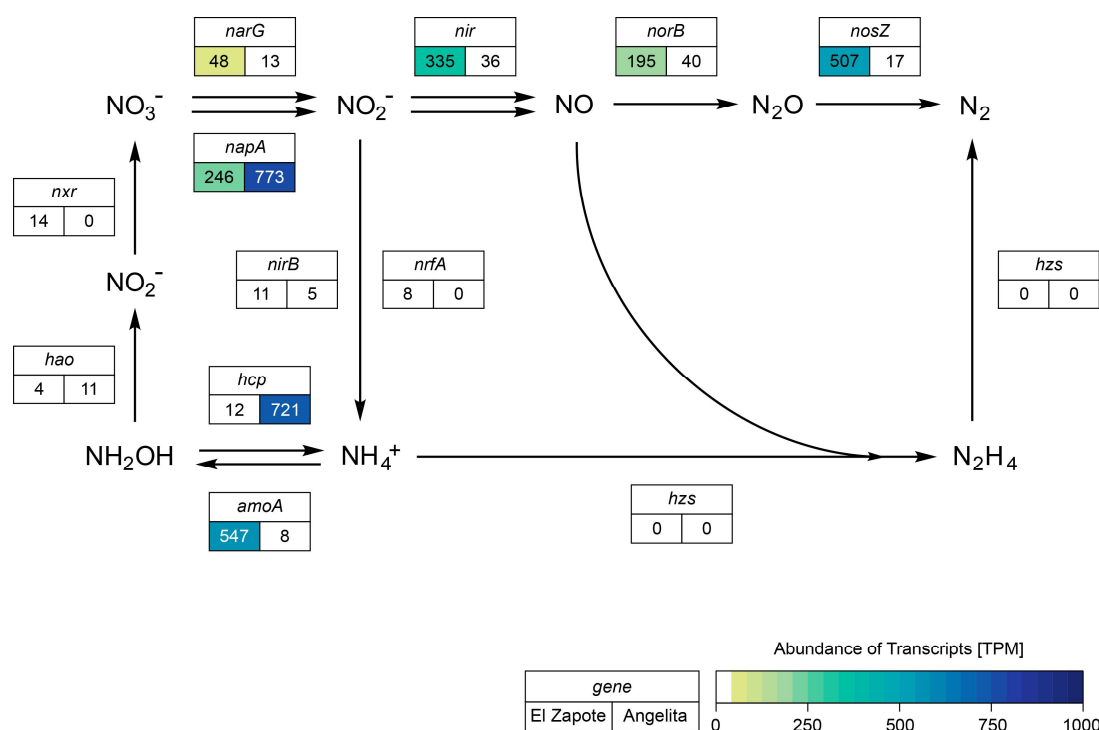
Figure 22: Metatranscriptomic analyses revealed the differential gene expression profiles of genes encoding enzymes that are involved in the nitrogen cycle of cenote Angelita and El Zapote. The gene expression levels were calculated in transcripts per million (TPM). For a comparative analysis, the respective transcript abundances in the metatranscriptome of the redoxcline of cenote El Zapote (with Hells Bells) and Angelita (without Hells Bells) are shown. Scheme based on Alvarez et al. (2014) and Rodionov et al. (2005).

During the evaluation of the gene expression levels of all genes of the nitrogen cycle, a gene was discovered in the metatranscriptome of cenote Angelita that had not been addressed here before. It was annotated as hydroxylamine reductase (gene name hybrid cluster protein; *hcp*) and is described in the context that it could be involved in the detoxification of by-products of the N cycle such as hydroxylamine. The *hpc* gene reached a transcription level of 721 TPM

in cenote Angelita and 12 TPM in metatranscriptome of cenote El Zapote. In both redoxclines however, the typical ANAMMOX genes *hzs* and *hdh* were not expressed at all (0 TPM).

As depicted in Figure 22, the two redoxclines differed in the nitrogen cycle mainly in the fact that in El Zapote a complete denitrification pathway seemed to be in place instead of an incomplete reduction of nitrate to nitrite (via NapA) as in cenote Angelita. In addition, only in the redoxcline of El Zapote ammonium oxidation seemed to be relevant. This assumption corresponds to the hydrogeochemical data, since ammonium oxidation was only indicated by the increasing concentration of nitrite at the upper edge of the redoxcline but not in the center of the redoxcline. Nitrite production by nitrate reduction was not observed in the hydrogeochemical profiles.

The metatranscriptomic results of the sulfur cycle of both redoxcline communities are shown in Figure 23 and 24. Between the two redoxcline communities a few differences in the expression of genes encoding periplasmic proteins involved in sulfur oxidation were discovered. The *soxY* (149 TPM), *soxZ* (265 TPM) and *soxA* (70 TPM) gene transcripts were much less abundant in the redoxcline of cenote Angelita than in El Zapote. Also, *soxB* was expressed only about one third as high (48 TPM). However, *soxC* was expressed by the redoxcline community of cenote Angelita (287 TPM), which was not the case in El Zapote. *SoxD* gene transcripts from the *soxCD* complex were not detected (0 TPM).

The expression of *soxCD* and potentially the presence of SoxCD enzymes could mean that the sulfur oxidizers in cenote Angelita do not need to use the pathway via sulfur globules to regenerate SoxYZ but use SoxCD for this step. Further differences were found in the transcription of genes encoding alternative enzymes that also catalyze sulfur oxidation in the periplasm. The flavocytochrome *c* (*fccAB*) genes were ten times lower expressed in the redoxcline of cenote Angelita (70 TPM), whereas transcript of the membrane-bound sulfide:quinone oxidoreductase (*sqr*) were ten times higher abundant (300 TPM) compared to El Zapote. The sulfur oxygenase reductase (*sor* 0 TPM) was not identified on the transcriptome level in neither of the two meta data sets. The two redoxcline microbiomes actively expressed the cytoplasmic enzymes DsrAB, AprAB and Sat that are involved in both sulfide oxidation and sulfate reduction. In detail, microorganisms involved in the sulfur cycle of cenote Angelita highly expressed *dsrA*/*B* with 524 TPM/171 TPM, *aprA*/*B* with 359 TPM/ 456 TPM and *sat* with 266 TPM.
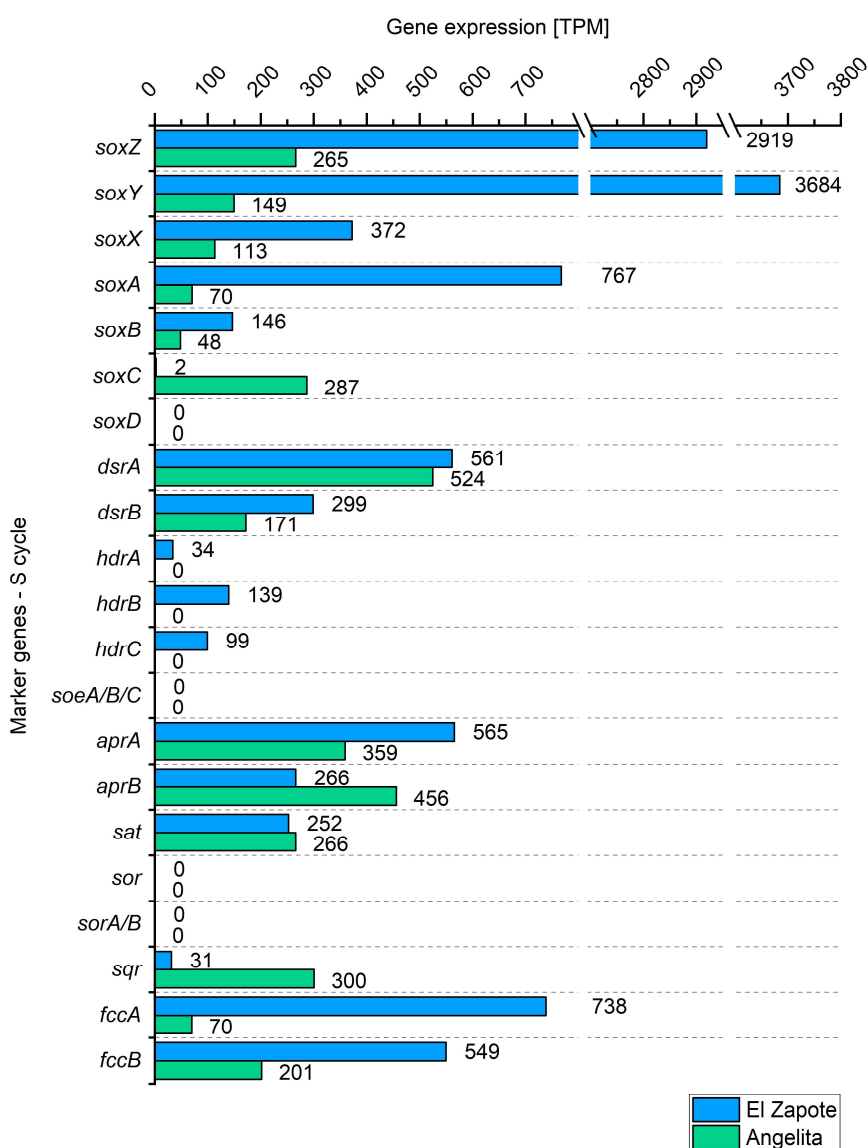
Figure 23: Dominant microbial metabolic pathways of the sulfur cycle. The transcript abundances were calculated in transcripts per million (TPM). Gene expression levels of genes involved in the sulfur cycle are shown for the redoxcline community of Angelita without Hells Bells (shown in green) and cenote El Zapote with Hells Bells (shown in blue).

As before for El Zapote, the question whether the microorganisms catalyze either sulfide oxidation or sulfate reduction should also be answered for the redoxcline community of cenote Angelita, since these three enzymes play a role in both contrasting processes. Therefore, another classification of the *dsrA* genes to the oxidative or reductive type of encoded DsrA was also performed for the dominant *dsrA*-expressing orders. For the Nitrosomonadales, Chlorobiales, Chromatiales and unassigned γ-Proteobacteria the *dsrA* gene sequences were confirmed as the reverse, oxidative form of DsrA. The BLAST result for the *dsrA* gene of Thiotrichales yielded only insufficient *e*-values for an exact

classification. However, as Thiotrichales are described as a sulfur-oxidizing order the *dsrA* transcripts should also be considered as the sulfide oxidizing form (Supplementary Table S7-11). The heterodisulfide reductase (*hdrA/B/C*) genes that were expressed by the community in the cenote El Zapote redoxcline (34/139/99 TPM) were not expressed at all in the redoxcline of cenote Angelita. The respective genes of the membrane-bound sulfite oxidoreductase SoeABC were not expressed at all in neither of the two environmental settings. Thus, the contribution of SoeABC to the oxidation of sulfite in the cytoplasm seemed to be negligible in both cases.
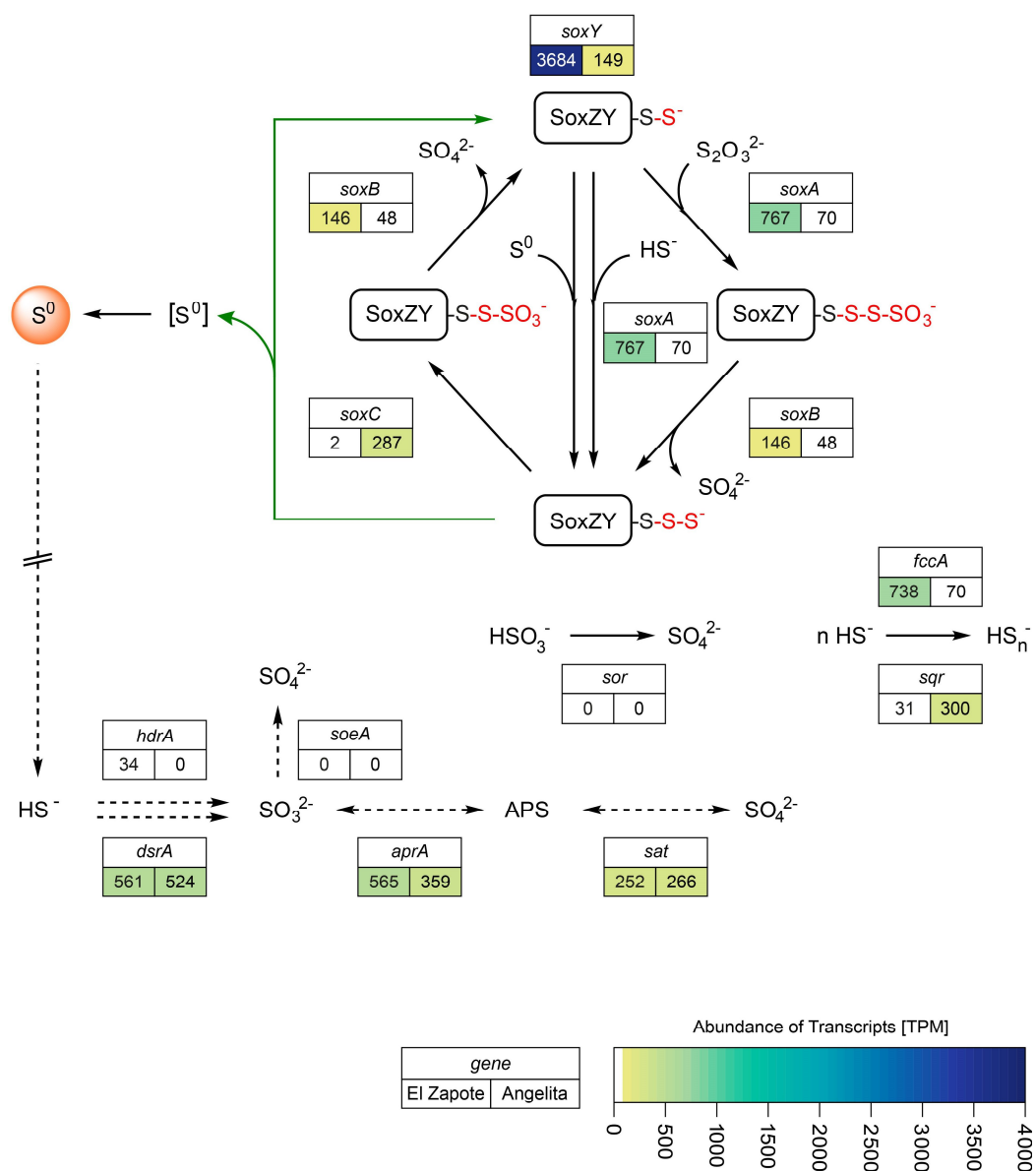
Figure 24: The sulfur cycle – metatranscriptomic profiles of the redoxcline communities of cenote Angelita (without Hells Bells) and El Zapote (with Hells Bells). The transcript abundances were calculated in transcripts per million (TPM). Scheme based on Alvarez et al. (2014) and Rodionov et al. (2005).

Besides the nitrogen and sulfur cycle, the process of photosynthesis was also addressed in the metatranscriptome-based metabolic profiling of the redoxcline community of cenote Angelita (Fig. 25).
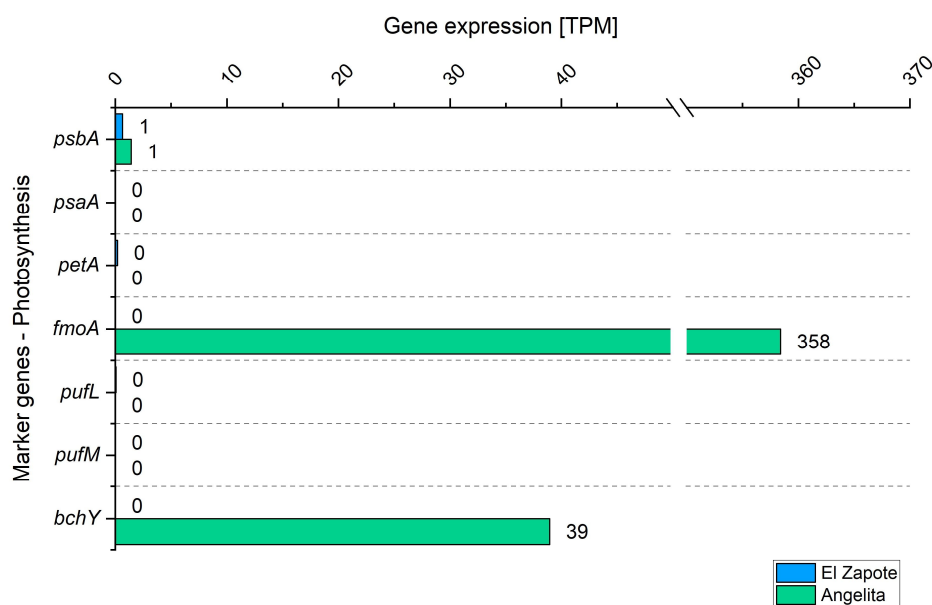
Figure 25: Transcription levels of genes involved in photosynthesis. The gene expression levels were calculated in transcripts per million (TPM). The gene expression profiles of the redoxcline community of cenote El Zapote with Hells Bells (shown in blue) and Angelita without Hells Bells (shown in green) are included.

It was noticed that among the observed genes related to photosynthesis, only two were expressed (> 1 TPM). These two genes encode BchY and the Fenna-Matthews-Olson protein FmoA. As a bacteriochlorophyll, FmoA is involved in the energy transfer from chlorosomes to the reaction center located at the cytoplasmic membrane of green sulfur bacteria. Thus, the *fmoA* gene is a specific marker for anoxygenic photosynthesis conducting green sulfur bacteria and Chloroacidobacteria (Imhoff, 2016). The *fmoA* gene expression level reached 358 TPM.

The second actively expressed gene, *bchY*, is another but more general marker gene for anoxygenic phototrophs as oxygenic phototrophs lack this gene. It encodes the chlorophyllide a reductase subunit Y, which is relevant for the biosynthesis of bacteriochlorophyll (Imhoff, 2016). 39 TPM could be calculated for the respective transcript abundance. Lastly, the third marker for anoxygenic photosynthesis, the *pufLM* genes, were not expressed by the microbial community in the redoxcline. These genes are specific for all phototrophic purple Proteobacteria and Chloroflexaceae and encode proteins of the reaction

center of the bacterial type II photosystem (Imhoff, 2016). Transcripts of genes of the PS I chlorophyll a apoprotein A1 (PsaA), the PS II reaction center D1 protein (PsbA), apocytochrome f of the cytochrome *b6f* complex (PetA), the bacteriochlorophyll synthesizing enzyme *BchP* were hardly transcribed in the redoxcline of cenote Angelita, just like in El Zapote (< 1 TPM).

Considering the determined microbial diversity in the redoxcline of cenote Angelita, the high abundance of *fmoA* transcripts as marker for anoxygenic photosynthesis conducting green sulfur bacteria goes in line with the high presence of Chlorobiales. Whereas anoxygenic photosynthesis thus seems to be a key process in the redoxcline of cenote Angelita without Hells Bells, this was not the case in El Zapote.

In the methane cycle, a few more differences between the two redoxcline communities can be identified (Fig. 26). While in El Zapote the particulate methane monooxygenase was expressed with 243 TPM, no transcripts were found in the metatranscriptome of cenote Angelita (*pmoA* 0 TPM). This was also true for the genes of the methanol (*mxaF* 0 TPM) and formaldehyde dehydrogenase (*fdhA* 0TPM). However, 43 TPMs could be assigned to the gene encoding the formate dehydrogenase. Just as in Zapote, no *mcrA* transcripts could be found that could be relevant for methanogenesis or in the reverse process of anaerobic methane oxidation.
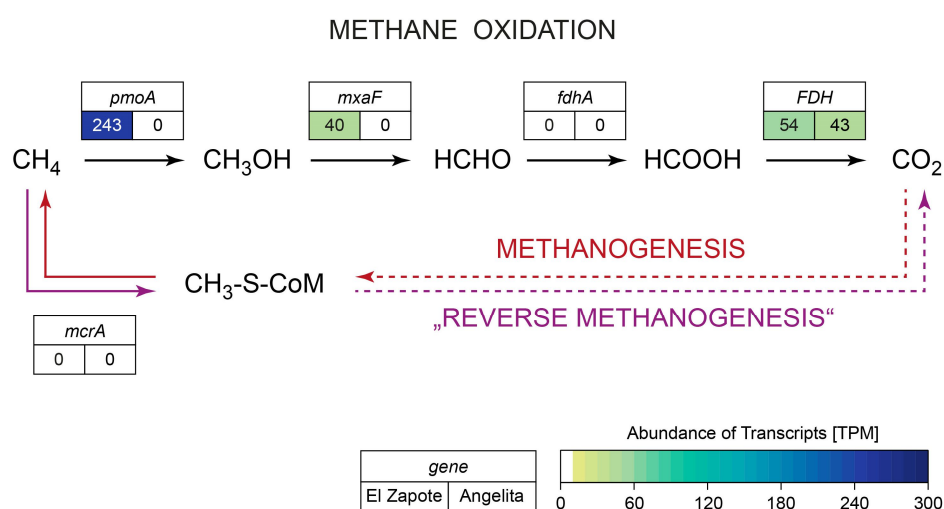
Figure 26: Transcript abundances of genes encoding enzymes that are involved in the methane cycle of cenote Angelita and cenote El Zapote. The gene expression levels were calculated in transcripts per million (TPM) and are shown in context of the respective catalyzed reaction.

Among the autotrophic pathways, differences in transcription profiles were again revealed between the two cenotes (Fig. 27).
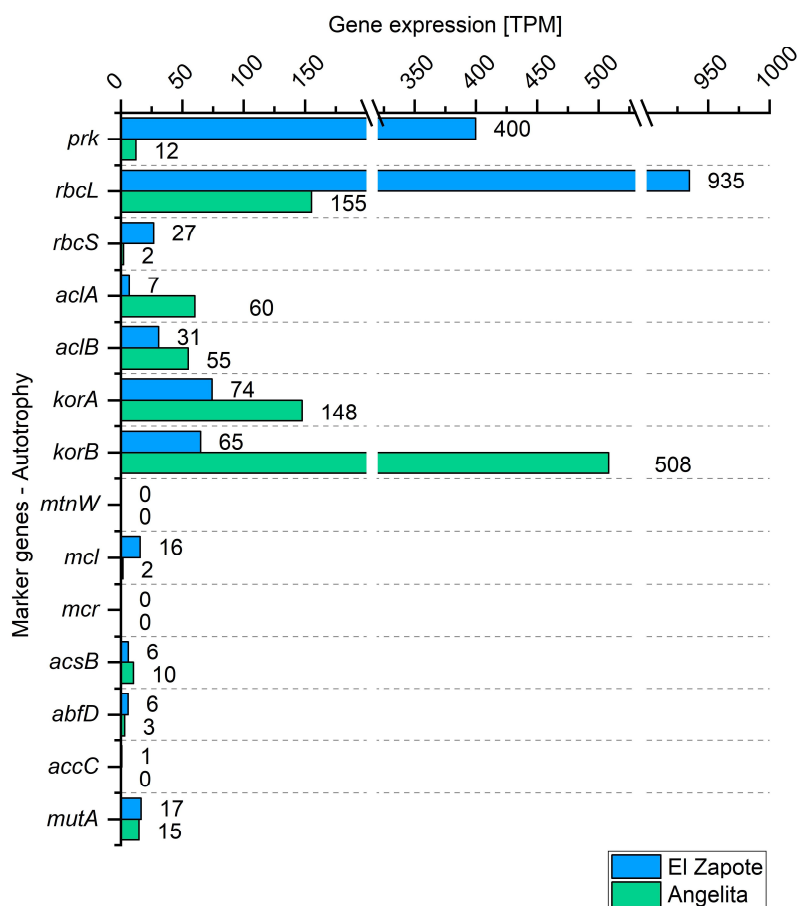
Figure 27: The metatranscriptomic analysis revealed the transcription levels of genes involved in different autotrophic pathways. The respective transcript abundances [TPM] in the metatranscriptome of the redoxcline of cenote El Zapote with Hells Bells (shown in blue) and Angelita without Hells Bells (shown in green) are included.

While the metatranscriptome of cenote El Zapote clearly showed the highest expression for genes of the Calvin cycle, the phosphoribulokinase (*prk* 12 TPM) and rubisCo large chain (*rbcL* 155 TPM) were less expressed in the redoxcline of cenote Angelita. In contrast, all genes of the rTCA cycle exceeded the respective transcript levels of El Zapote. This concerned the ATP citrate lyase (*aclA* 60 TPM; *aclB* 55 TPM) and especially the 2-oxoglutarate ferredoxin oxidoreductase (*korA* 148 TPM; *korB* 508 TPM). The marker gene *mtnW*, which encodes the 2,3-diketo-5-methylthiopentyl-1-phosphate enolase of the cysteine and methionine metabolism, was in both redoxcline communities hardly expressed (0 TPM). Just like in the redoxcline of El Zapote, the genes *mcl* (encoding the malyl-CoA/(S)-

citramalyl-CoA lyase; 2 TPM) and *mcr* (encoding the malonyl-CoA reductase; 0 TPM) of the 3-HP bicycle were only marginally expressed.

Transcripts of the marker gene of the Wood-Ljungdahl pathway, the acetyl-CoA synthase (*acsB*), were also only low abundant in both metatranscriptomes (El Zapote 6 TPM; Angelita 10 TPM). The transcript abundances of the three marker genes involved in the 3-HP-4-HB cycle were quite similar in both cenotes, with and without Hells Bells. The acetyl-CoA/propionyl-CoA carboxylase (*accC*; El Zapote 1 TPM; Angelita 0 TPM), the methylmalonyl-CoA mutase (*mutA*; El Zapote 17 TPM; Angelita 15 TPM) and the 4-hydroxybutyryl-CoA dehydratase (*abfD*; El Zapote 6 TPM; Angelita 3 TPM) transcripts reached only 17 TPM at maximum. Taken together, based on the transcript abundances, the Calvin cycle was not the only dominant metabolic pathway used for carbon dioxide fixation in cenote Angelita. The marker genes were much lower expressed compared to El Zapote. Additionally, the rTCA cycle might be another important autotrophic pathway in the redoxcline of cenote Angelita.

In conclusion, the comparative metatranscriptomic analysis revealed that the process of photosynthesis is most likely a major energy metabolism in cenote Angelita without Hells Bells, which was not the case in the redoxcline of El Zapote. Furthermore, carbon dioxide fixation mainly occurs via the Calvin and rTCA cycle. The oxidation of sulfide apparently does not only play an important role in cenote El Zapote, but also in cenote Angelita. In the nitrogen cycle, the two cenotes mainly differed in the expression of genes of the denitrification pathway. While in El Zapote all genes for the complete denitrification were expressed, only transcripts of the nitrate reductase were highly abundant in Angelita. After these findings, the next question to be addressed was, if the redoxcline communities to be compared share the same microbial key players or if the microbial community differs significantly between the two cenotes.

With the same approach as described for the El Zapote redoxcline community, the key gene expressing microbes were also determined for cenote Angelita (Fig. 28). For the sulfur cycle, which includes the *sox* genes, *fccA*, *sqr*, *dsrA*, *aprA* and *sat*, it is clearly shown that the Chlorobiales (phylum Chlorobi) represented a dominant order.
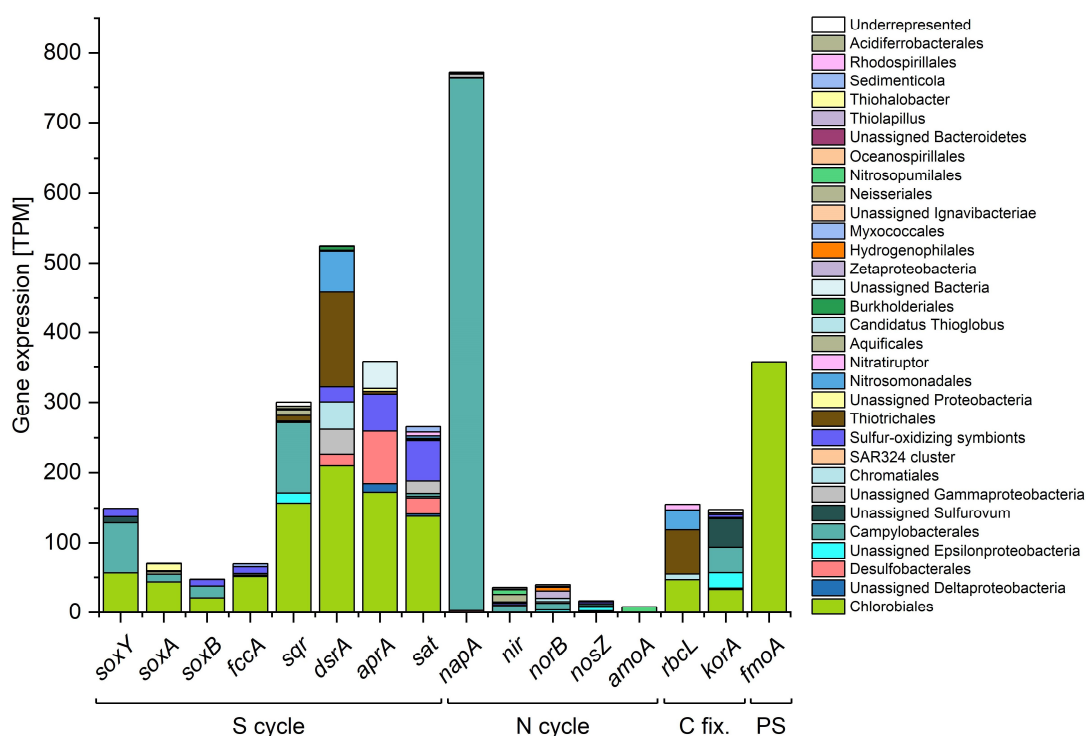
Figure 28: Taxonomic assignment of transcripts of key marker genes from the redoxcline community of cenote Angelita. The respective transcript abundances [TPM] and the taxonomy (at the order level) of the gene-expressing organisms in the planktonic phase of the redoxcline of cenote Angelita (without Hells Bells) are shown.

Besides the Chlorobiales, the order of Campylobacterales, which belong to the ε-Proteobacteria, were identified as key players in the sulfur cycle of the redoxcline of cenote Angelita. However, these only dominated in the expression of genes encoding periplasmic sulfur oxidation enzymes (*sox*, *fccA* and *sqr*). In contrast, the Desulfobacterales only showed transcripts of cytoplasmic enzymes (*dsrA*, *aprA*, *sat*). Apart from green sulfur bacteria, genes of cytoplasmic enzymes involved in the sulfide oxidation and sulfate reduction (*dsrAB*, *aprAB*, *sat*) were also expressed by the orders Thiotrichales, Desulfobacterales, Nitrosomonadales and unassigned γ-, ε- and δ-Proteobacteria. As described above, the BLAST against the *dsrAB* gene database (Müller et al., 2015) allowed the classification of the *dsrA* sequences of the order Chlorobiales, Chromatiales, Nitrosomonadales and unassigned γ-Proteobacteria as the oxidative type of DsrAB to catalyze the sulfur oxidation pathway (Supplementary Tables S7-11).

Among genes of the denitrification pathway (*napA*, *nir*, *norB*, *nosZ*), only the catalytic subunit of the nitrate reductase *napA* was dominantly expressed. *NapA* gene transcripts could

almost exclusively be assigned to the Campylobacterales. The ammonia monooxygenase subunit A (*amoA*) genes were only expressed by the Thaumarchaeota order Nitrosopumilales. Similar to the taxonomic distribution of *dsrA*-expressing orders, the large subunit of the RubisCo was mainly transcribed by Thiotrichales and Nitrosomonadales.

In summary, the community in the redoxcline of cenote Angelita (devoid of Hells Bells) differs in several aspects from the one studied at El Zapote (with Hells Bells). Mainly Chlorobiales and Campylobacterales were identified as dominant in the key processes in the redoxcline of cenote Angelita, which were not represented in El Zapote. Therefore, one of the most striking differences is that the process of anoxygenic photosynthesis by Chlorobiales plays a decisive role, which was not the case in El Zapote. Furthermore, among all genes relevant for the complete denitrification, only *napA* was highly expressed. Additionally, *amoA,* which is involved in the oxidation of ammonia, was less abundant on the metatransciptomic level than in El Zapote.

3.4   Proofing the hypothesis on the laboratory scale

After the metagenomic and -transcriptomic profiling of the microbial community in the redoxcline of cenote El Zapote (with Hells Bells), the working hypothesis evolved that the order Hydrogenophilales may promote local calcite precipitation by nitrate-dependent sulfide oxidation and autotrophic growth. Most likely, oxidant-deficiency in the redoxcline sets the foundation for an incomplete sulfide oxidation with the product of elemental sulfur instead of sulfate. The next aim was to test this hypothesis by mimicking the environmental conditions as they are in the redoxcline of cenote El Zapote and to proof calcite precipitation by these bacteria on the laboratory scale. For this purpose, the microbial key players of the order Hydrogenophilales had to be isolated from the complex community in the redoxcline. As the different enrichment and isolation approaches were not successful over a period of nine months, an alternative organism was sought that came closest to the Hydrogenophilales from the metabolic point of view and thrives under similar conditions. Therefore, *Thiobacillus denitrificans* was chosen, an obligate chemolithoautotrophic, facultatively anaerobic, Gram-negative *β*-Proteobacterium that also uses the Sox system for sulfur oxidation (Beller et al., 2006) like the Hydrogenophilales.

A minimal mineral medium saturated with calcium carbonate containing sulfide as electron donor and nitrate as electron acceptor (ratio 10:1) was designed to mimic the water chemistry of the redoxcline (see section 2.2.4). The meandric microfluidic chips system was chosen as the cultivation environment, which on the one hand allowed to create gradients along the chip (Hansen et al., 2019), but as a flow-through system also provided constant conditions through the permanent supply of fresh medium with electron acceptor and donor. A duplicate of chips inoculated with *T. denitrificans* was complemented with an abiotic control to verify that calcite precipitation only occured in presence of the sulfur oxidizer.

Four weeks after the inoculation of the meandric chip systems with *T. denitrificans*, the cultivation and abiotic control chips were examined microscopically to analyze if calcium carbonate crystals could be identified. *T. denitrificans* had not yet formed a dense biofilm at this time, but many individual cells could be observed (Fig. 29). In fact, in both cultivation chips crystals were observed. In the abiotic control, however, no cells and crystals could be found throughout the chip. The crystals appeared in a rhombohedral shape. Although the flow-through system only allowed a simplified simulation of the highly complex hydrogeochemistry of the redoxcline, the fact that crystals were detected only in the cultivation chip but not in the abiotic control indicates that the precipitation was based on the presence and metabolic activity of *T. denitrificans*.
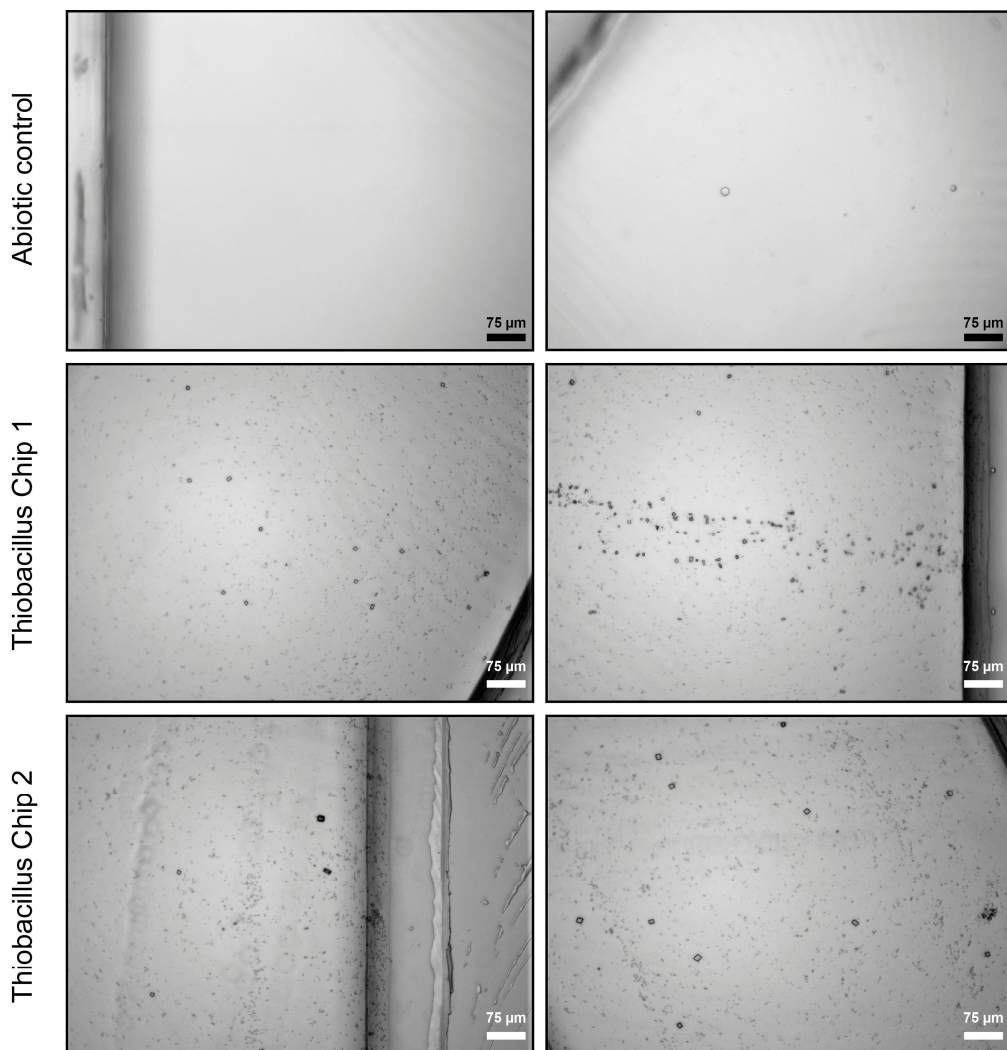
Figure 29: Simulation experiment of calcite precipitation by *Thiobacillus denitrificans* in the meandric chip system. *T. denitrificans* was cultured for four weeks in a redoxcline-derived medium in meandric chip systems (in a dublicate). Subsequently, the abiotic control and the dublicate were examined for the occurrence of carbonate crystals. Images were acquired using Leica microscope type DM5500B through a 10× bright field objective.

3.5 Isolation of Thaumarchaeota

In the context of this study on the microbial ecology and diversity in the redoxcline of El Zapote, the phylum of Thaumarchaeota has attracted attention by its high contribution of transcripts to the total metatranscriptome (13 %; Fig. 12). This was surprising for two reasons. Firstly, Thaumarchaeota made up less than two percent of the whole community. And secondly, Thaumarchaeota are known for a very slow growth with generation times > 20 h (in culture even 23 days are reported (Rosenberg et al., 2014a; Tourna et al., 2011)).

The idea arose that the Thaumarchaeota from the redoxcline of El Zapote could be an interesting and challenging candidate for an ongoing project in the research group that revolves around the cultivation of so far non-cultivable microorganisms. In detail, a subproject focuses on the development of an antibody-based approach that allows specific enrichments of microorganisms from complex environmental samples based on metagenomic and metatranscriptomic data.

This approach is based on secondary antibodies that are coupled to magnetic beads (Fig. 30). These beads are incubated with the primary antibody to allow the secondary antibody to bind to the primary one. The target cells bind to the primary antibody and can be isolated from the complex community via the magnetic bead-antibody-cell complex. A more detailed description of the isolation protocol is given in section 2.2.5.
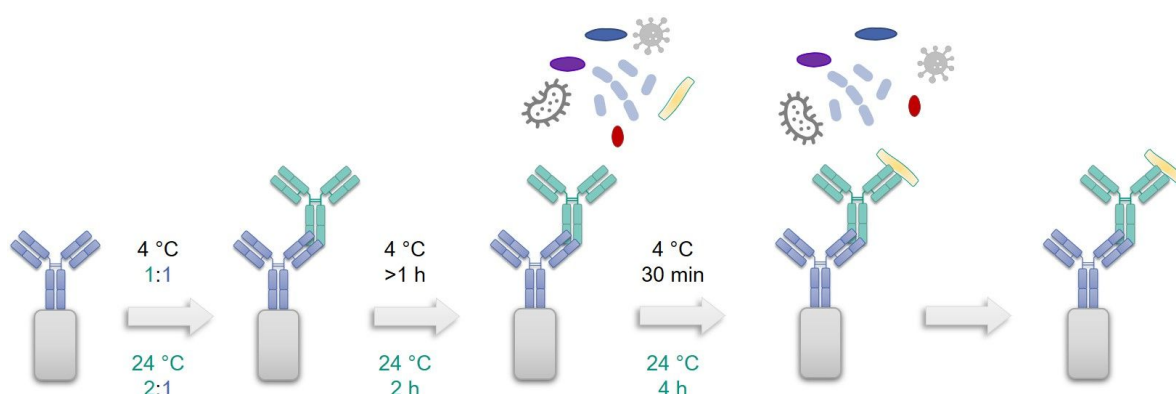
Figure 30: Workflow of the antibody-based pulldown method. In the first step, the desired primary antibody is bound to the magnetic bead-coupled secondary antibody. After four washing steps (using a magnetic rack), the complex microbial community is incubated with the cells of interest. The primary antibody binds to the epitope on the target cells. Subsequently, the magnetic bead-antibody-cell complex is separated from the bead supernatant by applying a magnetic field and the bound cells remain in the bead pellet. Parameters listed above the arrows correspond to the standard protocol (from New England BioLabs, Goat Anti-Rabbit IgG Magnetic Beads Protocol), those written below the arrows in green correspond to the parameters optimized for the isolation of Thaumarchaeota. These optimizations include a higher incubation temperature (24 °C), a higher primary:secondary antibody ratio (2:1) and longer incubation times.

In order to adapt this isolation method specifically to Thaumarchaeota from the upper redoxcline of El Zapote, first of all an appropriate cell surface protein needed to be defined as an antigen to which the primary antibody can bind. In this case, the determination of an optimal antigen was very simple. In fact, the group of Thaumarchaeota was also selected for this project because the metatranscriptomic analysis revealed that the ammonium oxidizers highly expressed a selection of genes that encode surface layer (S-layer) proteins. Among

those, the "Putative PKD domain protein", "S-layer protein" and "S-layer domain-containing protein". In total, almost 22 000 TPM were assigned to these genes.

In this context, the unspecified, in total 751 amino acids (AA) long "S-layer protein" was studied in more detail. Since a complete gene sequence related to this particular protein could not be found or assembled in the metagenome, the protein sequence of the common best hit in the Uniprot database (ID A0A388QJN8_9ARCH; 78.5 kDa in size) was used. Using the protein transmembrane helices prediction tool TMHMM (Krogh et al., 2001), it could be determined that AA 1-11 of the S-layer protein extend into the periplasm, AA 12-34 form a transmembrane domain, and AA 35-751 are most likely located extracellularly.

Subsequently, a protein structure modelling was performed using the Iterative Threading ASSEmbly Refinement (I-TASSER) server (Roy et al., 2010; Yang et al., 2015; Yang & Zhang, 2015). A boomerang-like structure was obtained as the most likely model for the Thaumarchaeota S-layer protein (Fig. 31). Based on this model, the N-terminal domain of the S-layer protein exhibits α-helices, whereas the C-terminal boomerang structure mainly consists of β-sheets. Finally, this protein was chosen as the target for the antibody-based isolation method. Therefore, the next step was to find an appropriate epitope that is freely accessible to an antibody and optimally exhibits no glycosylation site. Additional factors such as antigenicity, charge of the peptide and hydrophobicity were also taken into account. In the extracellular domain of the protein, the peptide sequence "ANRNSRADEDLDVN" (from AA 503-516) was finally identified as the optimal epitope of the antigen (Fig. 31).

Finally, the first experiments on the isolation of Thaumarchaeota from the upper redoxcline of El Zapote were initiated using the corresponding antibody against this S-layer protein epitope. The isolation procedure according to the standard protocol (from New England BioLabs, Goat Anti-Rabbit IgG Magnetic Beads Protocol) was not successful for Thaumarchaeota, until some adjustments were made (Fig. 30). Every incubation step was conducted at 24 °C, which reflects the temperature in the upper redoxcline of El Zapote, instead of 4 °C. The incubation time of the complex of magnetic beads coupled to the primary and secondary antibody together with the cells of interest was prolonged to 4 h (instead of 30 min). Furthermore, the ratio of the primary to the secondary antibody was adjusted to 2:1 (instead of 1:1) and cells in the redoxcline sample were pelleted, concentrated and

resuspended in Thaumarchaeota redoxcline medium, in which the antibody-based isolation approach was conducted.
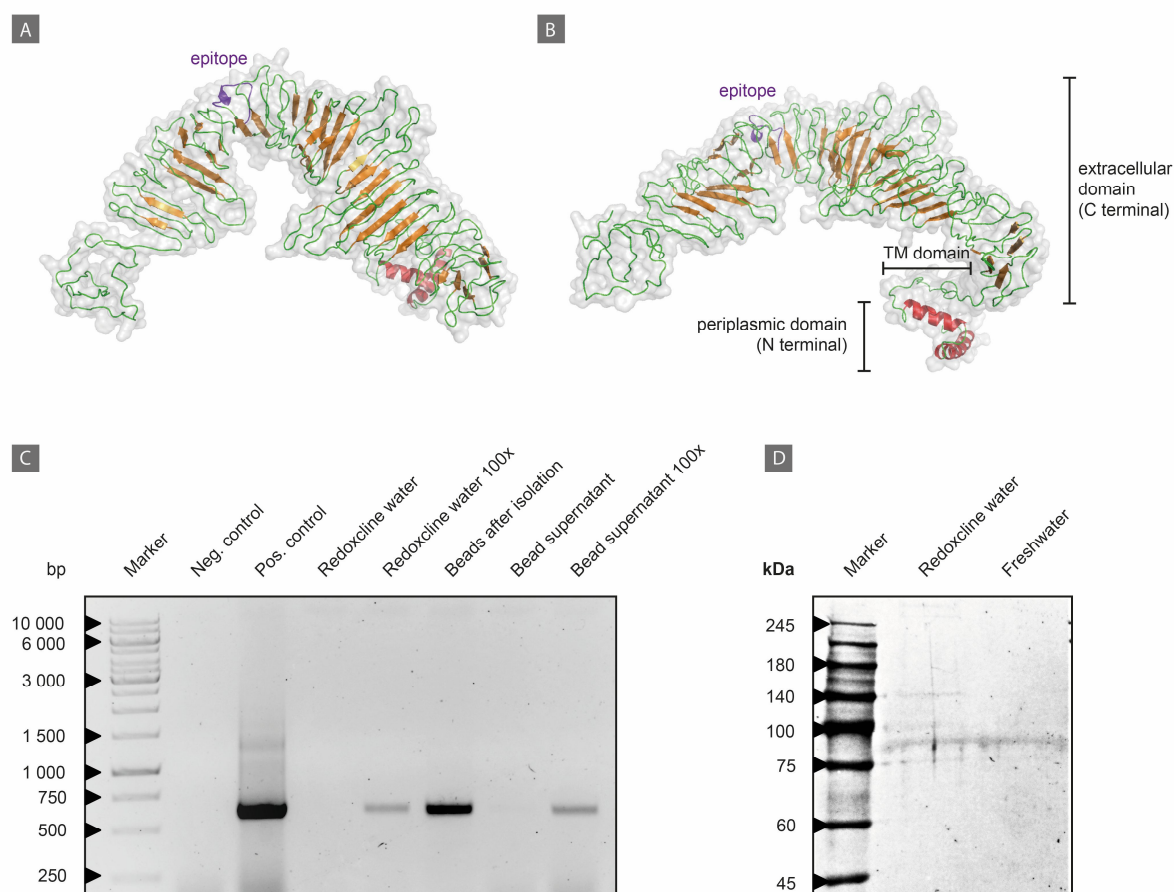
Figure 31: Isolation of Thaumarchaeota via the antibody-based pulldown method. A) Top view on the stucture model of the highly expressed S-layer protein of Thaumarchaeota from the redoxcline of El Zapote. The peptide and epitope of this protein as the target for the respective antibody for the isolation approach is highlighted in purple. B) Side view on the structure model showing the periplasmic, transmembrane (TM) and extracellular domain of this S-layer protein. C) PCR results on the ammonia monooxygenase subunit A (*amoA*) of archaea loaded on an agarose gel (product size 635 bp). The redoxcline water (positive for Thaumarchaeota) was used for the isolation approach. After the isolation procedure, the magnetic beads and bead supernatant were also tested on the presence of Thaumarchaeota via PCR on the *amoA* gene. The redoxcline water and bead supernatant were additionally concentrated 100x. D) Western blot on cell lysates of the microbial community in the upper redoxcline and freshwater, both positive for Thaumarchaeota, to verify that the anti-Thaumachaeota S-layer protein antibody binds specifically to proteins of the correct size (78.5 kDA). The immunostaining was based on the metatranscriptome-derived antibody (rabbit) against the Thaumarchaeota S-layer protein as primary antibody in combination with α-rabbit-IgG-AP conjugate.

After these adjustments, it was possible to detect Thaumarchaeota on the beads after the isolation approach. The presence of Thaumarchaeota was verified by PCR on the subunit A of the marker gene ammonia monooxygenase (*amoA*) (Fig. 31 C). On the agarose gel, the

positive band for the amplified *amoA* gene indicates that Thaumarchaeota bound to the magnetic bead-antibody complex. It could also be shown that a PCR on the original community was only clearly positive after concentrating (100 x). The same applied to the bead supernatant after the Thaumarchaeota isolation procedure. However, the *amoA* band of magnetic beads was the most intense. Subsequently, the specific amplification of the archaeal *amoA* gene was confirmed after sequencing of the respective PCR product. In principle, these results indicated that the bioinformatically derived antibody seems to be suitable for the isolation of Thaumarchaeota, since these were successfully detectable on the magnetic beads.

Furthermore, it was verified that the antibody specifically binds the intended target, the S-layer protein of Thaumarchaeota. Therefore, cell lysates were prepared from samples of the upper redoxcline and freshwater from the cenote El Zapote (both positive for Thaumarchaeota) and analyzed in a Western blot (Fig. 31 D). In both cell lysates, a band was detected between the 75 and 100 kDa marker bands. The approximate size of the S-layer protein is ~78.5 kDa.

Finally, the isolation method should be studied in a more quantitative way to determine an enrichment factor for the Thaumarchaeota isolation approach. Unfortunately, it was repeatedly not successful to generate whole genome amplifications for cells bound to the magnetic beads. Therefore, in the first step, only 16S rRNA amplicon sequencing of cells on the beads, in the bead supernatant and the redoxcline sample was performed using the universal primers 341F and 1492R. The PCR products were sequenced on a MinIon sequencer (Oxford Nanopore Technologies; see section 2.5.3). According to the 16S rRNA gene amplicon data, Thaumarchaeota only represented 1 % of the original redoxcline community, whereas 4 % were classified as Thaumarchaeota on the magnetic beads (Table 26). After the isolation approach, only 0.2 % were identified as Thaumarchaeota in the bead supernatant. The positive *amoA* PCR on the magnetic beads and the fact that Thaumarchaeota were less represented in the bead supernatant after the isolation approach suggests that the antibody-based isolation was successful. However, all three samples are dominated by Proteobacteria, and the enrichment factor is still greatly improvable. In this light, it should be verified whether the calculated relative abundance indeed reflects the presence of Thaumarchaeota or whether factors such as a primer bias affected the result here.

Table 26: Relative abundance [%] of Archaea and Bacteria in OTUs (on the pylum level) based on the 16S rRNA gene amplification. The taxonomic annotation is based on the SILVA 16S rRNA database. The abundance of Thaumarchaeota was determined before (redoxcline water) and after (bead supernatant and on magnetic beads) the antibody-based isolation approach. Only the top three phyla are shown.

Phylum	Relative abundance [%]		
	Magnetic beads	Bead supernatant	Redoxcline water
Proteobacteria	88	94	89
Thaumarchaeota	4	0.2	1
Cyanobacteria	4	3	8
Other Bacteria	3.5	2.9	1.3

4 DISCUSSION

Pelagic redoxclines represent important biogeochemical sinks for toxic hydrogen sulfide and thereby represent a barrier for sulfide to reach adjacent upper water layers (Walsh et al., 2009). It is predicted that along with rising temperatures, increasing eutrophication, and the associated enhanced stratification of water bodies, oxygen minimal zones will continue to spread, thus setting the basis for the increased occurrence of sulfidic environments (Diaz & Rosenberg, 2008; Stramma et al., 2008). A well-known extreme that illustrates the ecological effects of hydrogen sulfide are so-called dead zones, which are characterized by the death of aquatic life (Diaz & Rosenberg, 2008). In sulfidic environments, sulfur-oxidizing bacteria can have a detoxifying effect by oxidizing reduced sulfur species, thereby reducing the concentration of toxic sulfide and converting it to less toxic sulfur species (Grote et al., 2012). Research on the hydrobiogeochemistry of redoxclines elucidates the complex role of microorganisms in this process and the respective environmental key controlling factors for the detoxification of sulfide. This study on the microbial ecology of the cenote El Zapote with Hells Bells and Angelita devoid of calcite formations led to a fundamental understanding of the complex biogeochemistry of pelagic redoxclines. In the first step, the analysis of the microbial diversity throughout the water column of cenote El Zapote revealed that the microbiome of the redoxcline, the growth zone for Hells Bells, differs from the adjacent water layers. Further, bacteria of the order Hydrogenophilales were identified as the microbial key players that favor calcite precipitation by an incomplete, nitrate-driven sulfide oxidation. This model on microbially induced calcite precipitation was experimentally confirmed on a laboratory scale. In cenote Angelita devoid of Hells Bells, a complete chemolithoautotrophic sulfide oxidation to sulfate and anoxygenic photosynthesis were identified as the key processes that inhibit calcite supersaturation and thus of calcite speleothem formation.

4.1 Unique characteristics of the redoxcline as Hells Bells growth zone of El Zapote

With their study on the hydrogeochemistry of the redoxcline, Ritter et al. (2019) were able to identify that the redoxcline represents the growth zone for Hells Bells in the cenote El Zapote. Furthermore, it was concluded that the microbiology in the redoxcline may significantly contribute to the local calcite supersaturation and thus to the formation of the turbid layer and growth of calcite speleothems (Ritter et al., 2019; Stinnesbeck et al., 2018). Based on these findings, the first step of this thesis was to determine if the microbial community of the redoxcline differs from the adjacent water layers.

The 16S rRNA amplicon results verified that the water body of the cenote is highly stratified not only in the context of the hydrogeochemistry but also regarding the microbiomes in the redoxcline and adjacent water layers. The redoxcline represents a microbial and hydrogeochemical transition zone from the oxic freshwater to the stable halocline below, which isolates the deeper sulfidic saltwater from the upper freshwater. The redoxcline shares specific bacteria and archaea with both the freshwater and halocline, whereas the microbiomes of these two water layers differ significantly. The redoxcline community is strongly dominated by Proteobacteria, among which the largest group is represented by the Hydrogenophilaceae (35 %). This family also occurred in the halocline and freshwater but was much lower abundant in these water zones. In the halocline, the Hydrogenophilaceae were outcompeted by other sulfur-oxidizing bacteria of the ε-Proteobacteria family Sulfurovaceae (29 %). It was to be expected that sulfur oxidizers play a dominant role in the sulfur cycle of the redoxcline. However, it was surprising that they are represented by the family Hydrogenophilaceae, which, unlike ε-Proteobacteria, have not yet been described in the context of pelagic redoxclines (see section 4.6).

Thaumarchaeota were the dominant archaea in the planktonic phase in both the redoxcline and freshwater zone of cenote El Zapote. Thaumarchaeota were already described in the context of other pelagic redoxclines, such as in the Baltic sea (Berg et al., 2015). As Thaumarchaeota live obligatory aerobic but are highly adapted to minimal oxygen availability (Pester et al., 2011), it was expected that they occupy the niche in the (upper) redoxcline and freshwater where oxygen as electron acceptor is limited or even hypoxic conditions prevail. Thaumarchaeota also stood out of the metatranscriptome-based

abundance analysis as 13 % of all transcripts could be assigned to them (Fig. 12). Of course, slow growth does not necessarily mean low degree of transcription, but nevertheless, it was remarkable that Thaumarchaeota (with generation times > 20 h (Rosenberg et al., 2014a)) were that dominant on the metatranscriptomic level. This aspect is taken up again in chapter 4.5, where it is described that these ammonium-oxidizing archaea highly expressed several S-layer protein-encoding genes. However, the fact that Thaumarchaeota were still detectable in the halocline of cenote El Zapote was somewhat surprising, since anoxic conditions are to be expected there. Either they are actually able to cope with the harsh conditions in the halocline (including high sulfide concentrations) or they were only detectable on the DNA level through dead cells but are in fact not viable under these conditions.

The results on microbial diversity in the redoxcline are partially consistent with those of Stinnesbeck et al. (2018). Accordingly, Hydrogenophilales were also identified as one of the most dominant groups in the planktonic phase of El Zapote. However, in the study by Stinnesbeck et al. (2018), the water column of the cenote was analyzed as a whole, rather than zone-specifically as in the context of this work. By specifically sampling and analyzing the microbial communities in the freshwater, central redoxcline and halocline, the microbial diversity could be higher resolved along the vertical opposing gradients of reduced and oxidized chemical species. Therefore, the abundance of organisms adapted to strictly anaerobic conditions increases along the oxygen gradient towards the halocline. In the halo- and redoxcline the Chloroflexi family Anaerolineaceae and sulfate-reducing Desulfaculaceae were detected among which all members are described to live strictly anaerobic (Kuever, 2014; Rosenberg et al., 2014a). Even anaerobic methanotrophic Euryarchaeota of the cluster ANME-1b, for which even low concentrations of oxygen represent a selection factor (Knittel et al., 2005), were identified in the biofilm in the redoxcline and as well as in the planktonic phase of the halocline.

Accordingly, the microbial taxa identified by Stinnesbeck et al. (2018) could now be assigned to specific habitats: exemplarily, the Hydrogenophilaceae to the redoxcline, the ε-Proteobacteria to the redoxcline and halocline, the Nitrospirae to the freshwater zone. Nevertheless, a major difference could be identified. Chlorobi as green sulfur bacteria were identified by Stinnesbeck et al. (2018) both in the planktonic phase and in the biofilm on the Hells Bells. The presence of Chlorobi in the water depths analyzed could neither be

confirmed by 16S rRNA amplicon nor by metatranscriptomic/-genomic diversity analyses (Fig. 10 and 12).

The order Hydrogenophilales was also the most dominant in the metagenome- and metatranscriptome-based diversity analysis. Since this order accounts for the greatest difference among the three microbial (planktonic) communities to be compared, it supports the hypothesis that the Hydrogenophilales may play a central role in the microbial ecology and biochemical cycling of the redoxcline. Apart from their potential key role in the redoxcline of El Zapote, the dominant group of Hydrogenophilaceae could also be interesting in that they may form a new, so far undescribed genus within the Hydrogenophilales. Their sequenced 16S rRNA gene revealed a similarity of 93.7 % to "uncultured Hydrogenophilales" based on the SILVA database. Considering an identity cutoff of 95 % for taxa of the same genus (Schloss & Handelsman, 2005), this analysis indicates that the El Zapote redoxcline may inhabit representatives of a previously unexplored genus within the order Hydrogenophilales.

The highly abundant bacteria of the order Hydrogenophilales (planktonic phase) were not detectable on the Hells Bells reaching into the redoxcline. On the speleothem surface other Proteobacteria of the family Rhodocyclaceae und the obligat anaerobic Chloroflexi family Anaerolineaceae replaced them as dominant groups. However, the metagenome-based diversity analysis revealed that the Rhodocyclales made up only 3 % of the community instead of 24 % (as calculated based on the amplicon data). The family Anaerolineaceae is described in the context of hydrocarbon degradation, fermentation and in association with methanogenic consortia (Liang et al., 2015). Therefore, due to the dominance of the Anaerolineaceae, a very different metabolism compared to sulfur oxidation in the planktonic phase may play a key role on the surface of the Hells Bells speleothems. The microbial diversity on the Hells Bells speleothems will be discussed in more detail in section 4.2, together with the role of the biofilm in the growth of calcite speleothems.

In short, the microbial community in the redoxcline of cenote El Zapote is primarily characterized by the dominance of the family Hydrogenophilaceae. Based on these results, the next aim was to elucidate the dominant metabolic pathways catalyzed by the identified microbial community in the redoxcline.

4.2 Microbial ecology of the redoxcline - dominant metabolic pathways and microbial key players

This chapter revolves around the major findings of Leberecht et al. (in revision). This study revealed for the first time the precise microbial composition of the microbial community in the pelagic redoxcline of El Zapote, together with the key organisms in the observed hydrogeochemical reactions. Thus, it provides important insights into key metabolic processes that appear to be linked with the local calcite precipitation in that water zone. To address the central question of whether the microbiome is involved in calcite precipitation in the turbid layer of El Zapote, a metatranscriptomic and -genomic profiling of the redoxcline community was conducted. Since the calculated transcript abundances presented as part of this environmental study are not equivalent to enzyme activities or substrate turnover rates, gene expression levels were linked to the local hydrogeochemical *in-situ* parameters in order to provide robust conclusions.

4.2.1 The planktonic phase

The metatranscriptomic analysis revealed that the process of sulfur oxidation plays a central role in the redoxcline, which represents the interface between oxygenated and reduced sulfidic waters. In the sulfur cycle, the microbial community in the redoxcline mainly used the sulfide oxidation pathway via SoxYZXAB/FccAB, Dsr/Hdr, Apr and Sat with minor contributions of Sqr, but not via the alternatives. In the expression of most of these relevant genes, the Hydrogenophilales, Nitrosomonadales, and unassigned *β*-Proteobacteria were the most prominent. The Hydrogenophilales dominated in the expression of periplasmic SoxYZ, SoxXA and SoxB. However, they lacked transcripts of *soxCD*, which implicates that the regeneration of SoxZY carrier proteins most likely occurs via the production of the intermediate or final product of elemental sulfur globules (Frigaard & Dahl, 2008; Sauvé et al., 2007). However, the fact that the Hydrogenophilales and Nitrosomonadales also highly expressed the cytoplasmic proteins DsrAB, AprAB and Sat raises the question if the sulfur oxidizing bacteria actually oxidize the available hydrogen sulfide via elemental sulfur to sulfate or if the sulfur oxidation process mainly halts after the production of elemental sulfur. As described before, these enzymes are both involved in the contrary processes of sulfide oxidation and sulfate reduction. Therefore, a classification of the respective *dsrA* genes was conducted to verify, which of these processes is catalyzed by these bacteria.

Both the Hydrogenophilales and Nitrosomonadales *dsrA* genes were classified as encoding the oxidative, reverse form of the dissimilatory sulfite reductase for the oxidation of sulfide (section 3.2.1). This classification, together with the fact that *sat* was almost exclusively expressed by these organisms (Fig. 17) emphasizes that the process of sulfide oxidation clearly prevails. Nevertheless, sulfate production is not indicated by the hydrogeochemical data of the redoxcline (Fig. 9). On the one hand, this could mean that sulfate is not produced or that the sulfate formed is immediately reduced again in a cryptic cycle by sulfate reducing organisms. However, the latter seems rather unlikely, since *sat* as the gene encoding the first enzyme responsible for sulfate reduction is dominantly (to almost exclusively) expressed by sulfur oxidizers (Fig. 17). However, even if sulfate reduction was to occur, it could be beneficial in terms of microbially induced calcite precipitation, since sulfate (as sulfuric acid) is a much stronger acid than hydrogen sulfide, so that the reduction of sulfate would promote alkalinity (chapter 1.1.3; Baumgartner et al., 2006) and thus calcite precipitation. Still, the absence of *soxCD* transcripts and the fact that no production of sulfate was detected in the redoxcline suggests that zero-valent sulfur may be the final product of the sulfur oxidation process.

However, the absence of produced sulfate alone is not sufficient to support the bioinformatic results. Considering the central question of this thesis (whether microbiology in the redoxcline creates conditions for authigenic calcite precipitation), it is of particular importance to verify whether the sulfur-oxidizing bacteria oxidize hydrogen sulfide only to the state of zero-valent sulfur or completely to sulfate as the final product. The oxidation of sulfide would explain the alkalinity shift in the redoxcline and thus promote calcite precipitation, while the production of sulfate (as a stronger acid than HS^-) would lower the pH and thus result in calcite dissolution. In order to identify the product of sulfide oxidation, the presence of particulate sulfur in the center of the redoxcline was quantified by the research group of Isenbeck-Schröter (University of Heidelberg) during the second sampling in 2020 (Fig. 32), almost two years after the microbiome sampling.

If the abundances of particulate calcium and sulfur are now examined more closely, it is noticeable that both profiles showed a defined peak in the redoxcline, which coincided perfectly with the measured maximum turbidity in this zone (Fig. 32). For both particulate chemical species, a maximum value of ~28 μmol l^{-1} was detected in the respective water filtrates.
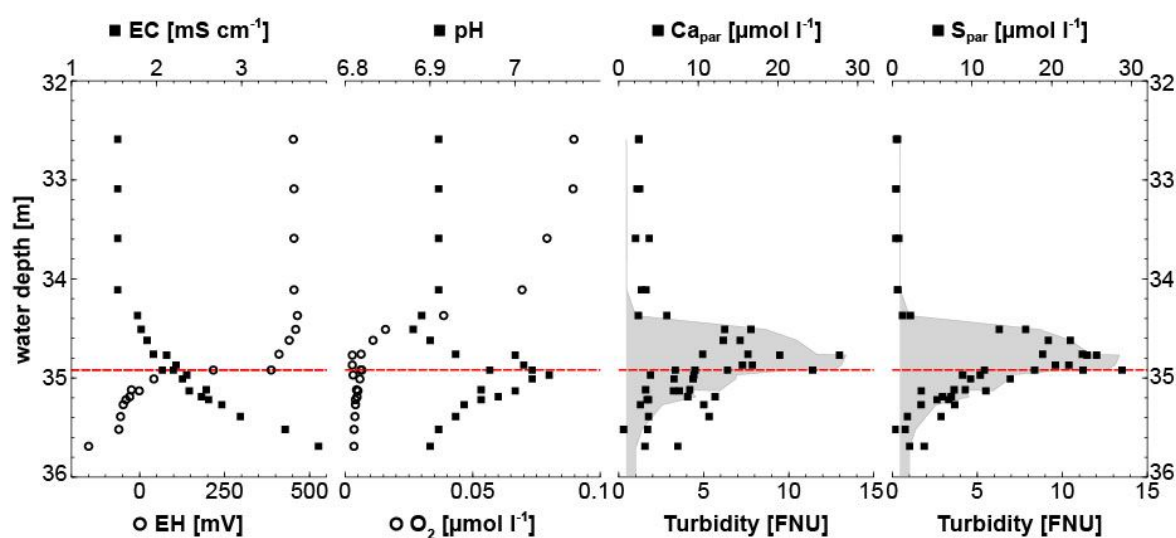
Figure 32: Quantification of the abundance of particulate sulfur and calcium in water filtrates of the redoxcline water of El Zapote. Using the optimized DCS system, the redoxcline water was analyzed regarding the presence of particulate sulfur and calcium [µmol l^{-1}] together with the local *in-situ* parameters such as the pH, the redox potential (EH) [mV], the electric conductivity (EC) [mS cm^{-1}], the turbidity [FNU] and the concentration of dissolved oxygen [µmol l^{-1}]. The red dashed line marks the water depth of the first appearance of sulfide. The gray area highlights the turbid layer. According to Leberecht et al. (in revision). Data generated by the research group of Isenbeck-Schröter, University of Heidelberg.

As a side note, the profiles of the electric conductivity and redox potential, which mark the position of the halocline and redoxcline, appear very similar to the ones measured two years before (in 2018). However, it was noticeable that the halocline and thus also the redoxcline were positioned approx. 0.8 m higher (~34.9 m) than in 2018 (~35.7 m). The pH measurement based on a new pH electrode revealed a stronger pH shift in the redoxcline as detected before. The pH ranged from 6.88 at the top to 7.04 in the central part of the redoxcline. Furthermore, the values describing the degree of turbidity were twice as high as detected before (in 2018).

Taken together, particulate sulfur indeed seems to accumulate in the redoxcline, together with particulate calcium, which most likely originates from authigenically precipitated $CaCO_3$. As a side note, it could be excluded that the detected particulate calcium and sulfur originated from calcium sulfate (gypsum). The whole water body of the cenote is undersaturated regarding $CaSO_4$ dihydrate, as indicated by the respective SI values for gypsum (the SI_{gypsum} = -1.8 to -1.5) (Leberecht et al. (in revision)). Furthermore, it should be considered that the abundance of particulate sulfur and calcium might be even higher than mentioned as these data only include particles larger than the filter pore size of 0.22 µm. Furthermore, Scanning Electron Microscopy (SEM) and Energy Dispersive X-Ray (EDX) analysis of

particulate matter from the redoxcline filtrated revealed that the particulate Ca on the filters originates from 4–10 μm sized Ca-carbonate particles. The particulate sulfur seemed to be distributed diffusely over the filters or was indicated as intracellular deposits of sulfur globules within microbial cells (Kühnel, 2020 (unpub.); Leberecht et al. (in revision)).

Now that all evidence indicates that particulate sulfur accumulates in the redoxcline, exactly where the microbial community conducts sulfide oxidation, the question arises as to why elemental sulfur and not sulfate (as the product of the complete oxidation) is produced. This implies the question whether an incomplete oxidation to zero-valent sulfur may be metabolically/energetically favorable for the microbial key players or rather enforced by the *in-situ* conditions in the redoxcline. Based on the metatranscriptomic data, the microbial key players in the sulfur cycle such as the Hydrogenophilales couple sulfide oxidation to the reduction of nitrate. Thereby, nitrate serves as electron acceptor (Fig. 17). In case of the order Hydrogenophilales, it can be assumed that these sulfur oxidizing bacteria reduce nitrate completely to dinitrogen as they expressed all genes relevant for the complete denitrification pathway. In contrast, the order Nitrosomonadales seems to reduce nitrate only to nitrite but not further (Fig. 17). In principal, both families are also able to grow aerobically via oxygen as the electron acceptor (Boden et al., 2017; Orlygsson & Kristjansson, 2014). However, as can be seen in the hydrogeochemical data of the redoxcline, the profiles of oxygen and sulfide do not intersect in the redoxcline (Fig. 9). The concentration of oxygen already falls below the detection limit at the upper edge of the redoxcline. In contrast, the trend of the nitrate concentration shows very clearly that nitrate is consumed exactly at the water depth and can no longer be measured where the electron donor hydrogen sulfide meets the electron acceptor nitrate. In this respect, the transcriptional and hydrogeochemical data support each other in the assumption that nitrate is used as an alternative electron acceptor in the center of the redoxcline.

The hydrogeochemical data also show that the available concentration of hydrogen sulfide is about 10 times higher than that of nitrate. If the concentrations of nitrate and hydrogen sulfide one meter above and below the center of the redoxcline are compared, the available concentrations diffusing towards the redoxcline are about 0.2 mmol l^{-1} for HS^- and 0.02 mmol l^{-1} for NO_3^-. This can be further supported by the determined converging fluxes for nitrate and hydrogen sulfide. The downward flux of nitrate with ~3.0 * 10^{-5} μmol m^{-2} s^{-1} is about one order of magnitude lower than the upward flux of hydrogen sulfide with

~7.9 * 10^{-4} µmol m^{-2} s^{-1} (Leberecht et al. (in revision); Ritter et al., 2019). Thus, the redoxcline seems to be clearly oxidant-limited with an electron donor to acceptor ratio of about 10:1. The implications for the metabolism of the sulfide oxidizers become clear when the stoichiometry and energetic aspects (calculated based on Thauer et al., (1977)) of the complete oxidation (Equations (E) 6) is set against that of the incomplete oxidation (E7) (according to Leberecht et al. (in revision)):
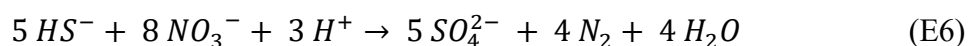
1) **Oxidation of HS$^-$ to SO$_4$$^{2-}$**

$$5\ HS^- + 8\ NO_3^- + 3\ H^+ \rightarrow 5\ SO_4^{2-} + 4\ N_2 + 4\ H_2O \tag{E6}$$

$\Delta G^{0'} = -3{,}722$ kJ/mol

Normalized per mole nitrate: $\Delta G^{0'} = -465$ kJ/mol

2) **Incomplete oxidation of HS$^-$ to S^0**

$$5\ HS^- + 2\ NO_3^- + 7\ H^+ \rightarrow 5\ S^0 + N_2 + 6\ H_2O \tag{E7}$$

$\Delta G^{0'} = -982$ kJ/mol

Normalized per mole nitrate: $\Delta G^{0'} = -491$ kJ/mol

Of course, sulfide-oxidizing bacteria gain more energy if they completely metabolize the available sulfide to sulfate (E6), than through the incomplete oxidation process (E7). But if the availability of nitrate is taken into account, which is about one tenth of that of sulfide, it becomes obvious that the complete oxidation requires 4 times the amount of nitrate as the incomplete oxidation. Normalizing the Gibbs free energy ($\Delta G^{0'}$) for both reactions to the corresponding amount of nitrate required, the incomplete oxidation then appears to be thermodynamically more beneficial. This means that under the conditions in the redoxcline, with nitrate as the limiting resource, bacteria are forced to stop sulfide oxidation at the stage of zero-valent sulfur due to electron acceptor limitation.

From the equations (E6 and 7) established, conclusions can be drawn about the pH changes in the redoxcline. During the complete oxidation of sulfide to sulfate (E6), less protons are consumed per mole hydrogen sulfide than during the incomplete oxidation (E7). In addition, as described above, the production of sulfate promotes acidification. In contrast, the partial oxidation results in a positive pH shift due to the consumption of hydrogen sulfide and the oxidation to the neutral state of S^0, together with the enhanced demand of protons (E7). Taken together, the positive pH peak in the redoxcline leading to local calcite supersaturation and thus calcite precipitation, as well as the accumulation of zero-valent sulfur most likely result from the incomplete nitrate-driven sulfide oxidation in the oxidant-deficient environment.

In addition to the dominant sulfur oxidizers, ammonium oxidizing Thaumarchaeota of the family Nitrosopumilaceae have also been noticed in the metatranscriptome of the redoxcline community. Thaumarchaeota were already reported in other oxygen minimum zones and pelagic redoxclines such as in the Baltic sea (Labrenz et al., 2010) and the Gulf of Alaska (Muck et al., 2019). In El Zapote, Thaumarchaeota most likely inhabit the niche where the converging profiles of oxygen and ammonia meet at the upper edge of the redoxcline. In the exact same water depth, both substrates fall below the detection limit indicating a simultaneous consumption by ammonium oxidizers. Furthermore, they leave their metabolic signature by the local increase in the nitrite concentration and the respective minimal pH shift towards slightly more acidic values at the top of the redoxcline. They are highly adapted to limited substrate availability (Martens-Habbena et al., 2009; Walker et al., 2010) and may therefore be responsible for consuming the remaining minimum oxygen concentrations and thereby creating anoxic conditions in the central redoxcline below. Taking up the issue of electron acceptor limitation in the redoxcline, it can be added that these archaea may support other microorganisms by producing nitrite. For organisms that express *nir* genes encoding nitrite reductases, such as the sulfur-oxidizing Hydrogenophilales, nitrite could serve as an alternative electron acceptor to oxygen and nitrate.

Additionally, Thaumarchaeota and the orders Hydrogenophilales and Nitrosomonadales could also further contribute to the calcite precipitation by carbon dioxide fixation (Castanier et al., 1999, 2000; Castro-Alonso et al., 2019). By their uptake of CO_2, which leads to a local positive pH shift around the cells, these ammonium and sulfur oxidizers may be responsible for the decrease of upwards diffusing HCO_3^- (Fig. 9) and increase of ^{13}C bicarbonate (Ritter et al., 2019) in the redoxcline. This signature in hydrogeochemistry, together with the high

expression levels of specific autotrophic genes indicate that carbon dioxide assimilation represents a relevant process in the redoxcline. The metatranscriptomic data revealed that the Hydrogenophilales and Nitrosomonadales fix carbon dioxide via the Calvin cycle (Fig. 17). Thaumarchaeota are known to have the most efficient aerobic autotrophic pathway, the 3-HP-4-HB cycle (Könneke et al., 2014). However, among the autotrophic pathways, the gene expression levels of genes of the 3-HP-4-HB cycle were one of the lowest (Fig. 13) and transcripts could not be assigned to Thaumarchaeota. Potentially, the gene annotation was non-specific. In principle, the high efficiency of the 3-HP-4-HB cycle may still compensate for very low gene transcription.

Since upwards diffusing methane reaches the redoxcline of El Zapote, it was also investigated whether important processes take place in the methane cycle. In the context of the methane metabolism only the marker gene for the aerobic methane oxidation was highly abundant on the metatranscriptomic level (243 TPM). This gene (*pmoA*) encodes the particulate methane monooxygenase and was almost exclusively expressed by the methanotrophic, methylotrophic γ-Proteobacteria family Methylococcaceae. Bacteria of the family Methylococcaceae have a strictly aerobic metabolism and gain energy from the dissimilatory oxidation of methane. They use methane and methanol as sole energy and carbon sources for biosynthesis (Rosenberg et al., 2014b). PmoA catalyzes the oxidative step from methane to methanol, however, thereby it uses NADH and oxygen and does not contribute to energy production (Fuchs et al., 2017). Therefore, the transcript abundance of this particular gene may not be related to the relevance of methane oxidation in the redoxcline.

In the following oxidation steps from methanol via formaldehyde and formate to CO_2, reducing equivalents are generated and the formation of ATP occurs. The corresponding gene expression levels for enzymes that catalyze these reactions were much lower or, as in the case of formaldehyde dehydrogenase, not detectable in the metatranscriptome. The methanol dehydrogenase encoding gene was moderately expressed (40 TPM). However, transcripts of the formaldehyde dehydrogenase, which is responsible for the oxidation of the toxic intermediate formaldehyde to formate, was not represented in the metatranscriptome. The formate dehydrogenase (53 TPM) that catalyzes the last oxidation reaction from formate to carbon dioxide was not only expressed by the described methanotrophs but dominantly transcribed by many other non-methanotrophic bacteria (such as the Rhodocyclales). Apparently, only transcripts of the formaldehyde dehydrogenase from the aerobic methane

oxidation pathway from Methylococcaceae were not found in the metatranscriptome. Either the Methylococcaceae use alternative reactions for this oxidation step or, more likely, transcript annotation may have been to unspecific.

If the gene expression of the methanol dehydrogenase, as the first enzyme of the pathway that contributes to energy production, was taken as an indicator for methane oxidation, it can be said that methane could indeed be oxidized aerobically. But considering the limited availability of oxygen, aerobic methane oxidation most likely occurs to a lower extent. This goes along with the decrease of methane in the redoxcline (Fig. 9). CO_2 production would lower the local pH and rather inhibit calcite precipitation (E8).

$$CH_4 + 2\,O_2 \rightarrow CO_2 + 2\,H_2O \qquad \text{(E8)}$$
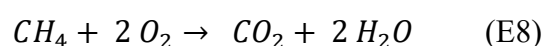
However, the emergence of CO_2 seems to be compensated by autotrophic organisms as no increase but decrease of the product of dissolved bicarbonate could be measured. According to the hydrogeochemical profile, anaerobic methane oxidation would have been expected as the concentrations of methane fall below the detection limit below the measurable oxygen occurrence (Fig. 9). Therefore, the gene *mcrA* was additionally tested for transcript abundance. This gene is involved both in methanogenesis and in anaerobic methane oxidation as the reverse methanogenesis pathway. However, no transcripts of this gene could be found in the metatranscriptome. This indicates that only evidence of aerobic methane oxidation was found. Methanotrophs are reported to grow in a variety of environmental scenes and in a wide range of oxygen availability and even cope with anoxic conditions for longer durations (Rosenberg et al., 2014b). Methylococcaceae as aerobic organisms are most likely represented in the metatranscriptome because the sampling method (FreeFlow bottle) averages over ~40 cm of water column and thus may still include microaerophilic organisms. As just described for Thaumarchaeota, the family Methylococcaceae may also contribute to the depletion of the remaining low oxygen concentrations thereby providing anoxic conditions in the central redoxcline and setting the foundation for anaerobic nitrate-driven sulfide oxidation.

Combining the hydrogeochemical results with the presented bioinformatic results on the microbial community in the redoxcline of El Zapote, the following model for the formation of the turbid layer and Hells Bells speleothems can be established (Fig. 33).
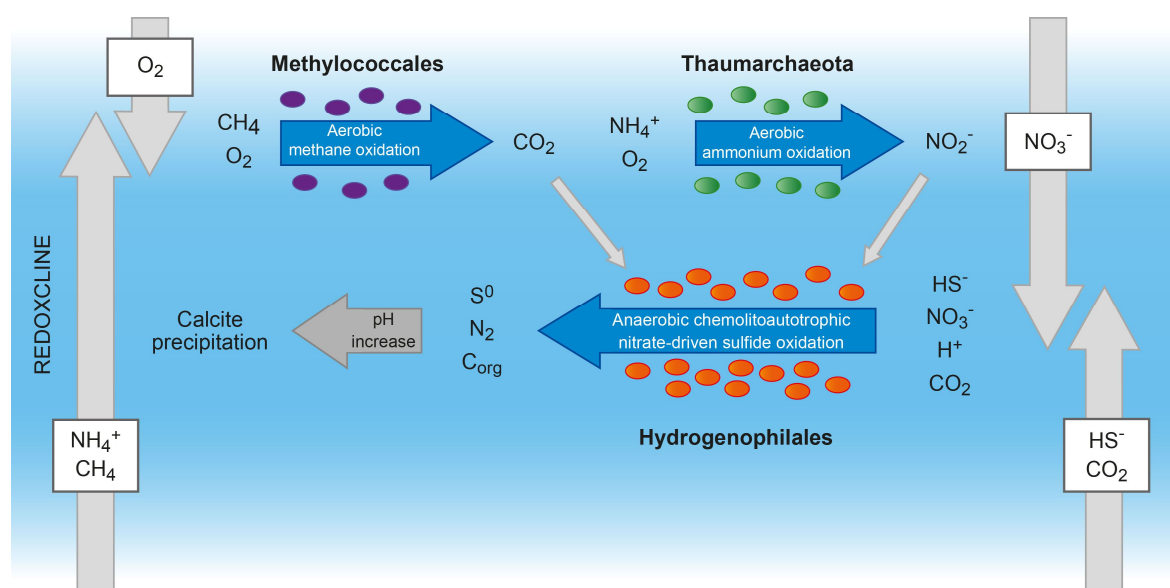
Figure 33: Microbially induced calcite precipitation by the process of nitrate-driven sulfide oxidation. The integration of hydrogeochemical, metagenomic and -transcriptomic data revealed the chemolithoautotrophic order Hydrogenophilales as the microbial key players in the redoxcline of El Zapote. These conduct nitrate-driven sulfide oxidation to the state of zero-valent sulfur and thereby set the foundation for calcite precipitation in an oxidant-deficient environment. Methane oxidizing Methylococcales and chemolithoautotrophic ammonium-oxidizing Thaumarchaoeta create anoxic conditions in the center of the redoxcline by depleting the remaining oxygen at the top of the redoxcline.

Chemolithoautotrophic Thaumarchaeota inhabit the niche at the top of the redoxcline, where the converging profiles of downwards diffusing oxygen and upwards diffusing ammonia coincide. Together with methane-oxidizing Methylococcales, they consume the remaining, but still very low concentration of oxygen and create anoxic conditions in the redoxcline water below. In the center of the redoxcline, the autotrophic sulfur-oxidizing bacteria of the order Hydrogenophilales and Nitrosomonadales thrive in the gradients of the electron donor hydrogen sulfide, bicarbonate and the electron acceptors nitrate and nitrite (the product of ammonium-oxidizing Thaumarchaeota). There, they conduct nitrate-driven sulfide oxidation. Electron acceptor limitation sets the foundation for an incomplete oxidation process that halts after the production of zero-valent sulfur instead of sulfate. This incomplete, proton-consuming oxidation process results in a metabolically induced positive pH shift towards alkalinity and thus favors calcite supersaturation and finally authigenic precipitation in the center of the redoxcline.

A very important factor that has not yet been discussed but is of great importance for the hydrogeochemistry and thus for the microbiology in the cenote, represents the vertical dynamics of the halocline. Although the water column of El Zapote is characterized by its

stagnancy, there is the additional component that the entire water column shifts vertically in dependence on climatic and weather conditions (Ritter et al., 2019). Strong rainfalls or recharge events (like Hurricanes), which leads to an increased freshwater infiltration into the Yucatán karst aquifer and to increasing of the freshwater body mass of the cenote, results in a compensatory drawdown of the halocline. In contrast, periods of droughts promote the temporal elevation of the halocline, and thus also of the redoxcline lying on top of it. Furthermore, the daily tides together with the seawater level control the movement of the halocline (Ritter, 2020). Certainly, this also means for the microbial community in the redoxcline that the availability of resources can temporarily change during the movement of the halocline. This oscillating dynamic is most likely responsible for the fact that Hells Bells are found in a relatively wide range of 10 m, and thus also outside of the current position of the redoxcline as the Hells Bells growth zone. Therefore, Ritter et al. (2019) described that the growth of Hells Bells occurs rather episodically than constantly and highly depends on the position of the growth zone, the redoxcline.

The dynamics of the halocline could also be responsible for the maximum particulate Ca being measured just above the pH in the redoxcline (Fig. 32). Driven by the density gradient towards the halocline, particulate matter in the redoxcline would also follow the movement of the halocline. Depending on the specific gravity (which describes the density ratio of two substances), particles should react with a varying degree of inertia. During a halocline elevation, small particles will be carried along faster whereas larger ones will most likely follow with a time lag. Accordingly, during a settling movement of the halocline, large particles will sink faster than small ones. A subsequent increase in the halocline would push the small particles, which could not reach their original position in the redoxcline again, further up. Only the particles that remain in the growth zone will continue to grow. If they have reached too large a mass, they will probably sink to the deeper water layers, where they will be dissolved again due to the lower pH towards the halocline and saltwater (Eschenröder, 2020; Leberecht et al., in revision). In short, the peak in particulate Ca is most likely due to the vertical dynamics of the halocline, which promotes an accumulation of small particles just above the actual pH peak.

Nitrate-driven sulfide oxidation by Hydrogenophilales has now been identified as a key process leading to pH increase and finally calcite precipitation in the planktonic phase of the oxidant-deficient redoxcline.

4.2.2 The biofilm on Hells Bells speleothems

Subsequently, the question was addressed whether the biofilm on the Hells Bells also promotes the growth of the speleothems, or whether the regulation occurs solely from the planktonic phase. The highly complex water column of El Zapote, which is very stagnant and stratified on one hand, but highly dynamic along the vertical axis on the other, complicates the idea that a biofilm as a stationary phase on the speleothems also plays a key role in the regulation of Hells Bells growth. In this study, the biofilms on Hells Bells that reached into the redoxcline were also analyzed – on the 16S rRNA gene, but also on the metagenomic diversity level.

Based on both data sets, Chloroflexi of the order Anaerolineales clearly dominate in the biofilm community on the speleothems in the redoxcline (Fig. 10 an 18). This order is not yet well described. However, Anaerolineales have been reported in studies in association with methanogenic alkanes-degrading consortia (Liang et al., 2015), anaerobic granular sludge and as thermophiles in bacterial mats in hot springs (Yamada et al., 2006). They are classified as strictly anaerobic organisms with a fermentative lifestyle. Anaerolineales are further described in context of syntrophic-like interactions with methanogens due to hydrogen production. Thereby, Anaerolineales may serve as hydrogen-producing partner for hydrogenotrophic methanogens (Xia et al., 2016; Yamada & Sekiguchi, 2009). In microbial communities, these fermenting bacteria may also play a role in providing lactate as electron donor to sulfate reducing bacteria (Drennan et al., 2016). Interestingly, both methanogens and sulfate reducing bacteria seem to co-exist in the biofilm on Hells Bells speleothems in the redoxcline. The Euryarchaeota class Methanomicrobia was identified in the biofilm community, which are described as methanogens that can use hydrogen and formate as electron donors (Garcia et al., 2006). The order Desulfobacterales (δ-Proteobacteria) represents a group of sulfate reducing bacteria, most of which are chemoorganoheterotrophic (Rosenberg et al., 2014c). In a biofilm scenario, the three dominant anaerobic groups of Anaerolinea, Desulfobacterales and Methanomicrobia could have established a synthrophic manner of co-existence. Anaerolineales may feed the Desulfobacterales with fermentation products such as lactate allowing them to conduct chemoorganoheterotrophic sulfate reduction. The hydrogen produced during fermentation (Sun et al., 2016) could provide hydrogenotrophic methanogens with hydrogen as an electron donor. Desulfobacterales in

turn may supply methanotrophic Methanomicrobia with the electron acceptor carbon dioxide. Non-methylotrophic methanogenesis is a known process in context of microbially induced calcite precipitation, as well as the dissimilatory reduction of sulfate (see section 1.1). Anaerolineales are described to metabolize proteinaceous carbon sources and carbohydrates. It would be interesting to verify if these organism could also promote calcite oversaturation by the elimination of known inhibitors of calcite precipitation within the biofilm such as carboxylated polysaccharides or acidic amino acids (Dupraz et al., 2009). Furthermore, degradation of extracellular polymeric substances (EPS) may also favor calcite precipitation (see section 1.1.4). However, due to the missing link to a metatranscriptomic profile of the biofilm community in the redoxcline, these processes and their effect on the carbonate equilibrium can only be discussed on a speculative basis.

In fact, there are a number of indications that support the hypothesis that no pronounced biofilm covers the Hells Bells surfaces. Firstly, despite several attempts and different sampling approaches, it was not possible to generate a metatranscriptome for the biofilm community. Low RNA yield due to degradation of mRNA upon sampling seems rather unlikely as the respective samples were immediately stabilized after collection (see section 2.1.3). Still, it cannot be excluded that further methodological optimizations would be necessary. However, assuming that this issue is not sampling-related, this could reflect that there are cells on the surface, but not in form of a pronounced confluent biofilm. Apparently, the quantity of cells was sufficient for DNA purification, but not for the isolation of mRNA for a metatranscriptomic analysis. While the metagenome reveals the genetic potential of the microbial community and provides information on which organisms are present, a metatranscriptome enables the establishment of an active functional profile (Shakya et al., 2019). The lack of mRNA may indicate that the microenvironment on the Hells Bells surface allows only limited growth and/or that the cells even persist in a low-activity state. Considering the substrate limitations in the redoxcline, this could mean that the cells are rather transcriptionally and metabolically inactive. The oscillating dynamics of the halocline potentially represent a great challenge for the formation of a biofilm. Whereas the microbial community in the water column of the redoxcline would just follow the movement of the halocline, the biofilm community must cope with changing redox regimes and fastly adapt to constrasting environments – the sulfidic, anoxic halocline or oxic freshwater. In addition to the vertical substrate gradients already described, horizontal gradients most likely

also play a role in the water column of El Zapote (Ritter, 2020). Electron donors such as methane, hydrogen sulfide and reduced carbon and nitrogen species diffuse through the organic degradation from the debris mound in the center of the cenote towards the redoxcline. By diffusion, radial gradients are likely to form reaching from the debris mound as the central source. Accordingly, the availability of various substrates is lowest with increasing distance from the debris mound. As a result, the cave walls and the Hells Bells that form on them are subjected to higher resource limitations, and chemolithotrophic processes occur to a more significant extent in the center of the water column. This may also contribute to the fact that the planktonic phase does not reassemble the microbial biofilm composition. Furthermore, these lateral gradients most likely set the foundation for the horizontal layering of the Hells Bells and speleothem growth towards the center of the cenote. This factor may further explain the horseshoe-like shape, the opening of which is directed towards the cave walls (Ritter et al., 2019).

Apart from the metabolic activity, microoganisms can also influence the carbonate equilibrium by the physical characteristics of their cellular surfaces and the surrounding extracellular polymeric substance (see section 1.1.4). Many studies revealed that the characteristics of the EPS matrix have a major impact on the morphology of the precipitating calcium carbonate mineral (Dupraz et al., 2009). Ritter et al. studied the petrographic characteristics of Hells Bells speleothems in more detail by scanning electron microscopy (SEM) imaging and identified dogtooth-like, blocky and bladed calcite crystals on the speleothem surface. Thus, it was concluded that the occurrence of dog-tooth calcite rather indicates an inorganic precipitation than a biologically-mediated growth within a biofilm (Ritter et al., 2019).

In summary, the factors described, such as the lack of mRNA, substrate limitation by horizontal gradients and the crystal morphology, indicate that no pronounced biofilm developed on the Hells Bells. Instead, a monolayer-like biofilm would be conceivable. The metagenome-based diversity analysis indicates that the biofilm community is very different from that in the planktonic phase. Due to the absence of sulfur-oxidizing bacteria, the key process identified to be responsible for the local calcite supersaturation in the planktonic phase of the redoxcline, the incomplete sulfide oxidation to S^0, does not seem to play a role in the sessile community on the Hells Bells speleothems. The oscillating movement of the halocline and thus of the Hells Bells growth zone (the redoxcline) in response to hydraulic

changes strongly enforces the model that the development of speleothems is controlled by the microbial metabolic cycling in the planktonic phase. A redox regime-dependent Hells Bells growth over ~120 thousand years (Ritter, 2020) therefore seems much more likely to be regulated from the planktonic phase than from a biofilm. Nevertheless, a participation of the biofilm in the speleothem development cannot be excluded.

4.3   What distinguishes El Zapote from cenotes without Hells Bells - a comparative analysis (from a microbiological point of view)

Having extensively studied the microbial ecology in the El Zapote redoxcline and identified the mechanism of microbially induced calcite precipitation in association with the formation of the turbid layer and Hells Bells speleothems, the next step was to perform a comparative analysis to cenote Angelita without Hells Bells to reveal additional key controlling factors for the emergence of Hells Bells.

Cenote Angelita represents the optimal comparative cenote for El Zapote because it is deep enough to have a similar stratification of the water column and is exposed to equivalent climatic conditions. But unlike El Zapote, cenote Angelita exhibits no underwater speleothems. While the hydrogeochemical differences have already been intensively studied by Ritter (2020), Klose (2018; unpub.) and Eschenröder (2020; unpub.), the aim of this work was to highlight differences in microbial metabolic cycling in the redoxclines of these two cenotes. This analysis intended to resolve to what degree does the microbiology contribute to the absence of Hells Bells and to extend the list of already identified key factors for the formation of Hells Bells (Ritter, 2020) and, if necessary, specify individual definitions.

Cenote Angelita represents a habitat with a microbial ecology that significantly differs from that of El Zapote. This may be primarily attributable to the different hydrogeochemical conditions. The redoxcline of Angelita overlaps with the halocline, whereas the redoxcline of El Zapote is located above the halocline. In contrast to El Zapote, where the electron acceptor to donor ratio was < 1, a different redox regime dominates in the redoxcline of cenote Angelita. In cenote Angelita the difference in the availability of electron donors and acceptors is smaller with a ratio of ≤ 1 (Fig. 19). Accordingly, the reducing power is higher in the redoxcline of El Zapote than in Angelita. In the central redoxcline of Angelita, the concentration of hydrogen sulfide falls below the detection limit, which indicates a complete

depletion due to microbially catalyzed oxidation of sulfide (Fig. 19). Furthermore, the sulfide and oxygen concentrations fall below the detection level at the same water level, which indicates that in cenote Angelita aerobic sulfide oxidation may occur to some extent, which was not the case in El Zapote. Therefore, in cenote Angelita there seems to be a redox regime that is less oxidant deficient compared to the redoxcline of cenote El Zapote. Furthermore, in cenote Angelita, advection probably plays a greater role than in El Zapote, so that the transport of resources such as the electron acceptors oxygen and nitrate is regulated by advection rather than by diffusion (Ritter, 2020).

Interestingly, the microbial community in the redoxcline of cenote Angelita differs significantly to the one studied at El Zapote with Hells Bells. The redoxcline of El Zapote is highly dominated by Hydrogenophilales, whereas cenote Angelita mainly inhabits ε-Proteobacteria and green sulfur bacteria of the order Chlorobiales (Fig. 20). The comparative diversity analysis indicated that the complexity of the microbiome in cenote Angelita is much lower as in El Zapote. In fact, this phenomenon rather reflects the successful optimization of the sampling method (by the research group of Isenbeck-Schöter, University of Heidelberg). Whereas the redoxcline of El Zapote was sampled with a FreeFlow bottle, that provides an average over ~40 cm of the water body, the optimized DCS system allows a resolution of ~5 cm. Considering the strong vertical counter-gradients in redoxclines, the resolution has a major impact. Whereas the sampling technique covered multiple niches and thus different niche-adapted organisms along the gradients at El Zapote, the central redoxcline was most likely sampled as the only niche at cenote Angelita. This can be confirmed by the fact that in the redoxcline community of cenote Angelita lower transcriptional activity occurs related to the methane and nitrogen cycle (Fig. 22 and 26). In the methane cycle of cenote Angelita, only the formate dehydrogenase was expressed, neither methanogenesis nor anaerobic or aerobic methane oxidation seems to occur. In the nitrogen cycle, only the nitrate reductase subunit A was highly expressed (773 TPM). In fact, it seems that the niche at the oxic-anoxic interface, or more precisely the zone, where sulfide meets electron acceptors, was sampled accurately at cenote Angelita.

As described above, the redoxcline of El Zapote is dominated by the sulfur-oxidizing bacteria of the order Hydrogenophilales. The microbial community of the redoxcline of cenote Angelita also mainly comprises bacteria that are relevant for the sulfur cycling in this water layer.

These include the orders Chlorobiales and Campylobacterales. Chlorobiales, however, stand out from the previously identified and described sulfur oxidizers in that they conduct anoxygenic photosynthesis. Both oxygenic and anoxygenic photosynthesis do not play a role in the redoxcline of El Zapote but the latter seems to be a key process in cenote Angelita. Thereby, the shape of the cenote caves probably plays a decisive role. In contrast to cenote El Zapote, cenote Angelita has a very wide shaft-like cave opening (Fig. 6). Consequently, the light conditions in cenote Angelita are quite different, with light reaching the redoxcline (Fig. 5). In the metatranscriptome, the process of anoxygenic photosynthesis was represented by the active expression of *bchY* encoding the chlorophyllide a reductase subunit Y for the biosynthesis of bacteriochlorophyll, and *fmoA,* encoding a bacteriochlorophyll relevant for the energy transfer from chlorosomes to the photosystem reaction center (Fig. 25).

In anoxygenic photosynthesis, hydrogen sulfide serves as electron donor (Imhoff, 2014), but unlike chemolithotrophic sulfur oxidation, the process is independent of external electron acceptors such as nitrate. In the gene expression profile of Chlorobiales, it is noticeable that they expressed *soxYZ*, *soxXA*, *soxB* (Fig. 28), but not *soxCD*. This means that equivalent to the community in the redoxcline of El Zapote, the Chlorobiales in the redoxcline of cenote Angelita oxidize hydrogen sulfide via the stage of S^0. Therefore, the metatranscriptomic data is in line with previous knowledge on green sulfur bacteria, which are known to form sulfur granules due to the lack of *soxCD* genes. Of note, Chlorobiales store S^0 extracellularly (Imhoff, 2014). The genes of the Sox system were much higher expressed by the community in the redoxcline of El Zapote compared to the one of cenote Angelita.

Another major difference was identified in the transcription of genes of the periplasmic flavocytochrome *c* (FccAB) and the membrane-bound sulfide:quinone oxidoreductase (SQR), which are involved in the oxidation of sulfides to polysulfides and/or elemental sulfur (Griesbeck et al., 2002). The community in El Zapote mainly expressed *fccA*, whereas the sulfide-oxidizing bacteria in the redoxcline of cenote Angelita mainly transcribed *sqr*. According to the metatranscriptomic data, Chlorobiales expressed both *fccA* and *sqr*. In phototrophic bacteria, both enzymes serve to introduce electrons into the photosynthetic electron flux (Griesbeck et al., 2001; Kushkevych et al., 2021). However, it is energetically more favorable to oxidize sulfide by SQR (Griesbeck et al., 2001). In this context, the increased *sqr* transcription by the phototrophic Chlorobiales can be very well explained.

Furthermore, there are some indications that the Chlorobiales in the redoxcline of cenote Angelita oxidize hydrogen sulfide through the intermediate stage of S^0 completely to sulfate. Firstly, the expression of genes encoding cytoplasmic sulfur-oxidizing enzymes, more specifically *dsrAB*, *aprAB*, and *sat*, is much higher than of the previously mentioned periplasmic enzymes (*sox* genes, *fccA*, *sqr*). Although the transcript abundance does not necessarily reflect metabolic turnover rates, this may indicate that the oxidation of S^0 to sulfate dominantly occurs. Secondly, the concentration of sulfide falls below the detection limit at the water level, exactly where the microbiome was sampled. In contrast to the hardly described key players in the redoxcline of El Zapote, the Hydrogenophilales, the metabolic behavior of Chlorobiales is already well studied. Thus, it is known that these green sulfur bacteria further metabolize the extracellularly stored sulfur stock of S^0 if the resource of the electron donor hydrogen sulfide is limited and sufficient light energy can be absorbed (Imhoff, 2014). Therefore, in the less electron acceptor-limited regime in the central redoxcline of cenote Angelita, a significant proportion of elemental sulfur is most likely oxidized to sulfate. The production of sulfate as sulfuric acid would also explain the negative pH shift from 6.9 above the redoxcline to about 6.7 towards the center of the redoxcline.

The pH-decreasing effect resulting from sulfate production could also be partially compensated by sulfate-reducing organisms. In the metatranscriptome, sulfate-reducing bacteria were also found to transcribe *dsrAB*, *aprAB*, and *sat* for the reduction of sulfate to hydrogen sulfide, the electron donor for anoxygenic photosynthesis conducting Chlorobiales. Chlorobiales are known to form synthrophic relationships with sulfate reducers (Imhoff, 2014). In the redoxcline of Angelita, bacteria of the order Desulfobacterales could be potential synthrophic partners (Fig. 28).

Chlorobiales as obligate phototrophic bacteria highly depend on the availability of light. Just as purple sulfur bacteria, green sulfur bacteria inhabit the niche of anoxic environments, where both sunlight (from above) and the electron donor hydrogen sulfide (from below) coincide. Therefore, they are dominantly represented in deeper water layers of stratified lakes, where these conditions are provided (Imhoff, 2014). The fact that green sulfur bacteria are much more abundant than purple sulfur bacteria (such as Ectothiorhodospiraceae, (Fig. 20)) in the central redoxcline of El Zapote indicates that the availability of light as the energy source for phototrophic life is rather limited. Green sulfur bacteria have an light-

harvesting apparatus optimized for low light conditions that involves specified organelles called chlorosomes (Frigaard, 2016; Imhoff, 2014). Of note, in the metatranscriptome a high expression of genes relevant for the formation of chlorosomes was also apparent. Furthermore, green sulfur bacteria are less sensitive to higher sulfide concentrations and often less tolerant even to minimal oxygen concentrations (Frigaard, 2016). Taken together, these properties allow the conclusion that light may be a limiting factor in the redoxcline of cenote Angelita and that nearly anoxic to anoxic conditions prevail.

In the context of microbially induced calcite precipitation the final product of the anoxygenic photosynthesis is of particular importance. As described above, green sulfur bacteria produce sulfate via the intermediate state of elemental sulfur when the absorbance of light is ensured and sulfide as the electron donor is limited (E9, E10). In contrast, sulfide oxidation halts after the formation of extracellular S^0 if light is limited and sulfide is available in excess (E11, E12) (Imhoff, 2014). Sulfate production would inhibit authigenic calcite precipitation, whereas the incomplete oxidation of sulfide and uptake of CO_2 and protons increase the pH and thus favor calcite supersaturation.

Oxidation of HS⁻ to SO₄²⁻ (including (E9) and excluding autotrophy (E10))

$$2\,CO_2 + \ HS^- + \ 2\,H_2O \rightarrow \ SO_4^{2-} + 2\,CH_2O + \ H^+ \qquad \text{(E9)}$$

$$HS^- + \ 4\,H_2O \rightarrow \ SO_4^{2-} + 9\,H^+ + 8\,e^- \qquad \text{(E10)}$$
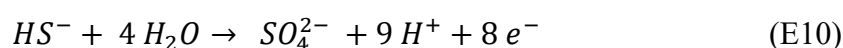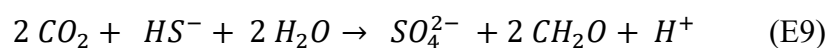
Oxidation of HS⁻ to S⁰ (including (E11) and excluding autotrophy (E12))

$$CO_2 + \ 2\,HS^- + 2\,H^+ \rightarrow \ 2\,S^0 + \ CH_2O + \ H_2O \qquad \text{(E11)}$$

$$HS^- \rightarrow S^0 + \ H^+ + 2\,e^- \qquad \text{(E12)}$$
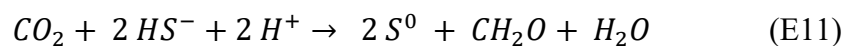
In fact, both sulfate production by sulfide oxidation and the formation of elemental sulfur could be measured in the redoxcline of cenote Angelita. Just as in the turbid layer of El Zapote, the turbid layer in cenote Angelita is the result of the accumulation of particulate calcite and S^0 (Eschenröder, 2020 (unpub.); Ritter, 2020). Ritter and Eschenröder stated that

the oxidation of sulfide most likely occurs aerobically. Furthermore, particulate calcite detected in the redoxcline of cenote Angelita is not authigenic, which means that it originated from other sources but did not mineralize in the redoxcline where it is found. In this study, metatranscriptomic analysis has now revealed that anoxygenic photosynthesis conducted by strictly anaerobic photoautotrophic Chlorobiales is responsible for the depletion of sulfide. Since sulfur oxidation in Chlorobiales proceeds in two steps and spatially separated - first from hydrogen sulfide to extracellular S^0, then from S^0 to cytoplasmic sulfate - it can be explained very well why sulfate production together with a negative pH shift, as well as S^0 can be detected simultaneously in the redoxcline. Since light intensity most likely varies greatly within a day, not to mention day and night, there might even be a certain circadian dynamic in the sulfur oxidation process.

Unfortunately, the metatranscriptomic data cannot answer the question to which proportion of sulfide is oxidized to sulfate or S^0. To gain this kind of quantitative information, on-site tracer experiments would be required. Based on the hydrogeochemical profiles, Ritter (2020) calculated that 35 % of the available hydrogen sulfide is oxidized to zero-valent sulfur and 65 % to sulfate. This calculation would explain the resulting pH shift very well, but the calculation is based on the assumption that oxygen and nitrate serve as electron acceptors for chemolithoautotrophic sulfide oxidation (Ritter, 2020). The consumption of hydrogen sulfide via the process of anoxygenic photosynthesis was not considered. Nevertheless, sulfide oxidation with the main product sulfate further explains the observed negative pH shift in the redoxcline and finally the absence of calcite formations due to calcite undersaturation in the redoxcline.

However, chemolithoautotrophic sulfur oxidizers were also identified in the redoxcline of cenote Angelita. These are representatives of the phylum of the ε-Proteobacteria, more precisely of the order Campylobacterales. In the metatranscriptome, they stood out by their expression of many periplasmic but no cytoplasmic sulfur oxidation-related enzymes, especially of *sox* genes, and *sqr*. These even expressed *soxC* (in contrast to Hydrogenophilales in El Zapote), suggesting that the Sox cycle is closed, and they do not need to form elemental sulfur to regenerate SoxYZ. Via SQR, they then probably form polysulfides. The expression of the marker genes of the rTCA cycle indicates that these sulfide oxidizers are autotrophic. Within the Campylobacterales, the transcripts originate from the families Helico- and Campylobacteraceae.

Besides other sulfidic environments, Helicobacteria have already been identified in the redoxcline in the Baltic sea, where these chemolithoautotrophs couple sulfur oxidation with denitrification (Grote et al., 2012). Likewise, Campylobacterales in the redoxcline of cenote Angelita appear to play a role not only in the sulfur but also in the nitrogen cycle. While genes encoding enzymes that catalyze nitrogen cycle reactions were generally only fairly expressed, the nitrate reductase subunit A (*napA*) stood out due to its high transcription (761 TPM) by Campylobacterales. All other genes relevant for the complete oxidation of NO_3^- to N_2 were significantly lower expressed (< 10 TPM). Whether the representatives of the Campylobacterales conduct a complete denitrification of nitrate to dinitrogen is uncertain for three reasons. Firstly, transcripts for *napA*, *nir*, *nor* and *nosZ* could only be assigned unspecifically to ε-Proteobacteria in some cases, and not further to Helico- or Campylobacteraceae. Secondly, their expression of the *napA* gene was significantly stronger than that of the rest of the genes relevant for denitrification (< 10 TPM). Therefore, Campylobacterales could also carry out only the first step, nitrate reduction to nitrite, since thermodynamically nitrate is a more favorable electron acceptor. However, no nitrite accumulation was measured in the center of the redoxcline, but just above it, where oxygen is still detectable, and nitrite is most likely formed by nitrification.

In the context of calcite precipitation, the reduction of nitrate to dinitrogen would have a positive effect on the pH, while the reduction of nitrate to nitrite would have a negligible impact. However, according to the *in-situ* parameters, the calculations of Ritter (2020) and the metatranscriptomic data presented, it can be assumed that both Campylobacterales and Chlorobiales reduce sulfide primarily to sulfate and thereby counteract calcite precipitation. A simultaneous complete denitrification would not compensate the pH-lowering effect and create calcite precipitating conditions.

In summary (Fig. 34), one of the main differences in the redoxcline of cenote El Zapote with Hells Bells and cenote Angelita devoid of calcite speleothems is based on different redox regimes and the fact that in cenote Angelita the availability of light allows anoxygenic photosynthesis to occur. As a light-dependent process, anoxygenic photosynthesis is likely to oxidize sulfide less constant than via chemolithoautotrophy. However, Chlorobiales have a highly developed photosystem that absorbs minute amounts of light. Just as by chemolithoautotrophic sulfide oxidizing Campylobacterales, which couple sulfur oxidation to nitrate reduction or denitrification, the main product of anoxygenic photosynthesis by

Chlorobiales is likely to be sulfate. The fact that elemental sulfur also accumulates in the redoxcline of cenote Angelita can be explained by the fact that sulfur oxidation by green sulfur bacteria always proceeds via the intermediate stage S^0. Either the process stops after the production of S^0 as in the case of light deficiency or these extracellular granules are degraded to sulfate when electron donor deficiency occurs. The main product of sulfate as sulfuric acid causes a local pH decrease, which in turn results in local calcite undersaturation and thus counteracts the development of calcite speleothems (Frigaard, 2016).
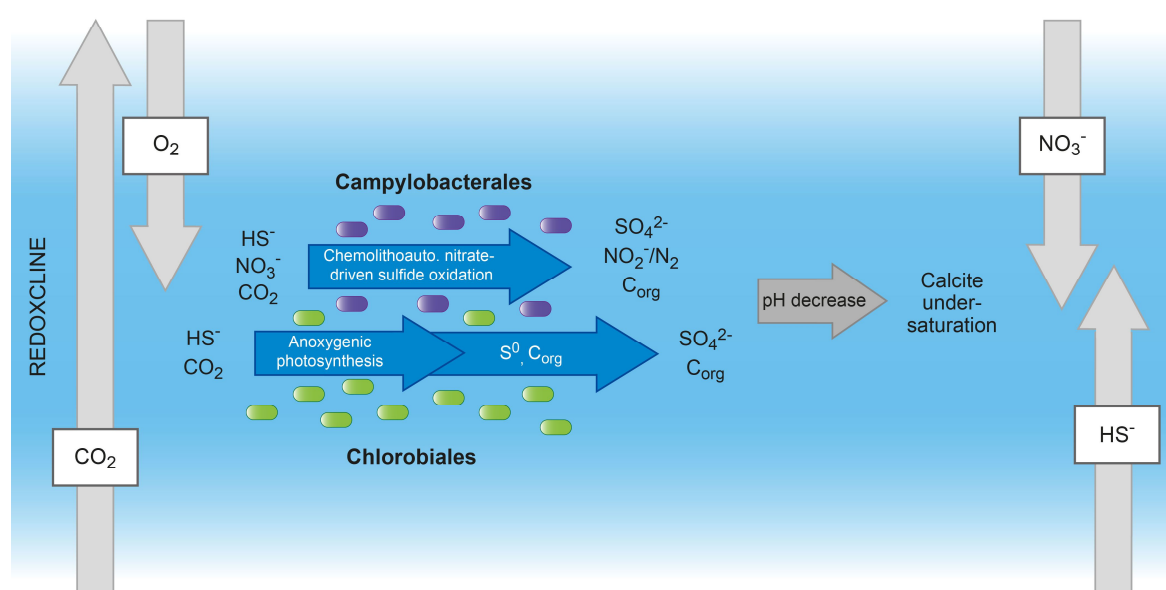
Figure 34: Microbial ecology of the central redoxcline of cenote Angelita devoid of Hells Bells. Unlike in cenote El Zapote with Hells Bells, anoxygenic photosythesis conducted by photolithoautotrophic green sulfur bacteria of the order Chlorobiales represents the major process. The availability of light and of the electron donor hydrogen sulfide determines if elemental sulfur (S^0) or sulfate is the main product of the anoxygenic photosynthesis. As the redox regime of cenote Angelita is less electron acceptor limited, it can be assumed, that the sulfur globules as the extracellular intermediate of the sulfide oxdiation process are predominantly further oxidized to sulfate. Besides Chlorobiales, chemolithoautotrophic Campylobacterales (ε-Proteobacteria) conduct nitrate-driven sulfide oxidation. It remains uncertain, if these catalyze only nitrate reduction or a complete denitrification to dinitrogen. The production of sulfate leads to a decrease in the local pH, which in turn results in calcite undersaturation and finally the inhibition of the development of speleothems in the redoxcline of cenote Angelita.

4.4 Proofing the hypothesis on the laboratory scale

Another major aim of this work was to prove the hypothesis that chemolithoautotrophic denitrifying, sulfur-oxidizing bacteria metabolically induce calcite precipitation on a laboratory scale. Since it was not possible to enrich the identified key players, the Hydrogenophilales, from the redoxcline of El Zapote, a related organism of the genus

Thiobacillus (order Nitrosomonadales) was selected, which shares the relevant metabolic characteristics with the order Hydrogenophilales.

Using microfluidic chip systems, it was possible to create a very simplified redoxcline environment (see section 3.4). This artificial gradient setting was characterized by anoxic conditions with oxidant limitation, with an electron acceptor to electron donor ratio of 1:10 as in the El Zapote redoxcline. The fact that crystals can only be observed in the presence of sulfur oxidizers strongly suggests that the metabolic activity of *Thiobacillus denitrificans* shifted the carbonate equilibrium towards supersaturation (Fig. 29). The electron acceptor deficiency here was most likely responsible for the incomplete chemolithoautotrophic sulfur oxidation to S^0 instead of the complete oxidation to sulfate. Furthermore, *Thiobacillus denitrificans* may have additionally served as cellular nucleation site. The proton-consuming process of the anaerobic incomplete oxidation of sulfide to S^0 most likely mediated calcite supersaturation in the artificial redoxcline environment. The rhombohedral shape of the crystals fits very well to the crystal structure described for calcite (Greer et al., 2017).

Certainly, the meandric chips system mimics the conditions in the redoxcline of El Zapote only to some extent. As a flow-through system, it does not provide a stratified, stagnant environment with diffusive substrate transport. Also, the cultivation chips did not mimic counter-gradients of nitrate and sulfide as in the redoxcline of El Zapote. Nevertheless, this system allowed the creation of anaerobic conditions and resource gradients along the cultivation chip. Accordingly, the substrate availability is higher in the front of the chip than towards the end. Therefore, it represented a suitable experimental environment with a stable, simplified substrate gradient comparable to the one in the redoxcline of El Zapote. Taken together, these results strongly support the model that nitrate-driven sulfide oxidation conducted by sulfide-oxidizing bacteria in the planktonic phase of the redoxcline of El Zapote promote authigenic calcite precipitation.

4.5 Isolation of Thaumarchaeota

The great challenge in studying so far undescribed bacteria and archaea can often be found in the fact that they live in very complex environmental niches to which they are highly adapted and may even be dependent on other organisms in the community (Cross et al., 2019; Staley, 2006). In such cases, it is very difficult to characterize these representatives in detail

because it is very demanding to mimic the environmental conditions during enrichment. Such an interesting, highly complex environmental setting was studied in this work, the redoxclines of cenote El Zapote. In the redoxcline of El Zapote, vertical counter-gradients of reduced and oxidized substrates are formed due to the dominant water stratification. In association with the investigation of the growth of Hells Bells speleothems and the contribution of microbiology in this process, Thaumarchaeota stood out for their high proportion of mRNA reads in the total metatranscriptome. Thaumarchaeota are notoriously challenging to cultivate (Rosenberg et al., 2014a). In connection with an ongoing project in the working group focusing on the cultivation of so far unculturable microbes, Thaumarchaeota from the redoxcline of cenote El Zapote were chosen as a candidate for the further development of an antibody-based isolation approach.

In this work, it was possible to identify a molecular target for the isolation of Thaumarchaeota from the upper redoxcline of cenote El Zapote using metatranscriptomic data. A highly expressed S-layer protein (78.5 kDa; 751 AA) should serve as an antigen for the antibody-based isolation method (Fig. 30). By modelling the protein structure and analyzing the peptide sequence, an appropriate epitope was found that exhibited optimal properties for antibody binding (Fig. 31 A). With the respective antibody, a number of optimizations of the standard workflow of the magnetic bead-based antibody isolation method were successfully implemented (Fig. 30). These optimizations included a higher primary:secondary antibody ratio (2:1) and longer incubation times. Furthermore, the incubation temperature was adjusted from 4 to 24 °C, which corresponds to the temperature of the redoxcline water in cenote El Zapote, from which the Thaumarchaeota were to be isolated.

After these adjustments, Thaumarchaeota were successfully detected on the magnetic beads by PCR following the isolation procedure. This result was a very good first milestone, indicating that the antibody does indeed bind to the Thaumarchaeota cell surface (Fig. 31 C). In addition, a western blot on the cell lysate of the redoxcline community showed that the antibody binds proteins that correspond to the size of the S-layer protein (Fig. 31 D). Future experiments with negative controls and other S-layer forming cells could verify that the antibody specifically binds to the intended target, the S-layer protein of Thaumarchaeota.

Based on these results, a quantitative analysis should be performed to provide an indication of the enrichment factor achieved via the established method. Since the proportion of

Thaumarchaeota according to metagenome-based diversity analysis is < 2% of the total community, it was assumed that the number of cells is not sufficient to sequence their genomes directly. Therefore, a genome amplification step was intended first. Genome amplification was repeatedly successful only for the bead supernatant and the redoxcline sample, but not for the cells on the beads. Since the lysis protocol was the same for all samples, the factor of an ineffective cell lysis can therefore be excluded. Since PCR on the 16S rRNA and *amoA* genes were possible on the cell lysate, which produces short DNA fragments, but whole genome amplification was not, the problem could be that large DNA fragments or even genomic DNA were interacting unintentionally with the magnetic beads so that these could not be regenerated from the beads. In future experiments, enzymatic antibody digestion could be used to try to release the intact cells from the antibody-bead complex in order to be able to exclude this factor.

In parallel, a 16S rRNA amplicon analysis was performed on the corresponding samples. In this context, the abundance of Thaumarchaeota was analyzed in the bead supernatant, on the beads and in the original sample. Nanopore sequencing revealed that Thaumarchaeota had a relative abundance of 1 % in the redoxcline water, 4 % on the magnetic beads, and 0.2 % in the bead supernatant. Thus, the results reflect the expected trend, as the abundance is highest in the bead isolate and lowest in the bead supernatant. Nevertheless, the enrichment factor still seems to be greatly improvable. It remains unclear whether these values actually represent the abundance of Thaumarchaeota. If so, then a great proportion of bacteria would also be isolated with this elaborated method. However, it is much more likely that a number of biases are involved. Firstly, it is known that archaea are often much less well covered by universal primers than bacteria (Eloe-Fadrosh et al., 2016; Narasingarao et al., 2012). This would explain the high proportion of bacteria in all samples. Secondly, the 16S rRNA amplicons were sequenced via Nanopore sequencing (see section 2.5.3). With this sequencing method, which is primarily designed for the sequencing of long fragments, the rate of incorrect base calling is significantly higher compared to other sequencing systems (Chandak et al., 2020), which could have had a major influence on the diversity analysis.

In summary, the initial results on the metatranscriptome-derived, antibody-based isolation method for Thaumarchaeota from the redoxcline of El Zapote are very promising. Thaumarchaeota can be detected by PCR on the magnetic beads after the isolation procedure. This sets the foundation for further optimization and future experiments will reveal the

performance of the method. Further experiments are needed to determine the specificity of the Thaumarchaeota-targeting approach, preferably by genome amplification of the bead-isolated cells. A successful and specific isolation of unexplored organisms from highly complex environmental niches (such as the Thaumarchaeota in this case) without prior enrichment and culturing, based on metagenomic and -transcriptomic data alone, will provide the basis for developing a pipeline for the cultivation of so far unculturable microbes.

4.6 Integral perspective

A deeper understanding of redoxclines as elementary transition zones is of particular interest as the occurrence of pelagic redoxclines in not restricted to cenotes of the Yucatán peninsula, but emerge worldwide in seasonal or permanently stratified water bodies. Therefore, redoxclines are found in sulfate-rich freshwater settings (Lake Cadagno, Switzerland (Camacho et al., 2001); Lake Banyoles, Spain (Noguerola et al., 2015)) but also in marine environments such as in (semi-) enclosed seas, bays and fjords (Baltic Sea (Grote et al., 2007); Black Sea (Glaubitz et al., 2010); Cariaco, Venezuela (Taylor et al., 2001); Mariager Fjord, Denmark (Zopfi et al., 2001), Framvaren Fjord, Norway (Behnke et al., 2010), Saanich Inlet, Canada (Walsh et al., 2009)).

For cenote El Zapote, which displays extraordinary bell-shaped underwater formations, the microbiological investigations (in form of this thesis) could be based on the previous, very conclusive hydrogeochemical studies (Ritter, 2020; Ritter et al., 2019; Stinnesbeck et al., 2018) and complement them to a holistic examination. The microbiological results presented in this thesis confirm the proposed model by Ritter et al. (2019) on the growth of Hells Bells speleothems. Ritter et al. discussed nitrate-driven sulfide oxidation as the key process promoting authigenic calcite precipitation. In this study, metagenomic and metatranscriptomic profiling revealed chemolithoautotrophic Hydrogenophilales conducting denitrifying sulfide oxidation to S^0 in the electron acceptor-limited redox regime as the microbial key players in El Zapote. This microbial process, summarized as nitrate-driven sulfide oxidation, leads to local alkalinity and calcite supersaturation, which in turn results in calcite precipitation, the formation of the turbid layer, and ultimately the growth of Hells Bells. In addition to the bioinformatic results, calcite precipitation by this metabolic process was experimentally demonstrated in a simplified, artificial redoxcline milieu (section 3.4). In

cenote Angelita without Hells Bells, which is less dominated by electron acceptor limitation, the main production of sulfate via photo- and chemolithoautotrophic pathways inhibits calcification.

The identified microbial process of nitrate-driven sulfide oxidation is not new per se. Bailey et al. (2009) and Himmler et al. (2018) already discussed this metabolic pathway in connection with microbially induced calcite precipitation in sedimentary communities. Himmler et al. (2018) studied the growth of stromatolites on methane seeps in the northern Arabian Sea. They found that authigenic calcite precipitation is triggered by the combined impact of nitrate-driven sulfide oxidation and anaerobic sulfate-driven methane oxidation (Himmler et al., 2018). However, it is not the denitrification process that plays a role here, but the dissimilatory nitrate reduction to ammonium. In addition, the product of sulfide oxidation is sulfate instead of S^0. Fossing et al. (1995), however, described the process for mat-forming *Thioploca* along the continental shelf transect off the Chilean coast. *Thioploca* combine denitrification with sulfide oxidation, which proceeds via the state of elemental sulfur stored in the cytoplasm (Fossing et al., 1995). Calcite precipitation was not reported for this sedimentary environment. Interestingly, nitrate-driven sulfide oxidation was also identified in the Baltic Sea (Bruckner et al., 2013). In the pelagic redoxcline of the Baltic Sea chemolithoautotrophic ε-Proteobacteria, mainly of the '*Sulfurimonas*' GD17 cluster, seem to occur in a similar niche and may therefore be the equivalent of Hydrogenophilales in the redoxcline of El Zapote (Bruckner et al., 2013).

As unique as Hells Bells may seem – research on Hells Bells speleothems revealed that the mechanism of formation is based on a process that plays, or if not yet investigated could play, a role in pelagic redoxclines worldwide. If for other redoxclines, the corresponding key processes and organisms involved are compared, it is noticeable that there are many important similarities (Table 27). Depending on whether light is available, anoxygenic photosynthesis can play an important role in the sulfur cycle of the redoxcline, as hydrogen sulfide serves as an electron donor for the photosynthetic process. In cenote Angelita without Hells Bells, which was examined in more detail in this study, this process, catalyzed by Chlorobiales, contributes significantly to sulfide consumption and sulfate production. The same is apparently the case in Lake Cadagno (Switzerland) and Lake Rogoznica (Croatia).

Table 27: Microbial ecology of pelagic redoxclines worldwide. The microbial key players and their metabolic activity in the redox gradients are listed.

Pelagic redoxcline location	Dominant taxon/taxa	Catalyzed process	Publication
Cenote El Zapote, Mexico	Hydrogenophilales, Nitrosomonadales	Chemolithoautotrophic incomplete nitrate-driven sulfide oxidation	This study
Cenote Angelita, Mexico	Chlorobiales; Campylobacterales (ε-Proteobacteria)	Anoxygenic photosynthesis; chemolithoautotrophic nitrate-driven sulfide oxidation	This study
Baltic sea	'*Sulfurimonas*' GD17 cluster (ε-Proteobacteria)	chemolithoautotrophic nitrate-driven sulfide oxidation	Grote et al. (2007, 2008) Bruckner et al. (2013)
Black sea	ε-Proteobacteria, green sulfur bacteria	chemoautotrophy	Grote et al. (2008) Jørgensen et al. (1991)
Cariaco basin, Venezuela	ε-Proteobacteria	chemoautotrophy	Lin et al. (2006)
Lake Cadagno, Switzerland	Chromatiaceae Chlorobiaceae	Anoxygenic photosynthesis	Danza et al. (2018)
Saanich Inlet, Canada	SUP05 clade (γ-Proteobacteria)	chemolithoautotrophic nitrate-driven sulfide oxidation	Walsh et al. (2009)
Lake Rogoznica, Croatia	Green sulfur bacteria (Chlorobi) during stratification vs. γ-Proteobacteria (GSP/SUP05 clade) after anoxic holomixis	Anoxygenic photosynthesis vs. chemotrophic sulfide oxidation after anoxic holomixis	Pjevac et al. (2015)

Chemolithoautotrophic sulfide oxidation seems to be carried out dominantly by ε-Proteobacteria instead, e.g. in the Baltic and Black Sea and Cariaco basin (Venezuela). Additionally, in the Canadian Saanich Inlet the SUP05 cluster of the γ-Proteobacteria seems to be relevant. That the process of sulfide oxidation is common to all redoxclines is not surprising but is based solely on the fact that they represent the water zone, in which hydrogen

sulfide (and other reduced electron donors) encounters downwards diffusing electron acceptors. Therefore, it represents the water layer of major biogeochemical transformations.

Interesting, however, is that the Hydrogenophilales as sulfur oxidizers and key players in the redoxcline of El Zapote (with Hells Bells) really stand out. In fact, some questions remain concerning the identity of Hydrogenophilales. There is still a lot to find out about this order as there are only a few well characterized species. In 2017, Boden et al. proposed the reclassification of Hydrogenophiaceae from the *β*-Proteobacteria and they are now assigned to the new class of Hydrogenophilalia, which so far includes two genera, *Hydrogenophilus* and *Tepidiphilus* (Boden et al., 2017). Three more closely described species of the Hydrogenophilales are thermophilic, facultatively chemolithoautotrophic hydrogen oxidizers - *Tepidiphilus margaritifer* (Manaia et al., 2003), *Hydrogenophilus hirschii* (Stöhr et al., 2001) and *Hydrogenophilus thermoluteolus* (Hayashi et al., 1999). These three representatives were identified in a hot spring, the Yellowstone National Park and in a thermophilic aerobic digester. The Hydrogenophilales studied at cenote El Zapote, however, live under mesophilic conditions with a redoxcline temperature of ~24.5 °C (Ritter et al., 2019). As described previously, the Hydrogenophilaceae of El Zapote most likely form a new genus within the class of Hydrogenophilalia. It is possible that these have metabolic features that remained unrecognized in the context of Hells Bells research, but which gives them a growth advantage over the chemolithoautotrophic *ε*-Proteobacteria dominant in other redoxclines. In any case, it will be of interest to further study the Hydrogenophilaceae and their function in the redoxcline in more detail. Previous attempts have shown that their enrichment is very challenging. Once the antibody-based isolation approach presented in this work is successfully established for isolating so far unculturable organisms such as Thaumarchaeota, this method could be adapted to target Hydrogenophilales, and the sulfur oxidizers could subsequently be studied in detail by single cell sequencing and cultivation.

Intensive research on the formation of Hells Bells from the hydrogeochemical (Ritter, 2020; Ritter et al., 2019; Stinnesbeck et al., 2018) and microbiological perspectives (Leberecht et al. (in revision); this thesis) has allowed to formulate a series of fundamental conditions for their development. Further, the identified requirements may help to assess, on the basis of the on-site hydrogeochemistry and microbial consortia, whether underwater speleothems are likely to occur in so far unexplored cenotes. Figure 35 shows a flow chart that summarizes all insights into the growth of Hells Bells and may give an orientation if calcite precipitation

is to be expected or rather not. While some hydrogeochemical requirements are specified only for the development of Hells Bells, all other aspects are also suitable for the prediction of calcite precipitation in pelagic redoxclines independent of speleothem development.

Ritter et al. (2019) established that the basic requirement for the development of Hells Bells is stagnancy to allow a predominant halocline to form and the water body to stratify. Therefore, the cenote must first be deep enough to reach the halocline at all. Furthermore, a high degree of organic matter mineralization must occur to create anoxic conditions in the halocline and provide reduced C, N and S compounds to the microbiome. Meromixis and water stagnancy in turn favor the development of redox gradients. Lightless conditions favor chemolithoautotrophy. Specifically for the growth of Hells Bells, a hydraulically controlled oscillating vertical movement of the halocline must be ensured (Ritter et al., 2019).

If these conditions are established, there are further factors that influence the microbial metabolic activity in the redoxcline thus the occurrence of Hells Bells. This involves the availability of electron donors and acceptors for the dominant metabolic processes, especially for sulfide oxidation. Furthermore, the availability of light determines whether anoxygenic photosynthesis plays a role in the redoxcline.

In an oxidant-deficient regime such as in cenote El Zapote with Hells Bells, proton-consuming processes dominate – more precisely, nitrate-driven sulfide oxidation (Ritter et al., 2019; Ritter, 2020; Leberecht et al. (in revision)). Sulfide oxidation can occur aerobically or anaerobically with alternative electron acceptors such as nitrate (in the case of El Zapote with subsequent complete denitrification). The result is an incomplete sulfur oxidation process with elemental sulfur as the neutral product instead of sulfate. Proton and hydrogen sulfide consumption results in pH increase and finally calcite precipitation.
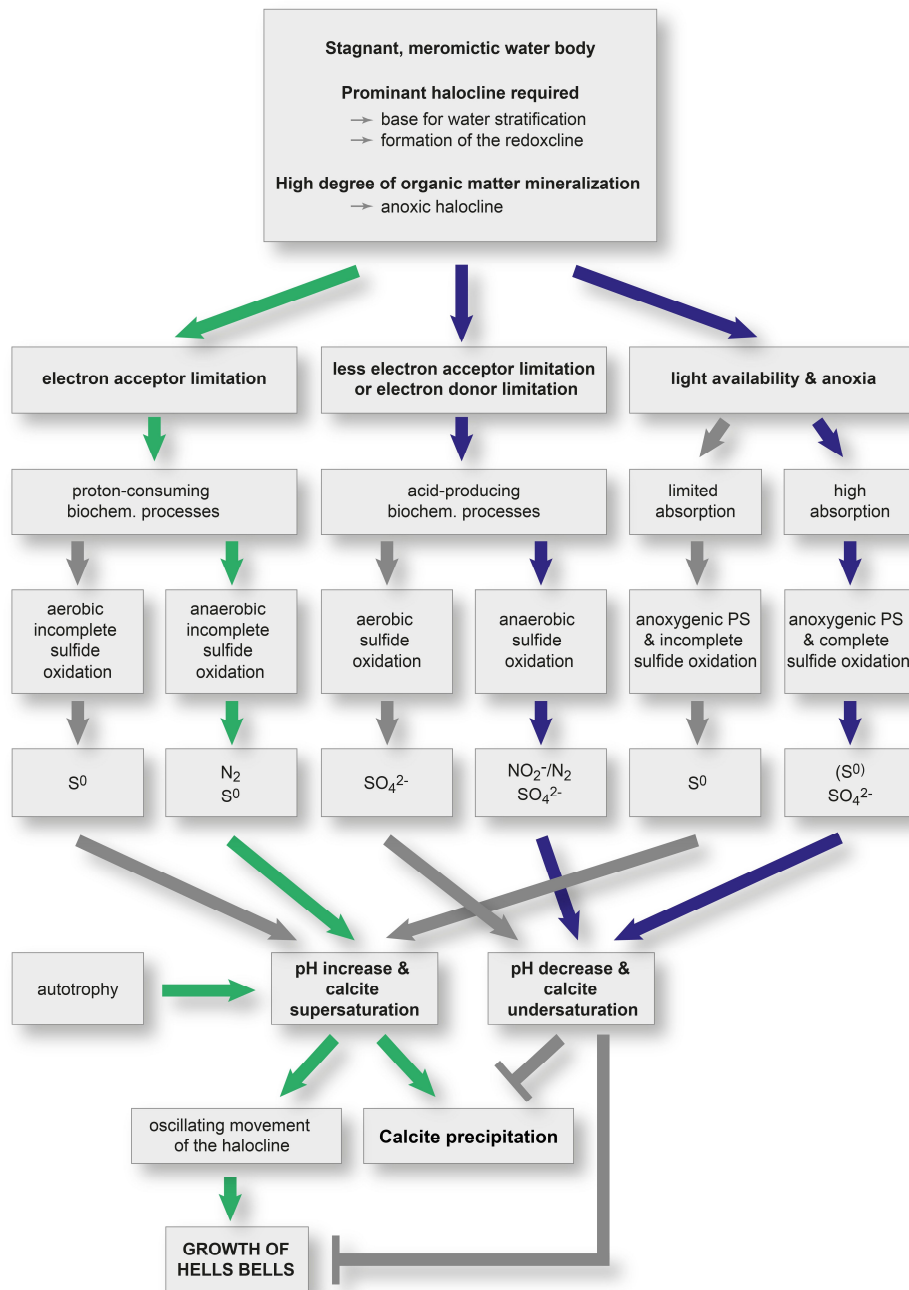
Figure 35: Flow chart for the developmental process of Hells Bells in pelagic redoxclines. The basic hydrogeochemical requirements for the occurrence of Hells Bells were defined by Ritter (2020) and Ritter et al. (2019). Depending on the redox regime and the availability of light, different microbially catalyzed sulfur oxidation processes occur. These have either inhibitory or promoting effects on calcite precipitation and thus on Hells Bells growth. Green arrows represent the scenario in the redoxcline of El Zapote with Hells Bells, blue arrows represent the conditions in the redoxcline of cenote Angelita without Hells Bells.

If, however, as in the case of cenote Angelita (without Hells Bells), the redoxcline is less oxidant deficient, the available amount of electron acceptor (e.g. O_2 or NO_3^-) is sufficient to oxidize hydrogen sulfide mainly to sulfate (as sulfuric acid). Due to sulfate production, the pH decreases and results in calcite undersaturation. Thus, no calcite precipitate and no Hells Bells growth occurs.

In cenotes like Angelita, where light still reaches the redoxcline (at least in minimal intensities), anoxygenic photosynthesis can be involved in the sulfur cycle. The incomplete oxidation of hydrogen sulfide promotes calcite precipitation, while complete oxidation counteracts it (Frigaard, 2016). However, it is still unclear whether there are Hells Bells that resulted from anoxygenic photosynthesis with incomplete hydrogen sulfide oxidation alone. Potentially, this light-dependent process is too dynamic to promote calcification in the long term.

4.7 Outlook

On the basis of the previous Hells Bells research, future studies could reveal whether cenotes with Hells Bells share only certain key microbial processes, or whether certain key players such as the Hydrogenophilales must also be involved in the biochemical cycling in redoxclines. Cenote Tortugas, which also displays smaller specimens of Hells Bells, would be another cenote that would advance the understanding of the occurrence of underwater speleothems. Ritter (2020) suggested that the lack of a prominent turbid layer could be due to the production of polysulfides instead of S^0. A metatranscriptomic analysis of the community in the redoxcline of cenote Tortugas could shed light on how the sulfur oxidizers are adapted to the even more extreme electron acceptor limitation and to what extent the microbiome differs from El Zapote. With each additional redoxcline studied and the particularities of the redox regime, the understanding of the interaction of the sulfur cycle and calcite precipitation deepens. This is of great interest, considering that oxygen minimal zones and thus sulfidic environments will continue to spread with rising temperatures (Diaz & Rosenberg, 2008).

In addition, it would be exciting in the next step to explore calcite precipitation beyond the redoxclines of cenotes. Using the list of fundamental hydrogeobiochemical requirements

established by Ritter (2020) and expanded in this work, it could be examined whether calcite precipitation is to be expected in other redoxclines.

In the context of the microbial key players in the redoxcline of El Zapote, there are still open questions that can be addressed. First, it would be exciting to clarify the taxonomic classification of the key players and whether they actually form a new genus within the Hydrogenophilaceae. In this context, the genomic features would also be examined in more detail. Furthermore, it could be investigated whether the Hydrogenophilaceae store elemental sulfur granules outside or inside the cells and have other special adaptations to electron acceptor limitation, such as nitrate concentrating mechanisms (like that of *Thioploca* (Fossing et al., 1995)) or the ability to reduce manganese (like the ε-Proteobacteria in the Baltic Sea (Henkel et al., 2019)).

However, to address these aspects, the key players would first have to be isolated. To circumvent the challenges of the enrichment through cultivation Hydrogenophilales could be isolated directly from the redoxcline water adapting the antibody-based isolation approach presented in this work to these unknown bacteria. The method itself will be tested in the next step for specificity to the target organisms (Thaumarchaeota) and enrichment efficiency. Thereby, an enzymatic antibody digestion could be tested to release the intact cells from the antibody-bead complex for the subsequent genome amplification and analysis. Furthermore, catalyzed reporter deposition fluorescence *in-situ* hybridization (CARD-FISH) could be another approach to verify that Thaumarchaeota cells successfully bound to the antibody-magnetic bead complex. Once this approach is successful with Thaumarchaeota as an exemplary target, an important basis for the further development of a pipeline for the direct isolation of organisms from complex communities has been established.

ACKNOWLEDGMENTS

I really thank you, Johannes, for challenging and supporting me so wonderfully over the three years of my PhD. Thank you for always trusting in my skills, for your support and your great optimism. You always had valuable advice for me when I was stranded. I am really grateful for how much I have evolved in your research group. You have really created a great working atmosphere that has always motivated and inspired me!

Furthermore, I want to express my thanks to Simon Ritter, Prof. Stinnesbeck and Prof. Isenbeck-Schröter. Thank you for getting me involved in such an exciting research project. You have welcomed me wonderfully into the Hells Bells team and I have enjoyed our collaboration very much. Thank you, Simon, for all the hydrogeological input you passed on to me over time and for all the exciting discussions. Thank you, Lukas Klose, Christian Scholz and Julian Eschenröder for two extraordinary sampling campaigns in Mexico. Thanks also go to John and Morgan and the whole AG Kaster for any help.

I'd like to thank the whole AG Gescher! Thank you very much for all your support and the great time with you. You don't find such a humorous, familiar team twice!

Many thanks go to Vicky for awakening my enthusiasm for the environmental microbiology. I learned a lot during our exciting sampling expeditions together in the Eifel.

Special thanks go to Melanie. Thank you for your generous help and support when I needed it most. Our frequent chai latte motivation sessions have gotten me through every challenging time and I enjoyed them very much. Thank you for always having an open ear for me!

Thank you, Sabrina, Lukas and Dennis, for getting me through my last stressful experiments. Sabrina, thank you that I could benefit a lot from your archaea-related frustration tolerance. You are by far the most helpful person. It was so good to have you in the environmental microbiology team.

Thank you, Jonas and Lukas, for so many funny non-sense discussions, as well as for your scientific input. Jonas, thank you so much for your support in every bioinformatic depression and for how much I have learned from you. Thank you, Edi, for helping me with every chip accident. Thank you, Miri and Janek, for bringing me on other thoughts when I was too

focused on my work. Miri, thank you also for all your great snacks, which have brought me so often through long days.

Last but not least, I would like to thank my parents, Anke and Finja, who made everything possible in the first place. Thank you that I can always count on you, for always supporting me and reminding me to trust in myself. I am so happy to have you!

Special thanks go out to my fiancé, Michael. Thank you for supporting me unconditionally through this challenging time and for always reminding me from time to time to consider a work-life balance. With your sense of humor, you always managed to get me thinking about something completely different when I needed it the most. Thank you so much for your constant encouragement and for turning worries into joy.

5 REFERENCES

Almagro Armenteros, J. J., Tsirigos, K. D., Sønderby, C. K., Petersen, T. N., Winther, O., Brunak, S., von Heijne, G., & Nielsen, H. (2019). SignalP 5.0 improves signal peptide predictions using deep neural networks. *Nature Biotechnology*, *37*(4), 420–423.

Altermann, W., Kazmierczak, J., Oren, A., & Wright, D. T. (2006). Cyanobacterial calcification and its rock-building potential during 3.5 billion years of earth history. *Geobiology*, *4*(3), 147–166.

Alvarez, L., Bricio, C., Blesa, A., Hidalgo, A., & Berenguer, J. (2014). Transferable denitrification capability of *Thermus thermophilus*. *Applied and Environmental Microbiology*, *80*(1), 19–28.

Arp, G., Reimer, A., & Reitner, J. (1999). Calcification in cyanobacterial biofilms of alkaline salt lakes. *European Journal of Phycology*, *34*(4), 393–403.

Bauer-Gottwein, P., Gondwe, B. R. N., Charvet, G., Marín, L. E., Rebolledo-Vieyra, M., & Merediz-Alonso, G. (2011). Review: The Yucatán Peninsula karst aquifer, Mexico. *Hydrogeology Journal*, *19*(3), 507–524.

Baumgartner, L. K., Reid, R. P., Dupraz, C., Decho, A. W., Buckley, D. H., Spear, J. R., Przekop, K. M., & Visscher, P. T. (2006). Sulfate reducing bacteria in microbial mats: Changing paradigms, new discoveries. *Sedimentary Geology*, *185*(3), 131–145.

Behnke, A., Barger, K. J., Bunge, J., & Stoeck, T. (2010). Spatio-temporal variations in protistan communities along an O2/H2S gradient in the anoxic Framvaren Fjord (Norway). *FEMS Microbiology Ecology*, *72*(1), 89–102.

Beller, H. R., Chain, P. S. G., Letain, T. E., Chakicherla, A., Larimer, F. W., Richardson, P. M., Coleman, M. A., Wood, A. P., & Kelly, D. P. (2006). The genome sequence of the obligately chemolithoautotrophic, facultatively anaerobic bacterium *Thiobacillus denitrificans*. *Journal of Bacteriology*, *188*(4), 1473–1488.

Berg, C., Vandieken, V., Thamdrup, B., & Jürgens, K. (2015). Significance of archaeal nitrification in hypoxic waters of the Baltic Sea. *The ISME Journal*, *9*(6), 1319–1332.

Beveridge, T. J., & Murray, R. G. (1976). Uptake and retention of metals by cell walls of *Bacillus subtilis*. *Journal of Bacteriology*, *127*(3), 1502–1518.

Boden, R., Hutt, L. P., & Rae, A. W. (2017). Reclassification of *Thiobacillus aquaesulis* (Wood & Kelly, 1995) as *Annwoodia aquaesulis* gen. nov., comb. nov., transfer of *Thiobacillus* (Beijerinck, 1904) from the Hydrogenophilales to the Nitrosomonadales, proposal of Hydrogenophilalia class. nov. *International Journal of Systematic and Evolutionary Microbiology*, *67*(5), 1191–1205.

Bolger, A. M., Lohse, M., & Usadel, B. (2014). Trimmomatic: A flexible trimmer for Illumina sequence data. *Bioinformatics*, *30*(15), 2114–2120.

Bontognali, T. R. R., D'Angeli, I. M., Tisato, N., Vasconcelos, C., Bernasconi, S. M., Gonzales, E. R. G., & De Waele, J. (2016). Mushroom speleothems: stromatolites that formed in the absence of phototrophs. *Frontiers in Earth Science, 4,* 49.

Bosak, T, Greene, S. E., & Newman, D. K. (2007). A likely role for anoxygenic photosynthetic microbes in the formation of ancient stromatolites. *Geobiology*, *5*(2), 119–126.

Bosak, Tanja. (2011). Calcite Precipitation, Microbially Induced. *Encyclopedia of Geobiology* (J. Reitner & V. Thiel (eds.); pp. 223–227). Springer Netherlands.

Boughanemi, S., Lyonnet, J., Infossi, P., Bauzan, M., Kosta, A., Lignon, S., Giudici-Orticoni, M.-T., & Guiral, M. (2016). Microbial oxidative sulfur metabolism: biochemical evidence of the membrane-bound heterodisulfide reductase-like complex of the bacterium *Aquifex aeolicus*. *FEMS Microbiology Letters*, *363*(15).

Brankovits, D., Pohlman, J. W., Niemann, H., Leigh, M. B., Leewis, M. C., Becker, K. W., Iliffe, T. M., Alvarez, F., Lehmann, M. F., & Phillips, B. (2017). Methane- and dissolved organic carbon-fueled microbial loop supports a tropical subterranean estuary ecosystem. *Nature Communications*, *8*(1), 1–12.

Bray, N. L., Pimentel, H., Melsted, P., & Pachter, L. (2016). Near-optimal probabilistic RNA-seq quantification. *Nature Biotechnology*, *34*(5*)*, 525–527.

Bruckner, C. G., Mammitzsch, K., Jost, G., Wendt, J., Labrenz, M., & Jürgens, K. (2013). Chemolithoautotrophic denitrification of epsilonproteobacteria in marine pelagic redox gradients. *Environmental Microbiology*, *15*(5), 1505–1513.

Buchfink, B., Xie, C., & Huson, D. H. (2015). Fast and sensitive protein alignment using DIAMOND. *Nature Methods*, *12*(1), 59–60.

Bundeleva, I. A., Shirokova, L. S., Bénézeth, P., Pokrovsky, O. S., Kompantseva, E. I., & Balor, S. (2012). Calcium carbonate precipitation by anoxygenic phototrophic bacteria. *Chemical Geology*, *291*, 116–131.

Burow, L. C., Woebken, D., Marshall, I. P. G., Singer, S. W., Pett-Ridge, J., Prufert-Bebout, L., Spormann, A. M., Bebout, B. M., Weber, P. K., & Hoehler, T. M. (2014). Identification of Desulfobacterales as primary hydrogenotrophs in a complex microbial mat community. *Geobiology*, *12*(3), 221–230.

Camacho, A., Erez, J., Chicote, A., Florín, M., Squires, M. M., Lehmann, C., & Backofen, R. (2001). Microbial microstratification, inorganic carbon photoassimilation and dark carbon fixation at the chemocline of the meromictic Lake Cadagno (Switzerland) and its relevance to the food web. *Aquatic Sciences*, *63*(1), 91–106.

Castanier, S., Le Metayer-Levrel, G., & Perthuisot, J.-P. (2000). Bacterial roles in the precipitation of carbonate minerals. In *Microbial sediments* (pp. 32–39). Springer Berlin Heidelberg.

Castanier, S., Le Métayer-Levrel, G., & Perthuisot, J.-P. (1999). Ca-carbonates precipitation and limestone genesis – the microbiogeologist point of view. *Sedimentary Geology*, *126*(1–4), 9–23.

Castro-Alonso, M. J., Montañez-Hernandez, L. E., Sanchez-Muñoz, M. A., Macias Franco, M. R., Narayanasamy, R., & Balagurusamy, N. (2019). Microbially induced calcium carbonate precipitation (MICP) and its potential in bioconcrete: microbiological and molecular concepts. *Frontiers in Materials*, *6*, 126.

Chandak, S., Neu, J., Tatwawadi, K., Mardia, J., Lau, B., Kubit, M., Hulett, R., Griffin, P., Wootters, M., Weissman, T., & Ji, H. (2020). Overcoming high nanopore basecaller error rates for DNA storage via basecaller-decoder integration and convolutional codes. *BioRxiv*, 2019.12.20.871939.

References

Chapin III, F. S., Matson, P. A., & Vitousek, P. (2011). *Principles of terrestrial ecosystem ecology*. Springer.

Chen, Z., Koh, M., Van Driessche, G., Van Beeumen, J., Bartsch, R., Meyer, T., Cusanovich, M., & Mathews, F. (1994). The structure of flavocytochrome *c* sulfide dehydrogenase from a purple phototrophic bacterium. *Science*, *266*(5184), 430–432.

Cort, J. R., Selan, U., Schulte, A., Grimm, F., Kennedy, M. A., & Dahl, C. (2008). *Allochromatium vinosum* DsrC: solution-state NMR structure, redox properties, and interaction with DsrEFH, a protein essential for purple sulfur bacterial sulfur oxidation. *Journal of Molecular Biology*, *382*(3), 692–707.

Costa, O. Y. A., Raaijmakers, J. M., & Kuramae, E. E. (2018). Microbial extracellular polymeric substances: ecological function and impact on soil aggregation. *Frontiers in Microbiology*, *9*, 1636.

Cross, K. L., Campbell, J. H., Balachandran, M., Campbell, A. G., Cooper, S. J., Griffen, A., Heaton, M., Joshi, S., Klingeman, D., Leys, E., Yang, Z., Parks, J. M., & Podar, M. (2019). Targeted isolation and cultivation of uncultivated bacteria by reverse genomics. *Nature Biotechnology*, *37*(11), 1314–1321.

Dahl, C., Franz, B., Hensen, D., Kesselheim, A., & Zigann, R. (2013). Sulfite oxidation in the purple sulfur bacterium *Allochromatium vinosum*: identification of SoeABC as a major player and relevance of SoxYZ in the process. *Microbiology*, *159*(Pt_12), 2626–2638.

Dahl, C., & Prange, A. (2006). Bacterial sulfur globules: occurrence, structure and metabolism. In J. M. Shively (Ed.), *Inclusions in Prokaryotes* (pp. 21–51). Springer Berlin Heidelberg.

Danza, F., Ravasi, D., Storelli, N., Roman, S., Lüdin, S., Bueche, M., & Tonolla, M. (2018). Bacterial diversity in the water column of meromictic Lake Cadagno and evidence for seasonal dynamics. *PloS One*, *13*(12), e0209743.

De Moel, P., Van der Helm, A., Rijn, M., Dijk, J., & Meer, W. (2013). Assessment of calculation methods for calcium carbonate saturation in drinking water for DIN 38404-10 compliance. *Drinking Water Engineering and Science Discussions*, *6*, 167–198.

Diaz, R. J., & Rosenberg, R. (2008). Spreading dead zones and consequences for marine ecosystems. *Science*, *321*(5891), 926–929.

Drennan, D. M., Almstrand, R., Lee, I., Landkamer, L., Figueroa, L., & Sharp, J. O. (2016). Organoheterotrophic bacterial abundance associates with zinc removal in lignocellulose-based sulfate-reducing systems. *Environmental Science & Technology*, *50*(1), 378–387.

Druschel, G. K., & Kappler, A. (2015). Geomicrobiology and microbial geochemistry. *Elements*, *11*(6), 389–394.

Dupraz, C., Reid, R. P., Braissant, O., Decho, A. W., Norman, R. S., & Visscher, P. T. (2009). Processes of carbonate precipitation in modern microbial mats. *Earth-Science Reviews*, *96*(3), 141–162.

Eloe-Fadrosh, E. A., Ivanova, N. N., Woyke, T., & Kyrpides, N. C. (2016). Metagenomics uncovers gaps in amplicon-based detection of microbial diversity. *Nature Microbiology*, *1*, 15032.

Enyedi, N. T., Makk, J., Kótai, L., Berényi, B., Klébert, S., Sebestyén, Z., Molnár, Z., Borsodi, A. K.,

Leél-Őssy, S., Demény, A., & Németh, P. (2020). Cave bacteria-induced amorphous calcium carbonate formation. *Scientific Reports*, *10*(1), 8696.

Erşan, Y. Ç., Belie, N. de, & Boon, N. (2015). Microbially induced CaCO3 precipitation through denitrification: An optimization study in minimal nutrient environment. *Biochemical Engineering Journal*, *101*, 108–118.

Fein, J. B., Daughney, C. J., Yee, N., & Davis, T. A. (1997). A chemical equilibrium model for metal adsorption onto bacterial surfaces. *Geochimica et Cosmochimica Acta*, *61*(16), 3319–3328.

Fossing, H., Gallardo, V. A., Jørgensen, B. B., Hüttel, M., Nielsen, L. P., Schulz, H., Canfield, D. E., Forster, S., Glud, R. N., Gundersen, J. K., Küver, J., Ramsing, N. B., Teske, A., Thamdrup, B., & Ulloa, O. (1995). Concentration and transport of nitrate by the mat-forming sulphur bacterium *Thioploca*. *Nature*, *374*(6524), 713–715.

Francis, C. A., Roberts, K. J., Beman, J. M., Santoro, A. E., & Oakley, B. B. (2005). Ubiquity and diversity of ammonia-oxidizing archaea in water columns and sediments of the ocean. *Proceedings of the National Academy of Sciences of the United States of America*, *102*(41), 14683–14688.

Frigaard, N.-U. (2016). Biotechnology of anoxygenic phototrophic bacteria. *Advances in Biochemical Engineering/Biotechnology*, *156*, 139–154.

Frigaard, N.-U., & Dahl, C. (2008). Sulfur metabolism in phototrophic sulfur bacteria. *Advances in Microbial Physiology, 54*, 103–200.

Fromme, P. (1996). Structure and function of photosystem I. *Current Opinion in Structural Biology*, *6*(4), 473–484.

Fuchs, G., Eitinger, T., Heider, J., Kothe, E., & Overmann, J. (2017). *Allgemeine Mikrobiologie* (10th ed.). Georg Thieme Verlag.

Garcia, J.-L., Ollivier, B., & Whitman, W. B. (2006). The order methanomicrobiales. *In* M. Dworkin, F. Stanley, E. Rosenberg, K.-H. Schleifer, & E. Stackebrandt (Eds.), *The Prokaryotes* (3rd ed.). Springer.

Gautret, P., & Trichet, J. (2005). Automicrites in modern cyanobacterial stromatolitic deposits of Rangiroa, Tuamotu Archipelago, French Polynesia: Biochemical parameters underlaying their formation. *Sedimentary Geology*, *178*(1), 55–73.

Glaubitz, S., Labrenz, M., Jost, G., & Jürgens, K. (2010). Diversity of active chemolithoautotrophic prokaryotes in the sulfidic zone of a Black Sea pelagic redoxcline as determined by rRNA-based stable isotope probing. *FEMS Microbiology Ecology*, *74*(1), 32–41.

Grabarczyk, D. B., & Berks, B. C. (2017). Intermediates in the Sox sulfur oxidation pathway are bound to a sulfane conjugate of the carrier protein SoxYZ. *PloS One*, *12*(3), e0173395.

Greer, H. F., Zhou, W., & Guo, L. (2017). Reversed crystal growth of calcite in naturally occurring travertine crust. *Crystals, 7*(2), 36.

Griesbeck, C., Hauska, G., & Schütz, M. (2000). Biological Sulfide Oxidation: Sulfide-Quinone Reductase (SQR), the Primary Reaction. *Recent research developments in microbiology, 4*, 179–203.

Griesbeck, C., Schütz, M., Schödl, T., Bathe, S., Nausch, L., Mederer, N., Vielreicher, M., & Hauska, G. (2002). Mechanism of sulfide-quinone reductase investigated using site-directed mutagenesis and sulfur analysis. *Biochemistry*, *41*(39), 11552–11565.

Grote, J., Jost, G., Labrenz, M., Herndl, G. J., & Jürgens, K. (2008). Epsilonproteobacteria represent the major portion of chemoautotrophic bacteria in sulfidic waters of pelagic redoxclines of the baltic and black seas. *Applied and Environmental Microbiology*, *74*(24), 7546–7551.

Grote, J., Labrenz, M., Pfeiffer, B., Jost, G., & Jürgens, K. (2007). Quantitative distributions of Epsilonproteobacteria and a *Sulfurimonas* subgroup in pelagic redoxclines of the central Baltic Sea. *Applied and Environmental Microbiology*, *73*(22), 7155–7161.

Grote, J., Schott, T., Bruckner, C. G., Glöckner, F. O., Jost, G., Teeling, H., Labrenz, M., & Jürgens, K. (2012). Genome and physiology of a model epsilonproteobacterium responsible for sulfide detoxification in marine oxygen depletion zones. *Proceedings of the National Academy of Sciences*, *109*(2), 506– 510.

Gruber-Vodicka, H. R., Seah, B. K., & Pruesse, E. (2019). phyloFlash — Rapid SSU rRNA profiling and targeted assembly from metagenomes. *BioRxiv*, 521922.

Gulley, J. D., B.Martin, J., & Brown, A. (2016). Organic carbon inputs, common ions and degassing: rethinking mixing dissolution in coastal eogenetic carbonate aquifers. *Earth Surface Processes and Landforms*, *41*(14), 2098–2110.

Hansen, S. H., Kabbeck, T., Radtke, C. P., Krause, S., Krolitzki, E., Peschke, T., Gasmi, J., Rabe, K. S., Wagner, M., Horn, H., Hubbuch, J., Gescher, J., & Niemeyer, C. M. (2019). Machine-assisted cultivation and analysis of biofilms. *Scientific Reports*, *9*(1).

Hayashi, N. R., Ishida, T., Yokota, A., Kodama, T., & Igarashi, Y. (1999). *Hydrogenophilus thermoluteolus* gen. nov., sp. nov., a thermophilic, facultatively chemolithoautotrophic, hydrogen-oxidizing bacterium. *International Journal of Systematic Bacteriology*, *49*(2), 783– 786.

Henkel, J. V, Dellwig, O., Pollehne, F., Herlemann, D. P. R., Leipe, T., & Schulz-Vogt, H. N. (2019). A bacterial isolate from the Black Sea oxidizes sulfide with manganese(IV) oxide. *Proceedings of the National Academy of Sciences*, *116*(25), 12153–12155.

Himmler, T., Smrzka, D., Zwicker, J., Kasten, S., Shapiro, R. S., Bohrmann, G., & Peckmann, J. (2018). Stromatolites below the photic zone in the northern Arabian Sea formed by calcifying chemotrophic microbial mats. *Geology*, *46*(4), 339–342.

Holmes, A. J., Tujula, N. A., Holley, M., Contos, A., James, J. M., Rogers, P., & Gillings, M. R. (2001). Phylogenetic structure of unusual aquatic microbial formations in Nullarbor caves, Australia. *Environmental Microbiology*, *3*(4), 256–264.

Huerta-Cepas, J., Forslund, K., Coelho, L. P., Szklarczyk, D., Jensen, L. J., von Mering, C., & Bork, P. (2017). Fast Genome-Wide Functional Annotation through Orthology Assignment by eggNOG-Mapper. *Molecular Biology and Evolution*, *34*(8), 2115–2122.

Huerta-Cepas, J., Szklarczyk, D., Heller, D., Hernández-Plaza, A., Forslund, S. K., Cook, H., Mende, D. R., Letunic, I., Rattei, T., Jensen, L. J., von Mering, C., & Bork, P. (2019). eggNOG 5.0: a hierarchical, functionally and phylogenetically annotated orthology resource based on 5090 organisms and 2502 viruses. *Nucleic Acids Research*, *47*(D1), D309–D314.

Huggett, R. (2003). Karst Landscapes. In *Fundamentals of geomorphology (Routledge Fundamentals of Physical Geography)* (p. 404). Routledge.

Hyatt, D., Chen, G. L., LoCascio, P. F., Land, M. L., Larimer, F. W., & Hauser, L. J. (2010). Prodigal: Prokaryotic gene recognition and translation initiation site identification. *BMC Bioinformatics*, *11*(1), 119.

Imhoff, J. F. (2014). Biology of Green Sulfur Bacteria. In *eLS*.

Imhoff, J. F. (2016). New dimensions in microbial ecology - functional genes in studies to unravel the biodiversity and role of functional microbial groups in the environment. *Microorganisms*, *4*(2), 19.

Jørgensen, B. B., Fossing, H., Wirsen, C. O., & Jannasch, H. W. (1991). Sulfide oxidation in the anoxic Black Sea chemocline. *Deep Sea Research Part A. Oceanographic Research Papers*, *38*, S1083–S1103.

Jung, M.-Y., Park, S.-J., Min, D., Kim, J.-S., Rijpstra, W. I. C., Sinninghe Damsté, J. S., Kim, G.-J., Madsen, E. L., & Rhee, S.-K. (2011). Enrichment and characterization of an autotrophic ammonia-oxidizing archaeon of mesophilic crenarchaeal group I.1a from an agricultural soil. *Applied and Environmental Microbiology*, *77*(24), 8635–8647.

Kamennaya, N. A., Ajo-Franklin, C. M., Northen, T., & Jansson, C. (2012). Cyanobacteria as biocatalysts for carbonate mineralization. *Minerals, 2*(4).

Kappler, U., & Bailey, S. (2005). Molecular basis of intramolecular electron transfer in sulfite-oxidizing enzymes is revealed by high resolution structure of a heterodimeric complex of the catalytic molybdopterin subunit and a *c*-type cytochrome subunit. *Journal of Biological Chemistry*, *280*(26), 24999–25007.

Kappler, U., Bennett, B., Rethmeier, J., Schwarz, G., Deutzmann, R., McEwan, A. G., & Dahl, C. (2000). Sulfite:cytochrome *c* oxidoreductase from *Thiobacillus novellus*. *Journal of Biological Chemistry*, *275*(18), 13202–13212.

Kelly, D. P., & Wood, A. P. (2000). Confirmation of *Thiobacillus denitrificans* as a species of the genus *Thiobacillus*, in the beta-subclass of the Proteobacteria, with strain NCIMB 9548 as the type strain. *International Journal of Systematic and Evolutionary Microbiology*, *50*(2), 547–550.

Knittel, K., Lösekann, T., Boetius, A., Kort, R., & Amann, R. (2005). Diversity and distribution of methanotrophic archaea at cold seeps. *Applied and Environmental Microbiology*, *71*(1), 467–479.

Koch, T., & Dahl, C. (2018). A novel bacterial sulfur oxidation pathway provides a new link between the cycles of organic and inorganic sulfur compounds. *The ISME Journal*, *12*(10), 2479–2491.

Könneke, M., Bernhard, A. E., De La Torre, J. R., Walker, C. B., Waterbury, J. B., & Stahl, D. A. (2005). Isolation of an autotrophic ammonia-oxidizing marine archaeon. *Nature*, *437*(7058), 543–546.

Könneke, M., Schubert, D. M., Brown, P. C., Hügler, M., Standfest, S., Schwander, T., Schada Von Borzyskowski, L., Erb, T. J., Stahl, D. A., & Berg, I. A. (2014). Ammonia-oxidizing archaea use the most energy-efficient aerobic pathway for CO2 fixation. *Proceedings of the National Academy of Sciences of the United States of America*, *111*(22), 8239–8244.

References

Kovacs, S. E., Reinhardt, E. G., Chatters, J. C., Rissolo, D., Schwarcz, H. P., Collins, S. V, Kim, S.-T., Nava Blank, A., & Luna Erreguerena, P. (2017). Calcite raft geochemistry as a hydrological proxy for Holocene aquifer conditions in Hoyo Negro and Ich Balam (Sac Actun Cave System), Quintana Roo, Mexico. *Quaternary Science Reviews*, *175*, 97–111.

Krogh, A., Larsson, B., von Heijne, G., & Sonnhammer, E. L. L. (2001). Predicting transmembrane protein topology with a hidden markov model: application to complete genomes. *Journal of Molecular Biology*, *305*(3), 567–580.

Kuever, J. (2014). The Family Desulfarculaceae. *In* E. Rosenberg, E. F. DeLong, S. Lory, E. Stackebrandt, & F. Thompson (eds.), *The Prokaryotes: Deltaproteobacteria and Epsilonproteobacteria* (pp. 41–44). Springer Berlin Heidelberg.

Kushkevych, I., Bosáková, V., Vítězová, M., & Rittmann, S. K.-M. R. (2021). Anoxygenic photosynthesis in photolithotrophic sulfur bacteria and their role in detoxication of hydrogen sulfide. In *Antioxidants* (Vol. 10, Issue 6).

Labrenz, M., Sintes, E., Toetzke, F., Zumsteg, A., Herndl, G. J., Seidler, M., & Jürgens, K. (2010). Relevance of a crenarchaeotal subcluster related to *Candidatus* Nitrosopumilus maritimus to ammonia oxidation in the suboxic zone of the central Baltic Sea. *The ISME Journal*, *4*(12), 1496–1508.

Laemmli, U. K. (1970). Cleavage of structural proteins during the assembly of the head of Bacteriophage T4. *Nature*, *227*(5259), 680–685.

Langmead, B., & Salzberg, S. L. (2012). Fast gapped-read alignment with Bowtie 2. *Nature Methods*, *9*(4), 357–359.

Li, D., Liu, C. M., Luo, R., Sadakane, K., & Lam, T. W. (2015). MEGAHIT: An ultra-fast single-node solution for large and complex metagenomics assembly via succinct de Bruijn graph. *Bioinformatics*, *31*(10), 1674–1676.

Li, D., Luo, R., Liu, C.-M., Leung, C.-M., Ting, H.-F., Sadakane, K., Yamashita, H., & Lam, T.-W. (2016). MEGAHIT v1.0: a fast and scalable metagenome assembler driven by advanced methodologies and community practices. *Methods*, *102*, 3–11.

Liang, B., Wang, L.-Y., Mbadinga, S. M., Liu, J.-F., Yang, S.-Z., Gu, J.-D., & Mu, B.-Z. (2015). Anaerolineaceae and Methanosaeta turned to be the dominant microorganisms in alkanes-dependent methanogenic culture after long-term of incubation. *AMB Express*, *5*(1), 117.

Lin, X., Wakeham, S. G., Putnam, I. F., Astor, Y. M., Scranton, M. I., Chistoserdov, A. Y., & Taylor, G. T. (2006). Comparison of vertical distributions of prokaryotic assemblages in the anoxic Cariaco Basin and Black Sea by use of fluorescence in situ hybridization. *Applied and Environmental Microbiology*, *72*(4), 2679–2690.

Lin, Y.-J., Dancea, F., Löhr, F., Klimmek, O., Pfeiffer-Marek, S., Nilges, M., Wienk, H., Kröger, A., & Rüterjans, H. (2004). Solution structure of the 30 kDa polysulfide-sulfur transferase homodimer from *Wolinella succinogenes*. *Biochemistry*, *43*(6), 1418–1424.

Löffler, M., Feldhues, J., Venceslau, S. S., Kammler, L., Grein, F., Pereira, I. A. C., & Dahl, C. (2020). DsrL mediates electron transfer between NADH and rDsrAB in *Allochromatium vinosum*. *Environmental Microbiology*, *22*(2), 783–795.

López-Martínez, R., Gázquez, F., Calaforra, J. M., Audra, P., Bigot, J. Y., Pi Puig, T., Alcántara-

Hernández, R. J., Navarro, Á., Crochet, P., & Corona Martínez, L. (2020). Bubble trail and folia in cenote Zapote, Mexico: petrographic evidence for abiotic precipitation driven by CO2 degassing below the water table. *International Journal of Speleology*, *49*(3), 1.

Manaia, C. M., Nogales, B., & Nunes, O. C. (2003). *Tepidiphilus margaritifer* gen. nov., sp. nov., isolated from a thermophilic aerobic digester. *International Journal of Systematic and Evolutionary Microbiology*, *53*(5), 1405–1410.

Marcia, M., Ermler, U., Peng, G., & Michel, H. (2009). The structure of *Aquifex aeolicus* sulfide:quinone oxidoreductase, a basis to understand sulfide detoxification and respiration. *Proceedings of the National Academy of Sciences*, *106*(24), 9625–9630.

Martens-Habbena, W., Berube, P. M., Urakawa, H., De La Torre, J. R., & Stahl, D. A. (2009). Ammonia oxidation kinetics determine niche separation of nitrifying Archaea and Bacteria. *Nature*, *461*(7266), 976–979.

Melim, L. A., Shinglman, K. M., Boston, P. J., Northup, D. E., Spilde, M. N., & Queen, M. J. (2001). Evidence for microbial involvement in pool finger precipitation, hidden cave, New Mexico. *Geomicrobiology Journal*, *18*(3), 311–329.

Muck, S., De Corte, D., Clifford, E. L., Bayer, B., Herndl, G. J., & Sintes, E. (2019). Niche differentiation of aerobic and anaerobic ammonia oxidizers in a high latitude deep oxygen minimum zone. *Frontiers in Microbiology*, *10*, 2141.

Müller, A. L., Kjeldsen, K. U., Rattei, T., Pester, M., & Loy, A. (2015). Phylogenetic and environmental diversity of DsrAB-type dissimilatory (bi)sulfite reductases. *The ISME Journal*, *9*(5), 1152–1165.

Mulo, P., Sicora, C., & Aro, E.-M. (2009). Cyanobacterial *psbA* gene family: optimization of oxygenic photosynthesis. *Cellular and Molecular Life Sciences*, *66*(23), 3697–3710.

Narasingarao, P., Podell, S., Ugalde, J. A., Brochier-Armanet, C., Emerson, J. B., Brocks, J. J., Heidelberg, K. B., Banfield, J. F., & Allen, E. E. (2012). De novo metagenomic assembly reveals abundant novel major lineage of Archaea in hypersaline microbial communities. *The ISME Journal*, *6*(1), 81–93.

Noguerola, I., Picazo, A., Llirós, M., Camacho, A., & Borrego, C. M. (2015). Diversity of freshwater Epsilonproteobacteria and dark inorganic carbon fixation in the sulphidic redoxcline of a meromictic karstic lake. *FEMS Microbiology Ecology*, *91*(7).

Orlygsson, J., & Kristjansson, J. K. (2014). The Family Hydrogenophilaceae. *In* E. Rosenberg, E. F. DeLong, S. Lory, E. Stackebrandt, & F. Thompson (eds.), *The Prokaryotes: Alphaproteobacteria and Betaproteobacteria* (pp. 859–868). Springer Berlin Heidelberg.

Perry, E., Marin, L., McClain, J., & Velazquez, G. (1995). Ring of Cenotes (sinkholes), northwest Yucatan, Mexico: Its hydrogeologic characteristics and possible association with the Chicxulub impact crater. *Geology*, *23*(1), 17–20.

Pester, M., Schleper, C., & Wagner, M. (2011). The Thaumarchaeota: an emerging view of their phylogeny and ecophysiology. *Current Opinion in Microbiology*, *14*(3), 300–306.

Pjevac, P., Korlević, M., Berg, J. S., Bura-Nakić, E., Ciglenečki, I., Amann, R., & Orlić, S. (2015). Community shift from phototrophic to chemotrophic sulfide oxidation following anoxic holomixis in a stratified seawater lake. *Applied and Environmental Microbiology*, *81*(1), 298–

308.

Popall, R. M., Bolhuis, H., Muyzer, G., & Sánchez-Román, M. (2020). Stromatolites as biosignatures of atmospheric oxygenation: carbonate biomineralization and UV-C resilience in a *Geitlerinema* sp.-dominated culture. *Frontiers in Microbiology*, *11*, 948.

Queen, J. M., & Melim, L. A. (2006). Biothems: Biologically influenced speleothems in caves of the Guadalupe Mountains, New Mexico, USA. *Caves and Karst of Southeastern New Mexico, New Mexico Geological Society Guidebook, 57th Field Conference*, 167–174.

Quentmeier, A., & Friedrich, C. G. (2001). The cysteine residue of the SoxY protein as the active site of protein-bound sulfur oxidation of *Paracoccus pantotrophus* GB17. *FEBS Letters*, *503*(2–3), 168–172.

Reid, R. P., Visscher, P. T., Decho, A. W., Stolz, J. F., Bebout, B. M., Dupraz, C., Macintyre, I. G., Paerl, H. W., Pinckney, J. L., Prufert-Bebout, L., Steppe, T. F., & DesMarais, D. J. (2000). The role of microbes in accretion, lamination and early lithification of modern marine stromatolites. *Nature*, *406*(6799), 989–992.

Reinartz, M., Tschäpe, J., Brüser, T., Trüper, H. G., & Dahl, C. (1998). Sulfide oxidation in the phototrophic sulfur bacterium *Chromatium vinosum*. *Archives of Microbiology*, *170*(1), 59–68.

Ritter, S. M. (2020). *Unravelling the formation of Hells Bells: underwater speleothems from the Yucatán Peninsula in Mexico. Doctoral dissertation* [Heidelberg University].

Ritter, S. M., Isenbeck-Schröter, M., Scholz, C., Keppler, F., Gescher, J., Klose, L., Schorndorf, N., Avilés Olguín, J., González-González, A., & Stinnesbeck, W. (2019). Subaqueous speleothems (Hells Bells) formed by the interplay of pelagic redoxcline biogeochemistry and specific hydraulic conditions in the El Zapote sinkhole, Yucatán Peninsula, Mexico. *Biogeosciences*, *16*, 2285–2305.

Rodionov, D. A., Dubchak, I. L., Arkin, A. P., Alm, E. J., & Gelfand, M. S. (2005). Dissimilatory metabolism of nitrogen oxides in bacteria: comparative reconstruction of transcriptional networks. *PLoS Computational Biology*, *1*(5), e55.

Rodríguez-Martínez, M., Sánchez, F., Walliser, E. O., & Reitner, J. (2012). An upper Turonian fine-grained shallow marine stromatolite bed from the Muñecas Formation, Northern Iberian Ranges, Spain. *Sedimentary Geology*, *263*, 96–108.

Rosenberg, E., DeLong, E. F., Lory, S., Stackebrandt, E., & Thompson, F. (2014a). *The Prokaryotes: Other Major Lineages of Bacteria and The Archaeale* (4th ed.). Springer Berlin Heidelberg.

Rosenberg, E., DeLong, E. F., Lory, S., Stackebrandt, E., & Thompson, F. (2014b). *The Prokaryotes: Gammaproteobacteria* (4th ed.). Springer Berlin Heidelberg.

Rosenberg, E., DeLong, E., Loy, S., Stackebrandt, E., & Thompson, F. (2014c). *The Prokaryotes: Deltaproteobacteria and Epsilonpoteobacteria* (4th ed.). Springer Berlin Heidelberg.

Rother, D., Henrich, H. J., Quentmeier, A., Bardischewsky, F., & Friedrich, C. G. (2001). Novel genes of the *sox* gene cluster, mutagenesis of the flavoprotein SoxF, and evidence for a general sulfur-oxidizing system in *Paracoccus pantotrophus* GB17. *Journal of Bacteriology*, *183*(15), 4499–4508.

Roy, A., Kucukural, A., & Zhang, Y. (2010). I-TASSER: a unified platform for automated protein

References

structure and function prediction. *Nature Protocols*, *5*(4), 725–738.

Sanger, F., Nicklen, S., & Coulson, A. R. (1977). DNA sequencing with chain-terminating inhibitors. *Proceedings of the National Academy of Sciences of the United States of America*, *74*(12), 5463–5467.

Sauder, L. A., Albertsen, M., Engel, K., Schwarz, J., Nielsen, P. H., Wagner, M., & Neufeld, J. D. (2017). Cultivation and characterization of *Candidatus* Nitrosocosmicus exaquare, an ammonia-oxidizing archaeon from a municipal wastewater treatment system. *The ISME Journal*, *11*(5), 1142–1157.

Sauvé, V., Bruno, S., Berks, B. C., & Hemmings, A. M. (2007). The SoxYZ complex carries sulfur cycle intermediates on a peptide swinging arm. *Journal of Biological Chemistry*, *282*(32), 23194–23204.

Scheller, S., Goenrich, M., Boecher, R., Thauer, R. K., & Jaun, B. (2010). The key nickel enzyme of methanogenesis catalyses the anaerobic oxidation of methane. *Nature*, *465*(7298), 606–608.

Schloss, P. D., & Handelsman, J. (2005). Introducing DOTUR, a computer program for defining operational taxonomic units and estimating species richness. *Applied and Environmental Microbiology*, *71*(3), 1501–1506.

Schmitter-Soto, J. J., Comín, F. A., Escobar-Briones, E., Herrera-Silveira, J., Alcocer, J., Suárez-Morales, E., Elías-Gutiérrez, M., Díaz-Arce, V., Marín, L. E., & Steinich, B. (2002). Hydrogeochemical and biological characteristics of cenotes in the Yucatán Peninsula (SE Mexico). *Hydrobiologia*, *467*(1), 215–228.

Schopf, J. W. (1983). *Earth's Earliest Biosphere: Its Origin and Evolution*. Princeton University Press.

Seifan, M., & Berenjian, A. (2019). Microbially induced calcium carbonate precipitation: a widespread phenomenon in the biological world. *Applied Microbiology and Biotechnology*, *103*(12), 4693–4708.

Shakya, M., Lo, C.-C., & Chain, P. S. G. (2019). Advances and challenges in metatranscriptomic analysis. *Frontiers in Genetics*, *10*, 904.

Staley, J. T. (2006). The bacterial species dilemma and the genomic-phylogenetic species concept. *Philosophical Transactions of the Royal Society of London. Series B, Biological Sciences*, *361*(1475), 1899–1909.

Stinnesbeck, S., Frey, E., Olguín, J. A., Stinnesbeck, W., Zell, P., Mallison, H., González, A. G., Núñez, E. A., Morlet, A. V., & Mata, A. T. (2017). *Xibalbaonyx oviceps*, a new megalonychid ground sloth (Folivora, Xenarthra) from the Late Pleistocene of the Yucatán Peninsula, Mexico, and its paleobiogeographic significance. *PalZ*, *91*(2), 245–271.

Stinnesbeck, W., Frey, E., Zell, P., Avilés, J., Hering, F., Frank, N., Arps, J., Geenen, A., Gescher, J., Isenbeck-Schröter, M., Ritter, S., Stinnesbeck, S., Núñez, E. A., Dahne, V. F., González, A. G., & Deininger, M. (2018). Hells Bells – unique speleothems from the Yucatán Peninsula, Mexico, generated under highly specific subaquatic conditions. *Palaeogeography, Palaeoclimatology, Palaeoecology*, *489*, 209–229.

Stockdreher, Y., Sturm, M., Josten, M., Sahl, H.-G., Dobler, N., Zigann, R., & Dahl, C. (2014). New proteins involved in sulfur trafficking in the cytoplasm of *Allochromatium vinosum*. *The Journal*

of Biological Chemistry, *289*(18), 12390–12403.

Stockdreher, Y., Venceslau, S. S., Josten, M., Sahl, H.-G., Pereira, I. A. C., & Dahl, C. (2012). Cytoplasmic sulfurtransferases in the purple sulfur bacterium *Allochromatium vinosum*: evidence for sulfur transfer from DsrEFH to DsrC. *PLOS ONE*, *7*(7), e40785.

Stöhr, R., Waberski, A., Liesack, W., Völker, H., Wehmeyer, U., & Thomm, M. (2001). *Hydrogenophilus hirschii* sp. nov., a novel thermophilic hydrogen-oxidizing beta-proteobacterium isolated from Yellowstone National Park. *International Journal of Systematic and Evolutionary Microbiology*, *51*(Pt 2), 481–488.

Stramma, L., Johnson, G. C., Sprintall, J., & Mohrholz, V. (2008). Expanding oxygen-minimum zones in the tropical oceans. *Science*, *320*(5876), 655–658.

Sun, L., Toyonaga, M., Ohashi, A., Matsuura, N., Tourlousse, D. M., Meng, X.-Y., Tamaki, H., Hanada, S., Cruz, R., Yamaguchi, T., & Sekiguchi, Y. (2016). Isolation and characterization of *Flexilinea flocculi* gen. nov., sp. nov., a filamentous, anaerobic bacterium belonging to the class Anaerolineae in the phylum Chloroflexi. *International Journal of Systematic and Evolutionary Microbiology*, *66*(2), 988–996.

Tanabe, T. S., Leimkühler, S., & Dahl, C. (2019). Chapter Seven - The functional diversity of the prokaryotic sulfur carrier protein TusA. *In* R. Poole (Ed.), *Advances in Microbial Physiology* (Vol. 75, pp. 233–277). Academic Press.

Taylor, G. T., Iabichella, M., Ho, T.-Y., Scranton, M. I., Thunell, R. C., Muller-Karger, F., & Varela, R. (2001). Chemoautotrophy in the redox transition zone of the Cariaco Basin: A significant midwater source of organic carbon production. *Limnology and Oceanography*, *46*(1), 148–163.

Thauer, R. K., Jungermann, K., & Decker, K. (1977). Energy conservation in chemotrophic anaerobic bacteria. *Bacteriological Reviews*, *41*(1), 100.

Thompson, J. B., Schultze-Lam, S., Beveridge, T. J., & Des Marais, D. J. (1997). Whiting events: biogenic origin due to the photosynthetic activity of cyanobacterial picoplankton. *Limnology and Oceanography*, *42*(1), 133–141.

Tourna, M., Stieglmeier, M., Spang, A., Könneke, M., Schintlmeister, A., Urich, T., Engel, M., Schloter, M., Wagner, M., Richter, A., & Schleper, C. (2011). *Nitrososphaera viennensis*, an ammonia oxidizing archaeon from soil. *Proceedings of the National Academy of Sciences*, *108*(20), 8420–8425.

Tourney, J., & Ngwenya, B. T. (2014). The role of bacterial extracellular polymeric substances in geomicrobiology. *Chemical Geology*, *386*, 115–132.

Visscher, P. T., Reid, R. P., Bebout, B. M., Hoeft, S. E., Macintyre, I. G., & Thompson, J. A. (1998). Formation of lithified micritic laminae in modern marine stromatolites (Bahamas): The role of sulfur cycling. *American Mineralogist*, *83*(11), 1482–1493.

Walker, C. B., de la Torre, J. R., Klotz, M. G., Urakawa, H., Pinel, N., Arp, D. J., Brochier-Armanet, C., Chain, P. S. G., Chan, P. P., Gollabgir, A., Hemp, J., Hügler, M., Karr, E. A., Könneke, M., Shin, M., Lawton, T. J., Lowe, T., Martens-Habbena, W., Sayavedra-Soto, L. A., … Stahl, D. A. (2010). *Nitrosopumilus maritimus* genome reveals unique mechanisms for nitrification and autotrophy in globally distributed marine crenarchaea. *Proceedings of the National Academy of Sciences of the United States of America*, *107*(19), 8818–8823.

Walsh, D. A., Zaikova, E., Howes, C. G., Song, Y. C., Wright, J. J., Tringe, S. G., Tortell, P. D., & Hallam, S. J. (2009). Metagenome of a versatile chemolithoautotroph from expanding oceanic dead zones. *Science*, *326*(5952), 578–582.

Widdel, F., and Bak, F. (1992). Gram-negative mesophilic sulfate-reducing bacteria. *In* M. Dworkin, S. Falkow, E. Rosenberg, K.-H. Schleifer, & E. Stackerbrandt (eds.), *The Prokaryotes* (2nd ed., pp. 3352–3378). Springer.

Xia, Y., Yubo, W., Wang, Y., Chin, F., & Zhang, T. (2016). Cellular adhesiveness and cellulolytic capacity in Anaerolineae revealed by omics-based genome interpretation. *Biotechnology for Biofuels*, *9*.

Yamada, T., & Sekiguchi, Y. (2009). Cultivation of uncultured Chloroflexi subphyla: significance and ecophysiology of formerly uncultured Chloroflexi "subphylum i" with natural and biotechnological relevance. *Microbes and Environments*, *24*(3), 205–216.

Yamada, T., Sekiguchi, Y., Hanada, S., Imachi, H., Ohashi, A., Harada, H., & Kamagata, Y. (2006). *Anaerolinea thermolimosa* sp. nov., *Levilinea saccharolytica* gen. nov., sp. nov. and *Leptolinea tardivitalis* gen. nov., sp. nov., novel filamentous anaerobes, and description of the new classes Anaerolineae classis nov. and Caldilineae classis nov. in the bacterial phylum Chloroflexi. *International Journal of Systematic and Evolutionary Microbiology*, *56*(6), 1331–1340.

Yang, J., Yan, R., Roy, A., Xu, D., Poisson, J., & Zhang, Y. (2015). The I-TASSER Suite: protein structure and function prediction. *Nature Methods*, *12*(1), 7–8.

Yang, J., & Zhang, Y. (2015). I-TASSER server: new development for protein structure and function predictions. *Nucleic Acids Research*, *43*(W1), W174–W181.

Zhu, T., & Dittrich, M. (2016). Carbonate precipitation through microbial activities in natural environment, and their potential in biotechnology: a review. *Frontiers in Bioengineering and Biotechnology*, *4*, 4.

Zopfi, J., Ferdelman, T. G., Jørgensen, B. B., Teske, A., & Thamdrup, B. (2001). Influence of water column dynamics on sulfide oxidation and other major biogeochemical processes in the chemocline of Mariager Fjord (Denmark). *Marine Chemistry*, *74*(1), 29–51.

Zumft, W. G. (1997). Cell biology and molecular basis of denitrification. *Microbiology and Molecular Biology Reviews*, *61*(4), 533–616.

UNPUBLISHED THESES

Klose, L. (2018). Hydrogeologischer und hydrogeochemischer Vergleich unterschiedlicher Cenoten auf der Yucatán Halbinsel, Mexiko. Heidelberg University, pp. 120.

Schorndorf, N. (2018). Uranium series dating, stable isotopes and geochemistry of "Hells Bells" speleothems from the Yucatán Peninsula. Heidelberg University, pp. 79.

Kühnel, S. (2020). Untersuchung von Partikelbildung in verschiedenen pelagischen Redoxklinen. Heidelberg University.

6 APPENDIX

6.1 Digital appendix

The digital appendix of this thesis contains the custom python script 'lappleb.py' mentioned in section 2.6.2.

Furthermore, the submitted version of the following paper is provided, in which some of the presented results will be published:

Leberecht, K., Ritter, S. M., Lapp, C. J., Klose, L., Eschenröder, J., Scholz, C., Stinnesbeck, W., Kletzin, A., Isenbeck-Schröter, M., & Gescher, J. (in revision). Microbially promoted calcite precipitation in the pelagic redoxcline: Elucidating the formation of the turbid layer. *Geobiology*.

6.2 Supplementary Tables

Table S1: Overview of the 16S rRNA raw and trimmed reads and reads in OTUs belonging to Bacteria after phylogenetic analysis (based on the SILVA 16S v 132 97% reference database). According to Leberecht et al. (in revision).

Sample		Reads in pairs	No. of reads after trim	Average length after trim	Reads in OTUs
Fresh water	Replicate 1	312 800	312 750	231.0	83 841
	Replicate 2	277 554	277 526	230.9	83 249
Redoxcline	Replicate 1	384 056	384 002	230.2	99 454
	Replicate 2	409 700	409 668	230.7	102 162
Halocline	Replicate 1	364 602	364 538	229.3	71 396
	Replicate 2	357 142	357 076	231.1	72 396

Table S2: Overview of the 16S rRNA raw and trimmed reads and reads in OTUs belonging to Archaea after phylogenetic analysis (based on the SILVA 16S v 132 97% reference database). According to Leberecht et al. (in revision).

Sample		Reads in pairs	No. of reads after trim	Average length after trim	Reads in OTUs
Fresh water	Replicate	335 706	335 660	234.4	116 027
	Replicate	197 238	179 214	234.8	67 714
Redoxcline	Replicate	348 940	348 898	234.4	89 754
	Replicate	316 562	316 532	234.4	95 029
Halocline	Replicate	311 190	311 172	234.4	48 816
	Replicate	288 200	288 148	234.4	24 581

Table S3: Overview of metagenomic (MG) and metatranscriptomic (MT) raw and trimmed reads.

Sample	Reads in pairs (MG)/ Reads (MT)	No. of reads after trim
MG El Zapote (central redoxcline)	162 152 166	116 127 247
MT El Zapote (central redoxcline)	142 373 375	119 853 078
MG El Zapote Hells Bells biofilm (central redoxcline; merged duplicate from 2018 & 2020)	221 780 400	195 893 201
MG Angelita (central redoxcline)	98 721 270	18 550 005
MT Angelita (central redoxcline)	23 398 302	23 056 797

Table S4: BLAST result of the *dsrA* sequence from Hydrogenophilales (metagenome: El Zapote redoxcline) against the *dsrAB* database (Müller et al., 2015). The top 3 BLAST hits are listed. According to Leberecht et al. (in revision).

Hit	Description		Environ-ment	Operational classi-fication	E-value	% Identity
AkinLa18	alkaline lake sediment clone HSe226	Proteobacteria; Betaproteobacteria	Alkaliphilic/ Halophilic	Oxidative bacterial type *dsrAB*	0	76.5
AkinLa19	alkaline lake sediment clone HSe227	Proteobacteria; Betaproteobacteria	Alkaliphilic/ Halophilic	Oxidative bacterial type *dsrAB*	0	76.2
AkinLak9	alkaline lake sediment clone HSe122	Proteobacteria; Betaproteobacteria	Alkaliphilic/ Halophilic	Oxidative bacterial type *dsrAB*	0	76.2

Table S5: BLAST result of the *dsrA* sequence from Nitrosomonadales (metagenome: El Zapote redoxcline) against the *dsrAB* database (Müller et al., 2015). The top 3 BLAST hits are listed. According to Leberecht et al. (in revision).

Hit	Description		Environ-ment	Operational classi-fication	E-value	% Identity
ThbDeni5	*Thiobacillus denitrificans* NZ_AAFH010 00001	Proteobacteria; Betaproteobacteria	Soil	Oxidative bacterial type *dsrAB*	7.66 E-53	92.6
ThbThio4	*Thiobacillus thioparus*	Proteobacteria; Betaproteobacteria	Unknown/ Misc	Oxidative bacterial type *dsrAB*	1.69 E-49	91.4
AkinLak7	alkaline lake sediment clone HSe114	Proteobacteria; Betaproteobacteria	Alkali-philic/ Halophilic	Oxidative bacterial type *dsrAB*	1.78 E-49	91.4

Table S6: BLAST result of the *dsrA* sequence from Thiotrichales (metagenome: El Zapote redoxcline) against the *dsrAB* database (Müller et al., 2015). The top 3 BLAST hits are listed. According to Leberecht et al. (in revision).

Hit	Description		Environ-ment	Operational classification	E-value	% Identity
entry697	Marine metagenome lcl_2189573019_13 588_3986	Proteobacteria; Alphaproteo-bacteria	Marine	Oxidative bacterial type *dsrAB*	0	75.9
entry842	Alaska permafrost soil metagenome lcl_2124908044_66 702_4181194	Proteobacteria; Gammaproteo-bacteria	Soil	Oxidative bacterial type *dsrAB*	1.35 E-154	75.3
AkmEhrl3	*Alkalilimnicola ehrlichei* MLHE1 CP000453	Proteobacteria; Gammaproteo-bacteria	Alkali-philic/ Halophilic	Oxidative bacterial type *dsrAB*	0	75.1

Table S7: BLAST result of the *dsrA* sequence from Chlorobiales (metagenome: Angelita redoxcline) against the *dsrAB* database (Müller et al., 2015). The top 3 BLAST hits are listed.

Hit	Description		Environ-ment	Operational classification	E-value	% Identity
ChbTepi3	*Chlorobaculum tepidum* TLSNC_002932a	Chlorobi; Chlorobia; Chlorobiaceae	Thermo-philic	Oxidative bacterial type *dsrAB*	0	92.26
ClrTepid	*Chlorobaculum tepidum* TLSNC_002932b	Chlorobi; Chlorobia; Chlorobiaceae	Thermo-philic	Oxidative bacterial type *dsrAB*	0	92.18
ClrLim14	*Chlorobaculum limicola* DSM 257EU155046	Chlorobi; Chlorobia; Chlorobiaceae	Thermo-philic	Oxidative bacterial type *dsrAB*	0	91.76

Table S8: BLAST result of the *dsrA* sequence from Chromatiales (metagenome: Angelita redoxcline) against the *dsrAB* database (Müller et al., 2015). The top 3 BLAST hits are listed.

Hit	Description		Environ-ment	Operational classification	E-value	% Identity
entry700	Lake Washington sediment metagenomelcl_21 49837030_67518_1 978	Proteobacteria; Betaproteo-bacteria	Fresh-water	Oxidative bacterial type *dsrAB*	1.73 E-05	90.91
entry483	Lake Washington sediment metagenomelcl_20 06543005_4325_60 01898	Proteobacteria; Betaproteo-bacteria	Fresh-water	Oxidative bacterial type *dsrAB*	1.33 E-19	84.52
HrhHalo3	*Halorhodospira halophila* SL1NZ_AAOQ010 00001	Proteobacteria; Gamma-proteobacteria	Alkali-philic/ Halo-philic	Oxidative bacterial type *dsrAB*	6.42 E-49	83.33

Table S9: BLAST result of the *dsrA* sequence from Nitrosomonadales (metagenome: Angelita redoxcline) against the *dsrAB* database (Müller et al., 2015). The top 3 BLAST hits are listed.

Hit	Description		Environ-ment	Operational classification	E-value	% Identity
entry135	Hot spring metagenomelcl_ 2016842008_20 536_131781	Proteobacteria; Gamma-proteobacteria	Thermo-philic	Oxidative bacterial type *dsrAB*	1.77 E-11	91.49
FM246817	Uncultured marine FM246817	Proteobacteria; Alpha-proteobacteria	Marine	Oxidative bacterial type *dsrAB*	5.7 8E-24	87.5
FM246814	Uncultured marine FM246814	Proteobacteria; Alpha-proteobacteria	Marine	Oxidative bacterial type *dsrAB*	5.78 E-24	87.5

Table S10: BLAST result of the *dsrA* sequence from unassigned Gammaproteobacteria (metagenome: Angelita redoxcline) against the *dsrAB* database (Müller et al., 2015). The top 3 BLAST hits are listed.

Hit	Description		Environ-ment	Operational classification	E-value	% Identity
entry130	Marine microbial community metagenomelcl_2189 573008_57982_1466 2119	Proteobacteria; Betaproteo-bacteria	Marine	Oxidative bacterial type *dsrAB*	7.69 E-55	85.41
entry483	Lake Washington sediment metagenomelcl_2006 543005_4325_60018 98	Proteobacteria; Betaproteo-bacteria	Fresh-water	Oxidative bacterial type *dsrAB*	2.36 E-04	84.62
entry700	Lake Washington sediment metagenomelcl_2149 837030_67518_1978	Proteobacteria; Betaproteo-bacteria	Fresh-water	Oxidative bacterial type *dsrAB*	4.55 E-07	82.69

Table S11: BLAST result of the *dsrA* sequence from Thiotrichales (metagenome: Angelita redoxcline) against the *dsrAB* database (Müller et al., 2015). The top 3 BLAST hits are listed.

Hit	Description		Environ-ment	Operational classification	E-value	% Identity
JQ256785	Uncultured bacterium ws633F6JQ256 785	Proteobacteria; Gamma-proteobacteria	Marine	Oxidative bacterial type *dsrAB*	6.85	100
CP003108	*Desulfosporo-sinus orientis* DSM 765CP003108	Firmicutes; Clostridia; Desulfo-sporosinus	Soil	Reductive bacterial type *dsrAB*	0.16	95.24
UncS1662	Polluted aquifer clone LGWG13EF065 040	Proteobacteria; Deltaproteo-bacteria; Desulfobulb-aceae	Fresh-water	Reductive bacterial type *dsrAB*	1.09 E-03	92.59